An Electrochemical Impedance Spectroscopy Based Nitrate Sensor for Practical Application

A Project Report Submitted in Partial

Fulfillment of the Requirements

For the Degree of

Master of Engineering

In

Electrical and Electronics Engineering

By

Li Xie

School of Engineering and Advanced Technology

Massey University

Palmerston North

New Zealand

April 2016

Abstract

Water contamination not only affects human health, but can also damage the ecological system and the natural environment. Agriculture is the backbone of New Zealand's economy, however the sector has been identified as a primary source of nitrate contamination in many waterways. Therefore, monitoring of water quality in agricultural areas is paramount. The contemporary measurement methodologies applied for contaminant quantification are expensive, laboratory-based and time-consuming so the development of a low-cost, convenient sensing system is required. An electrochemical impedance spectroscopy based nitrate sensing system has been developed for nitrate detection. The system is designed to measure the nitrate concentration in water is stand-alone, robust, real-time and low-cost. The microcontroller in the designed system was used to generate the excitation signal applied to the sensor; for data processing and controlling time interval for the switch on/off the automatic sample-intake pump. The data in the microcontroller is transmitted to a computer for data storage and calculation via wireless communication. As the sensor geometry used in the project is the interdigital type which is very sensitive to the temperature, therefore, the sensor was initially tested in the deionized water at variable temperatures. From the result of testing in various temperature ranges, the temperature correction factor was obtained for nitrate measurement. The calibration samples were prepared by the serial dilution of a nitrate stock solution using sodium nitrate ($NaNO_3$) and ammonium nitrate (NH_4NO_3) with different concentrations. The sensor was immersed in the solution to observe the impedance change at various nitrate concentrations. The experimental result showed a good linear relationship between the concentration and real part of the measured impedance and the computational model for nitrate concentration was predicted based on the experimental results achieved. The sensor was also tested in the water samples collected from different local agricultural streams, and the results were validated with the applied laboratory testing results using contemporary techniques. The experimental results showed that the sensing system is more sensitive to the lower nitrate concentrations in the surface water. The system was prototyped and applied in the field. The real-time low-cost testing system displayed its potential for the in-situ continuous nitrate monitoring in the paddocks.

Acknowledgements

I would like to express my immense gratitude to my supervisor Prof. Subhas Chandra Mukhopadhyay for his great support, encouragement and help. He kept motivating me by giving me patient guidelines, advice and pointing me in the right direction throughout the work.

I would like to express my appreciation to my co-supervisor Dr. Lucy Burkitt for her patient guidance and advice on agricultural nitrate contamination of waterways.

I also would like to express my gratitude to Dr. Asif Zia for guiding me throughout the project. I would also thank Mr. Anindya Nag, Ms. Narsin Afsarimanesh, Mr. M. Eshrat Ealahi and Mr. Weizhong Shi for their active collaborations in the project. Thanks to Massey staff members Ms. Glenys Wallace, Mr. Ian Furkert, Mrs. Ann-Marie Jackson, Mr. John Edwards, Mr. Anthony Wade, Mr. Morio Fukuoka, Mr. Ken Mercer and Mr. Collin Plaw for their technical assistance and support during my work. I also would like to thank the School of Engineering and Advanced Technology, Massey University who provided me with funds and the opportunity to pursue my Masters' degree.

I want to pay special gratitude to my beloved parents and husband for their unconditional love and support. To my lovely and wonderful daughters Stephanie and Jamie, thanks for your patience and understandings throughout the year.

Table of Contents

Table of Figures

Lists of Tables

Research Output

Conference Proceedings

1. **L. Xie,** Zia A., Mukhopadhyay S.C, Burkitt L, "Electrochemical Impedimetric Sensing of Nitrate Contamination in Water", Proceedings of the 9th International Conference on Sensing Technology, December 8-10, 2015, Auckland, New Zealand, pp. 257-262.
2. Zia A., Afsarimanesh N., **L. Xie,** Nag A., Al-Bahadly I.H, P.L. Yu, " Improved Detection Limits for Phthalates by Selective Solid-phase Micro-extraction", Proceedings of the 9th International Conference on Sensing Technology, December 8-10, 2015, Auckland, New Zealand, pp. 733-738
3. **L. Xie,** Zia A., Alahi M.E.E, Mukhopadhyay S.C, Burkitt L, "Practical Nitrate Sensor Based on Electrochemical Impedance Measurement", Proceedings of 2016 IEEE International Instrumentation and Measurement Technology Conference, May 23-26, 2016, Taipei, Taiwan.

Journal Publications:

1. S. Mukhopadhyay, A. Nag, A. Zia, **X. Li,** and J. Kosel, "Novel sensing approach for LPG leakage detection: Part I: Operating Mechanism and Preliminary Results", **IEEE Sensor Journal. (Accepted).**
2. S. Mukhopadhyay, A. Nag, A. Zia, **X. Li,** and J. Kosel, "Novel sensing approach for LPG leakage detection: Part II: Effects of particle size, composition and coating layer thickness", **IEEE Sensor Journal. (Accepted).**

Conference Attendance:

Venue: ICST 2015, Auckland, New Zealand

Date: December 8-10, 2015

Conference Presentation

Title: Electrochemical Impedimetric Sensing of Nitrate Contamination in Water

Date: 9th December, 2015

Venue: ICST 2015, Auckland, New Zealand

Chapter 1: Introduction

1.1 Background of Project

In our planet, the water resource makes up 97% from the ocean and 3% from freshwater. Most of the freshwater (around 69%) is stored in the icecaps and glaciers, and there is only about 30% of total freshwater (around 1% of total water source) [1] found in the groundwater and surface water. Most freshwater comes from rainfall and snow which are dissolved from the atmosphere and flow into the sea or is absorbed by land or evaporates back in to the atmosphere. Moreover, freshwater extracted from rivers, lakes and ground are used for agriculture (70%), industrial processes (22%) and domestic use (8%) [2]. Freshwater is an essential natural resource which is necessary for all living organisms because it supplies drinking water and provides food and habitat. Freshwater also supports human recreational activities such as swimming, fishing and boating. Therefore, clean water is a key issue not only for human and animal health, but also the health of aquatic organisms.

The degree of urbanization has grown exponentially in the last few decades. This has resulted in a rapid increase of contamination in the waterways. One of the most important of these contaminants is the nitrate salt. Nitrate-nitrogen (NO_3-N) is the one of an essential element for the growth of all plants and animals in water as it is an important component for the supply of protein [3, 4]. It is also used in the agricultural sector to increase plant and therefore animal production. However, nitrate can become a contaminant if the concentration in the water rises above a certain threshold concentration, a common problem in surface and groundwater draining the agricultural areas all over the world [5, 6]. In New Zealand, the NO_3-N concentrations in groundwater are commonly higher than the threshold concentration in the agricultural areas, with figure 1.1.1 showing median concentrations around the country from 1995 to 2008 [7]. Figure 1.1.1 indicates that 80% of monitoring sites had were classified as ‘good’ condition with nitrate concentrations of less than 5.65 mg/L and around 5% of sites had nitrate concentrations that exceed the limit of drinking water (11.3 mg/L). In agricultural regions such as Canterbury, Manawatu, Taranaki and Waikato, nitrate concentrations above 5.65 mg/L, were more common.

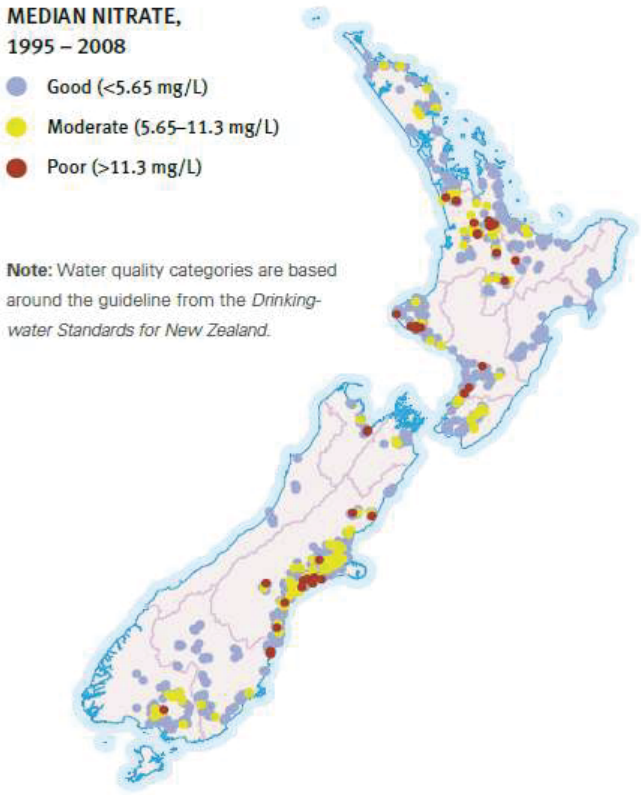

Figure 1.1.1: Median nitrate concentrations measured in groundwater (1995-2008) [7]

Figure 1.1.2 illustrates the trend in rivers condition, based on the monitoring sites in New Zealand. The nitrate concentration did not change over the 10 year analysis period at most of sites. Whereas, the nitrate concentration improved in 21% of the monitoring sites but 26% of sites got worse [8].

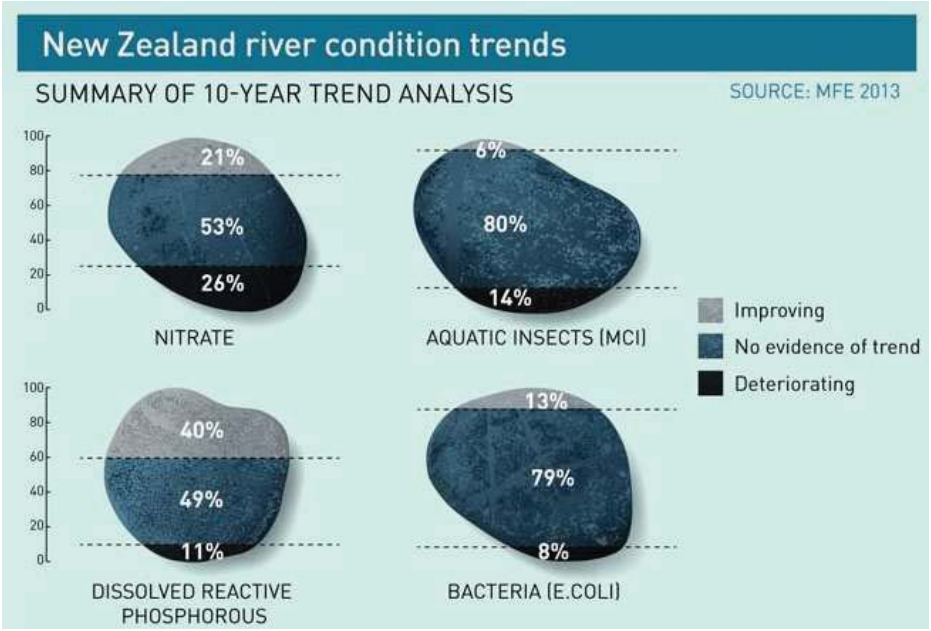

Figure 1.1.2: Summary of 10-year river condition trends reported in 2013 [8]

Agricultural activities are the major sources of nitrate [9] in the waterways. The urine of agricultural livestock is the main source of nitrate contamination [10] and nitrates in the form of urine are excreted by many domestic animals. For example, cows are really inefficient users of nitrogen therefore excrete a large proportion (>70%) of nitrogen that they consume, in their urine [11]. This results in concentrated patches of nitrate, which are prone to leaching into the groundwater and subsequently surface water. The application of nitrogen-rich fertilizer to grass and crops can also increase nitrate contamination of waterways [10, 12, 13]. Another source of nitrate contamination is from the disposal of human and animal sewage and industrial wastes either to the land or via direct release in to waterways.

Elevated NO_3-N concentration in surface waters can stimulate the growth of unwanted algae and aquatic plants leading to water pollution. The purity of water in these bodies can be degraded to the point of it being unsuitable for drinking or any domestic use, even after following a standardized purification procedure. When the nitrate is reduced to nitrite in the nitrogen cycle, it will cause methemoglobinemia due to failure to transfer oxygen to the tissues [14]. If nitrate concentration exceeds 11.3 mg/L in drinking water, it can have devastating effects on infant health [15] because they are more vulnerable to methemoglobinemia than the others. In addition, the rumen microbes in ruminants such as cattle and sheep can reduce the nitrate into the toxic nitrite form [16] and these livestock may have the same signs of nitrate poisoning such as blue membranes, lack of coordination and vomiting.

1.2 Current Measurement Status

Currently, water quality is routinely monitored by the regional councils around New Zealand. However, this is done by a manual collection of water samples from the field. For example, water samples collected from Massey University's Agricultural Experimental Station at Tuapaka, near Palmerston North are collected on a fortnightly basis and NO_3-N concentrations measured using the colorimeter method by Technicon Auto-Analyzer, in a laboratory.

1.2.1 Water Samples Collection

Tuapaka farm with a total area of 420 hectares is a hill country sheep and beef farm used for teaching and research. Parts of the farm are steep and difficult to access, particularly during winter, making water collection difficult and time consuming.

(a) Paddock down the hill

(b) Collect station up the hill

(c) Solar panel for power supply

Figure 1.2.1: Water Sample Collection

In figure 1.2.1 (a), there is a V-shape white board which was built to monitor stream flow which combined with nitrate concentration, allows the calculation of nitrate load (kg/ha) being lost in the waterway. One of the collection points as shown in figure 1.2.1 (b) and (c), the water comes from the uphill and flow into these box through the pipes. There is a counter outside each box used for calculating the flow rate of the stream for different weather condition (rainy or dry days give the different volume of water samples). The solar panel is used to supply power for the counter.

The water samples collected from the field may contain some soils, insects and so on. The unfiltered water may contain particles that may be conductive and dielectric in nature which could affect the impedance measurement. Particles size greater than 25 microns if enter the measurement system could cause the system to malfunction by short-circuiting the excitation and sensing electrodes on the sensor surface. In addition, the soil in the unfiltered water could create a mud layer on the sensing surface which can cause errors in the measurement values. Therefore, the water samples need to be filtered with a 0.22 micron filter before the water sample enters the measurement system.

1.2.2 Current Laboratory Measurement System

Technicon Auto-Analyzer uses continuous flow system (CFS), where samples are taken automatically from the sample tray and the appropriate reagents are added via a pump. Samples are passed through a manifold for mixing, filtering and heating. The colorimeter then measures the absorbance of color in the reaction of the sample and is displayed on the recorder [17].

Figure 1.2.2 shows the Technicon Auto Analyzer used to determine both of nitrate and ammonium concentration in the laboratory by the current method. The Autoanalyzer is set up with heating bath at 28-29^{o}C and uses 520 nm filters in the colorimeter. A red azo dye and an indo-phenol prussian blue dye is used to measure nitrate and ammonium respectively. Reagents used for NO_3-N detection include a catalyst solution, sodium hydroxide solution, hydrazinium sulphate solution and so on (as shown in figure 1.2.2 (b)). Reagents are pumped into the system for about 30 minutes to ensure the system is flushed completely. In the sample tray (Figure 1.2.2 (a)), the prepared nitrate standard and water samples are put in the sample tray. The probe will take each sample in the preset time interval into the system. The samples and reagents are mixed together in the system (Figure 1.2.2 (c)) and the measurement is done by a colorimeter (Figure 1.2.2 (d)). This recorder baseline should be set along with the colorimeter baseline control before the measurement starts by standard calibration.

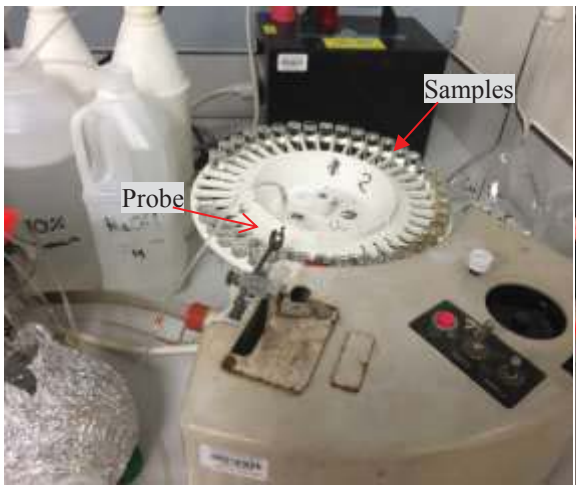

(a) Sample Tray

(b) Chemical Reagents

(c) Detection part (colorimeter)

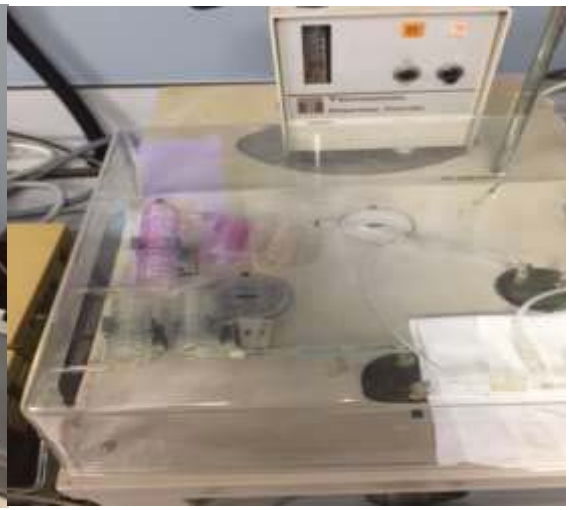

(d) Measured result

Figure 1.2.2: Technicon AutoAnalyzer currently used in the laboratory

This method requires expensive equipment and trained staff to conduct measurements in addition to the limitation on water sample collection, which can only be collected periodically. This approach risks missing key changes in NO_3-N concentration when river-flow rapidly rises or falls. Although high-frequency nitrate sample equipment is available, these cost in the order of $30-70,000.

1.3 Aims and Objectives

Through the importance of nitrate detection and the limitations of the current measurement options, the motivation of this project is to develop a sensing system which can be portable, suitable for in-situ measurement with a low cost for nitrate

detection in water and accurate. Considering the disadvantages of the current methodologies for detecting nitrate, this project aims to develop a sensing system based on the electrochemical impedance spectroscopy method using an interdigital sensor which can be installed in the field for continuous real-time monitoring.

Objectives of the project are to:

- investigate the characterization of the impedance of the sensor in variable temperature and humidity condition
- characterize the impedance of the sensor to detect nitrate concentration
- develop a low-cost and in-situ sensing system
- evaluate the developed system with the commercially available system
- implement the real-time monitoring of nitrate contamination in water

1.4 Organization of the Thesis

This thesis has been organized into five chapters. The introduction of the project is described in Chapter 1, which describes the issue of nitrate contamination in New Zealand waterways, the source and effect of nitrate contamination in natural water resources, the current measurement procedures and methodology and the objectives of this project. In Chapter 2, market research on the commercially available nitrate sensor is undertaken. The literature review of methods and sensors used for nitrate detection are also reported in Chapter 2. The detailed design of the nitrate sensing system has been described in Chapter 3. It includes the system overview, interfacing to the microcontroller, generation of input excitation signal applied to the sensor, measurement of the impedance and phase difference, design for the pump and valve control and the implementation of ZigBee-based data transmission from the microcontroller to the computer via wireless communication and graphic user interface. The experimental results are discussed in Chapter 4. As the interdigital sensor is sensitive to the temperature and humidity in the measurement environment, an experiment with variable temperature and humidity was undertaken and used to characterize the impedance of the sensor in different temperature, humidity conditions. Both of uncoated sensor and Parylene coated sensor were tested in the water solution to investigate the sensor impedance in variable nitrate concentrations

by the designed system and LCR meter. Water samples collected from different groundwater sources were also measured by the designed system, and the results were evaluated with the colorimetric method conducted in the laboratory. Finally, options for the future refinement of the system are discussed and conclusions are drawn in Chapter 5.

Chapter 2: Literature Review

2.1 Electrochemical Impedance Spectroscopy

Electrochemical Impedance Spectroscopy (EIS) is a method to determine the current response of an electrochemical cell by applying a small sinusoidal signal. EIS method is widely used in various applications such as detection of bacterial endotoxin in food [18], determination of the corrosive behavior of materials [19, 20], analysis of electrical properties for controlling soymilk coagulation process [21], evaluation of impedance response to the Phthalate concentration [22] and other biosensing applications [23]. In EIS method, a periodic sinusoidal voltage is applied to the sensor, so there is a phase shift between the applied voltage and current flow through the sensor. Therefore, the total impedance can be divided into the real part and the imaginary part.

Cole-Cole plot and Bode plot are two most important presentation methods to show the relationship between specific parameters. Cole-Cole plot is also known as Nyquist plot which represents the relationship between the real part of impedance (R_s) and imaginary part of impedance (X) in a particular frequency range. One disadvantage of Nyquist plot is that the frequency is not shown in the plot, so it is hard to understand visually which frequency value was used to record the points. In contrast, the frequency is plotted in the X-axes, and absolute impedance $|Z|$ and phase angle Θ is plotted on the Y-axes in the Bode plot. It can clearly show the frequency-dependent behavior of the electrochemical cell.

The Randles equivalent circuit is the mostly used to express EIS evaluation in electrical model form. Randles equivalent circuit consists of series resistance R_e, the parallel combination of double layer capacitance C_{dl} and charge transfer impedance Z_w and charge transfer resistance R_t [24] as shown in figure 2.1.1. The Nyquist plot for Randles circuit without Z_w is semi circle but there is diffusion on the semi-circle when Z_w is added. This happens when the electrode is covered with other coatings, so the electrochemical reaction is influenced.

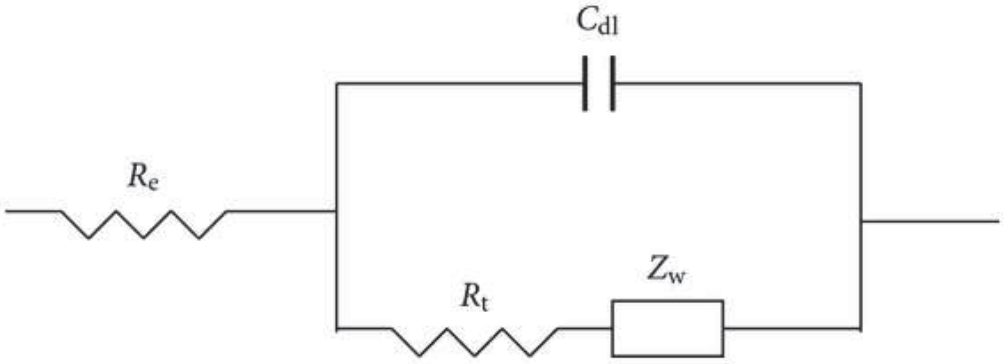

Figure 2.1.1: Randles equivalent circuit

Where:

- R_e: Series resistance
- C_{dl}: Double layer capacitance
- R_t: Charge transfer resistance
- Z_w: Charge transfer impedance

2.2 Fiber Optic Sensor

Fiber optic sensor [25] was developed quickly in the last three decades. It consists of three main elements: a light source to generate the light, optical fibers to pass through the light and a photodetector system to detect the optical signal. Fiber optic sensor can be divided into intrinsic and extrinsic sensors based on the use of fiber. The intrinsic sensor normally uses the phase-modulation techniques which require consistent light sources and only single mode fibers and the modulation happens using the fiber itself. In contrast, the fiber is used as a channel for transmitting in the extrinsic fiber optic sensor which is low cost and allows multimode fibers and inconsistent light sources. The extrinsic fiber optic sensor is widely used in remote sensing due to its small size, no requirement of electrical power, high-temperature operation and long working lifetime.

The optical sensor is also extensively used to detect the nitrate and nitrite [26] because it has some advantages such as high selectivity and sensitivity, low cost and simple. The optical sensor based on the Lauth's violet-triacetyl cellulose membrane film was developed to detect nitration concentration using absorption

spectrophotometry, and it could detect the nitrate concentration from 10.12 to 1012 ng/ml. Modified fiber optic sensor using fluorescing emission of suitable dyes was developed to detect the nitrate [27]. An extrinsic fiber optic sensor with Lophine as a sensitive layer to measure was used to detect nitrate in water [28]. It required the spectral wavelength between 300 and 1100 nm and it can detect the nitrate concentration between 1 and 70 mg/L with 20 millisecond response time.

An investigation using a broad range of wavelengths between 350 nm and 2500 nm of fiber optic sensors has been carried out to measure the spectral absorption of nitrate ions in water [29]. The ideal wavelength of 575 nm was determined using spectroradiometer.

The fiber grating sensor is usually fabricated with multiplexing of single fiber line, and it has high corrosion resistance and stability [25]. In addition, it can be easily embedded in an enormous diversity of material such as fiberglass, metals and thermoplastics. Researchers used fiber Bragg grating sensor to detect the nitrate concentration by analyzing the wavelength shift against the concentration of solution [30], and it achieved the maximum sensitivity at 1.322×10^{-3} nm/ppm.

Fiber optic sensor is used in many other applications. For example, the fluorescent dye is used as sensing lay to detect the dissolved carbon dioxide (CO_2) based on the pH modulation [31]. A pressure sensor fabricated directly on the tip of fiber with a thin silica diaphragm and a measure of 125 μm in diameter at 530/spl degree/C [32]. The fiber-optic temperature sensor based on the optoelectronic oscillator has been reported [33]. The refractive index of the fiber will change with a change in the temperature of the sensing fiber. Therefore, oscillator loop is changed by optical path length. The temperature is evaluated by tracking the peak of the oscillator. The fiber optic surface plasmon resonance is employed in the biology area like monitoring DNA hybridization and melting process using silica nano-bead signal amplification [34], detection of the urea in liquid [35]. Usually, three coating layers are used: silicon layer is used to protect silver layer from oxidation and enzyme layer from deactivation to improve the sensitivity. The resonance wavelength reduces with the increase in the urea concentration. The reported optic sensor can detect the urea concentration in the range of 0 - 160 nM and the sensitivity will decrease as the concentration is increased [35].

2.3 Electrochemical Biosensor

The combination of biological component and transducer are created to convert biological phenomenon into an electrical signal, called biosensor [36]. The biosensor is consists of bioreceptor which recognizes the analyte and detect mode that can electrochemical, optical and so on. Escherichia coli is used as a whole-cell fluorescence-based biosensor to determine the nitrate concentration in the water without any interference with other electrons [37].

Most of the biosensors for nitrate detection are based on the nitrate reductase [38-40]. Novel enzyme-catalyzed oxygen removal system was developed for application in nitrate biosensor under ambient air. The oxygen removal system includes an oxidase enzyme, an oxidase-specific substrate, and catalase for dismutation [38]. To determine the nitrate on the electrochemical biosensor, the following materials were used: 10 ml mixture of EDTA, D-glucose, MV and MOPS at pH 7.0 in deionized water as a buffer, NaR as biorecognition element and GOx as oxygen reduction catalyst. The system can detect the nitrate concentration in the field condition, but the results were affected by deactivating NaR.

Gokhale et al. developed an enzymatic biosensor for nitrate ion detection based on the nanostructured membrane [39]. Immobilized nitrate reductase in a conductive polymer matrix was used to generate an amperometric response. This biosensor strongly depends on the condition of electropolymerization and morphology of PEDOT nanowire arrays. It showed a good response to nitrate with the detecting limit of 0.16 ppm and sensitivity of around 92 μA/mM by applying oxidation potential at 1.1 V and 300 seconds for polymerization time. It also showed a linear relationship between the current density and concentration range of 200 ppb to 1100 ppb.

Another research for nitrate detection based on simplified nitrate reductase (SNaR) by potential spectroscopy technique was done by Wang el at. [40]. Using thin-layer potential coulometry followed by spectroscopic technique to detect Griess reaction products. This spectroscopic Griess evaluation showed the high sensitivity of 8000 AU/M and reproducibility at linear range of 1 to 160 μM without using oxygen removal. Even if a high concentration of other common anions is presented, SNaR also displays high selectivity to nitrate. The advantages of using thin-layer include

restriction of a diffusion layer which makes the reduction of nitrate faster and more effective, and only small amount of sample required.

2.4 Microwave Sensors

Microwave sensing is another novel technology which has various applications like humidity detection [41], measurement of water solution concentration [42, 43], real-time monitoring of glucose in the diabetic patient [44], real-time monitoring in water [45, 46] and so on.

Microwave sensing is based on the interaction between the material under test and resonating modes using high-frequency range (GHz). It used resonator support various mode but the TM_{010} was preferred mode because it can provide measurement in the simple, subtle way and the measuring error is reduced [42]. It can evaluate both organic and inorganic water solution and the sensitivity for detect NaCl is 0.4 dB/(mg/ml) within the concentration range of 0 to 1%. On the other hand, an etched-disc microstrip resonator based on the electromagnetic field distribution was developed to determine the impurities in the water by measuring the dielectric constant of the water. This microstrip resonator showed some benefits like easy fabrication, simple structure, and low cost and so on [43].

In further research, a microwave sensor was developed to monitor the water composition in real-time monitoring [45, 46]. A flexible substrate with interdigitated silver metal pattern was designed as the sensing element, and the sensor could be installed in various places such as water pipe, tube or even curved surface. The sensor was tested under air, deionized and tap water to observe the changing in the resonant frequencies.

There are two signals (reflected signal and transmitted signal) used for microwave analysis based on the conductivity and permittivity. It indicated that the narrow band analysis enables the most sensitive to nutrients in wastewater [46]. Therefore, the cylindrical resonant cavity was operated on TM_{010} mode with a frequency of 2.5 GHz and sample water flow into the cavity through PTFE pipe in the experiment. The system was designed to work at ambient temperature in order to reduce the interference of temperature with permittivity. The experimental results show the peak frequency was increased with the rise in the concentration.

2.5 Novel Interdigital Sensors

Interdigital sensors are finger-like structures on a solid substrate designed for single-sided access to the sample and based on the operation of a parallel plate capacitor. Figure 2.5.1 shows the geometric structure of the interdigital sensor. The planar fabric of the electrodes is formed to perform non-invasive, single-side measurement which offers significant advantages of the interdigital sensor. Other benefits include a simple autonomous operational system, high sensitivity [47] and non-destructive testing.

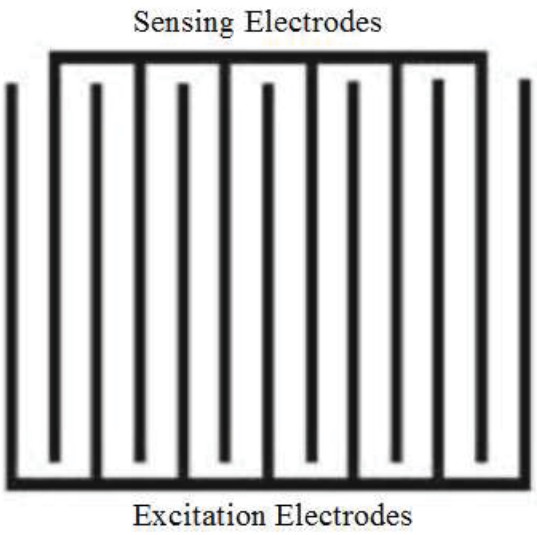

Figure 2.5.1: Geometric structure of interdigital sensor

When a time-dependent voltage signal is applied to the terminals, an electric field is generated between the electrodes of opposite polarity. The electric field passes through the material under test (MUT) and is modified by it. This electric field was used to evaluate some parameters of MUT such as impedance, chemical material, and density and so on [48].

The distance between two adjacent electrodes is called the pitch length. Figure 2.5.2 illustrates the penetration depth of electric field depends on the pitch length. Different pitch length (l_1, l_2, l_3) gives different corresponding penetration depth. The penetration depth is increased with the rise in the pitch length but the electric field strength generated at adjacent electrodes will get weak as it is inversely proportional to pitch length [49].

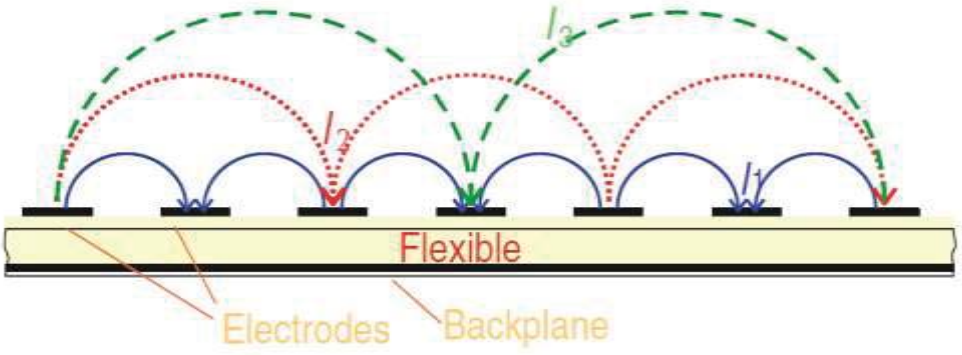

Figure 2.5.2: Electric field for different pitch length [49]

Figure 2.5.3 shows the geometry of excitation pattern for novel multi-sensing electrodes in the interdigital sensor. The electric field generated between excitation and sensing electrodes. Due to different pitch length and the penetration depth, it provides an almost uniform electric field on the sensing surface and thus increases the sensitivity of the interdigital sensor [50].

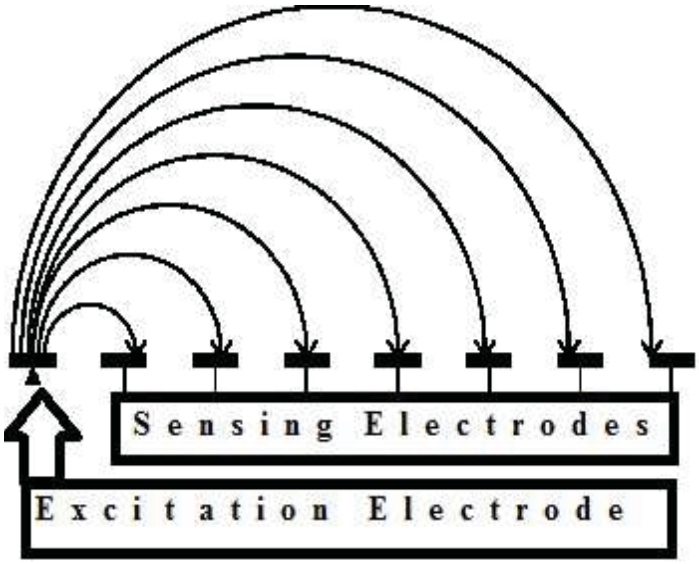

Figure 2.5.3: Geometry of excitation pattern for multi-sensing electrode

The interdigital sensors are fabricated based on the different configurations. Figure 2.5.4 shows the schematic diagram of the sensor configuration. 1-5-50 refers to the repeated pattern of five sensing electrode with respect to each excitation electrode with a distance of 50 microns between two consecutive electrodes [51].

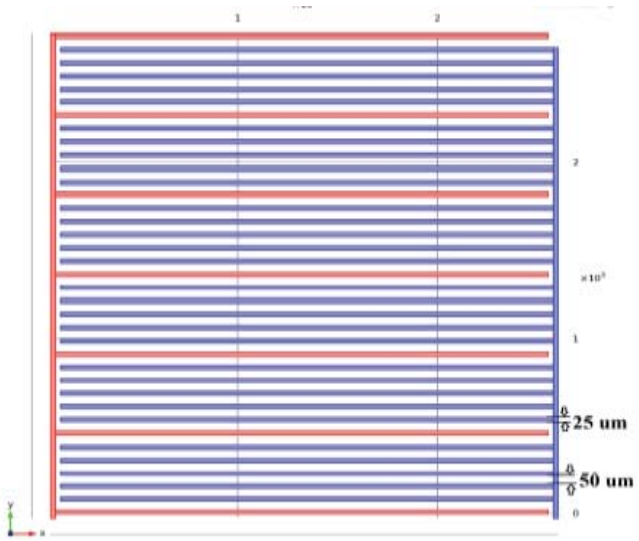

Figure 2.5.4: Sensor configuration (1-5-50)

Due to the planar structure, some of the electric field-lines bulge out from one terminal to the adjacent terminal of opposite polarity. If any material is kept in close proximity to the sensing surface, the permittivity values of the penetrating electric field changes. This change is studied via different spectroscopic techniques to analyze the properties of the material.

The interdigital sensors are used in varieties of applications in environmental monitoring [51-55], the manufacturing process [56], gas sensor [57], photosensitive detection [58], humidity and moisture sensing system [59-62] and so on.

One of the applications was to develop an interdigital sensor based on the electrochemical impedance spectroscopy technique to explore the presence of phthalates in aqueous media [51-53]. The interdigital sensor with gold sensing electrodes was fabricated on a silicon substrate using micro-electrochemical system device fabrication technology. In additional, Parylene C polymer was used as the coating layer to protect the sensing electrode from oxidization.

Another sensing system based on the interdigital sensor was developed to detect domoic acid [54, 55] in the seafood such as mussels, claws and oysters. Three different configurations of sensors had been designed and fabricated. All of three sensors have the same sensing surface area (4.75 mm x 5.00 mm) and the pitch length of 0.25 mm but the distance between two nearby positive and negative electrodes were changed. The first sensor was designed at 1-11-25, the second one

was 1-5-25 and third one was 1-3-25. The first sensor has shown the better uniformity of electric field.

The dielectric characterization of the interdigital sensor was used to evaluate epoxy-based resin's dielectric property which can observe the ionic conduction in the curing process in [56]. The movement of the peak in a dielectric loss means the different transition of the resin which can then be implemented for on-line cure monitoring.

2.6 Novel Electromagnetic Sensor

An electromagnetic sensor is a combination of meander coils with the interdigital sensor, thus show both inductive and capacitive properties. Yunus et al. [63] had developed a system to detect the nitrate based on the electromagnetic sensor. Two different types of connections between interdigital sensor and meander coils were discussed: parallel and series configuration. Figure 2.6.1 shows the schematic diagram of interdigital sensor and meander coils connected in parallel and figure 2.6.2 shows the series connection. Both the top view (left-hand side) and bottom view (right-hand side) were illustrated. One turn of the coil and five turns of meander coils connected to the interdigital sensor in parallel connection and series connection respectively. The Wattyl Killrust Incralac is used as an acrylic resin-based. The sensors were tested at two frequencies: 10 MHz and 500 kHz for nitrate detection. The sensor has more negative electrodes showed the most sensitive to nitrate and good correlation between the nitrate concentration and sensitivity.

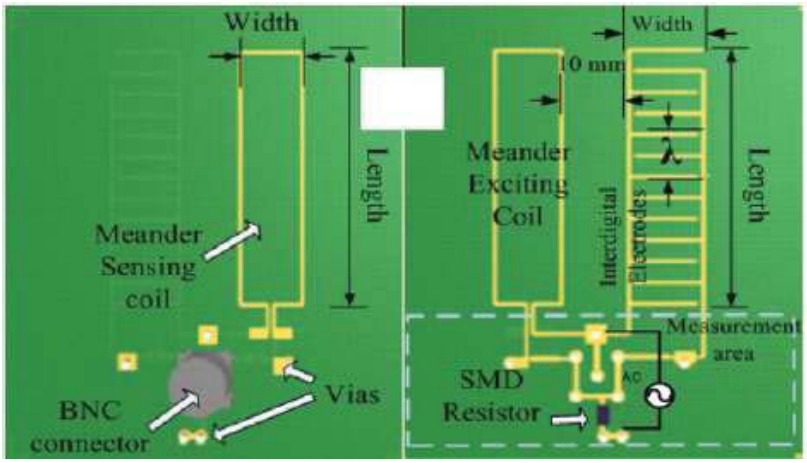

Figure 2.6.1: Schematic diagram of sensor connected in parallel [63]

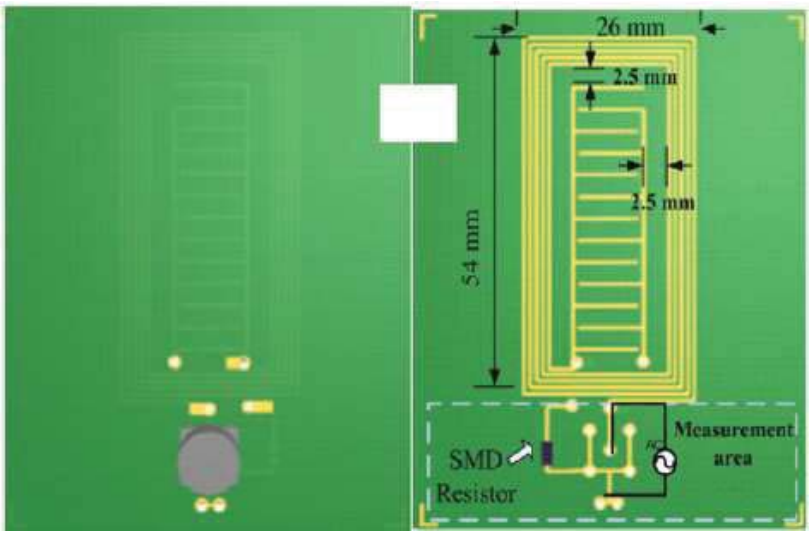

Figure 2.6 2: Schematic diagram of sensor connected in series [63]

Further research to detect the nitrate concentration was based on the radial basis functions (RBF) neural network using planar electromagnetic sensor [64]. RBF has three layers: input layer, hidden layer and output layer. The input layer is the sensor node that measures impedance for detecting the nitrate; hidden layer provide the analyzed function, and the output layer is the linear combination of hidden functions. The planar electromagnetic sensor was immersed into the nitrate water sample and its output signal fed into the RBF Neural Network which can be analyzed to estimate different nitrate concentrations in water. It provided the detection range from 5.5 mg/L to 110 mg/L.

Capacitive sensor based pH determination has been reported [65]. Applications of the interdigital sensor with meander coils includes inspection of printed circuit board, estimation of near-surface material properties, quality monitoring of dairy products and meat [66]. The exciting coil generates a magnetic field which passes through the conductor of the PCB. The eddy current is generated in the conductor which interacts with the generated magnetic field [67]. The resultant magnetic field produces induced voltage across the sensing coil. The voltage across the sensing coil was measured and analyzed so any defects existed in the PCB could be detected. The purpose of evaluating near-surface properties was to avoid unexpected accidents due to the material fatigue and aging [68]. Planar electromagnetic sensor is used for the nondestructive evaluation, and it can be used to measure the transfer impedance of coil for detection of any defects in the near-surface materials. The transfer impedance was calculated based on the finite element analysis, and results were obtained by an

off-line grid system which used to determine the near-surface material properties from real measured data [69]. Another application was to estimate the properties of the dielectric material in the diary product. The impedance changes with fat content in the milk [66]. The dielectric permittivity of fat has an effect on both of the resistance and reactance of impedance of the sensor. Both the magnitude and phase of the impedance were used for evaluation of the properties of the material under test. The frequency was another key element for the optimum result so the most precise frequency should be selected for measurement.

2.7 Nitrate Detection Methods

The techniques for the detection of nitrate are either simultaneously or sequentially. Simultaneous technique means the detection is independent of other analytes in one measurement [70] such as capillary electrophoresis [71-74] and electrochemical [75-82].

2.7.1 Electrochemical detection

Electrochemical detection is based on the evaluation of potential, current or charge to characterize an analyte's chemical reaction or determine its concentration.

Zn (II), the complex-based coating on polymeric membranes, was developed to determine the nitrate concentration range from 5.0 x 10^{-5} to 1.0 x10^{-1} M. This developed system based on the potentiometric sensor showed a fast response time of fewer than 25 seconds and an excellent detection limit of around 10^{-5} M [75]. Another potentiometric nitrate sensor was developed by Cuartero et al. [76]. This sensor consists of an all-solid-state nitrate selective electrode with lipophilic carbon nanotubes and a miniaturized reference electrode. It has the detecting limit of 5 x 10^{-7} M with the response time of 5 seconds.

The amperometric method is used to measure the current at a given electrode to analyze the response of analyte as the current is changing with varying of concentration. Badea et al. [77] developed the electrochemical sensor to detect nitrate based on the Cellulose Acetate membrane. A three-electrode electrochemical sensor was designed based on nitrate-selective polypyrrole (Ppy) as working electrode [78, 79]. The working principles of this system are that a large number of nanopores will

be produced on the surface of the Ppy nanofiber when the working electrode is doping into the nitrate solution. The nitrate detection can be achieved by charge distribution within doped Ppy nanofibers [78]. Similarly, the nitrate was detected by using doped Ppy nanowires integrated with microfluidics [79].

The voltammetric method is also used to detect the nitrate concentration at a copper electrode [80, 82] without reagent electrodes. Based on the deposition of macroporous structure, the copper deposit showed selectivity for the nitrate ion with the detection range of 10 to 200 µM. Lonardi et al. [81] researched on nitrate sensor using silver nanoparticles embedded with polymethacrylic acid matrix electrode. The detection range is linear from 0-20 mM with limit of 0.5 mM by the voltammetric sensor. In [82], an in-situ copper plated boron-doped diamond microelectrode array was developed to detect nitrate with a limit of 0.76 µM.

Table 2.7 1: Electrochemical detection summary

Working method	Working Electrode	Detection limit	Reference
Potentiometric	Zn(II)	1×10^{-5} M	[75]
Potentiometric	Lipophilic Carbon Nanotubes	5×10^{-7} M	[76]
Amperometric	Cellulose Acetate	1×10^{-6} M	[77]
Amperometric	Ppy nanofibers	1×10^{-4} M	[78]
Amperometric	Ppy nanowires	4.5×10^{-6} M	[79]
Voltammetric	Copper	1×10^{-5} M	[80]
Voltammetric	Silver nanoparticles	5×10^{-4} M	[81]
Voltammetric	Copper	7.6×10^{-7} M	[82]

Table 2.7.1 summarizes the electrochemical detection based on methods like potentiometric, amperometric and voltammetric. There are some advantages of electrochemical detection include:

- Simple and cost effective

- Suitable for in-situ measurement
- Fast response and wide detection limit

On the other side, the disadvantages are:

- The sensitivity relies on the working electrode
- Requires prepared reagent solutions
- Interference with other ions like phosphate, sulphate, chloride, etc. in the water

2.7.2 Ion Chromatography

Ion chromatography is used to measure the concentration of major anions in the water by separating their ionized samples based on their interface to a resin. The individual separation depends on their charge, species type and size. Sample solutions go through a pressurized column where the column constituents absorb the ions (called eluent). As the eluent runs through the column and the absorbed ions start separating from the column. The ionic concentration is determined by the retention time of different species as shown in figure 2.7.2.1 [83].

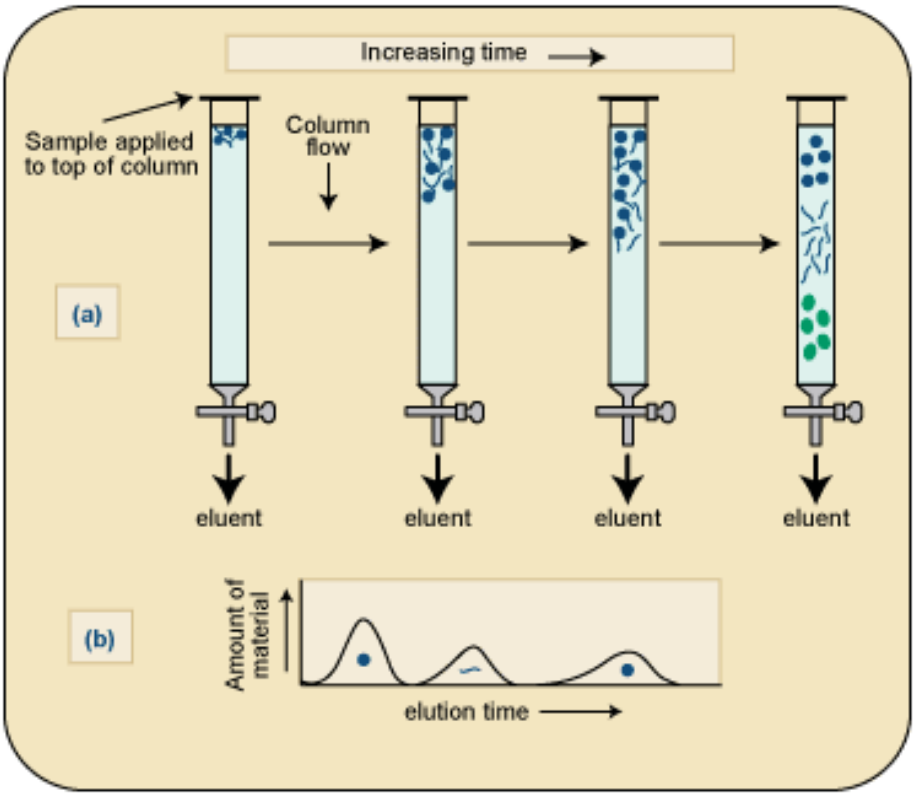

Figure 2.7.2.1: Schematic diagram of Ion Chromatography Method [83]

Due to its high accuracy of measurement, it is widely used in determining nitrate concentration in process streams based on the conductometric detection [84], milk samples [85] and monitor the wastewater quality in the fertilizer industry [86]. However, the expensive equipment is required for this method, and it is designed for the bench top in the laboratory base.

2.7.3 Flow Injection Analysis methods

The flow injection analysis technique has been used for the past forty decades. It is an automated method where the input sample is injected into the reagents carrier. The mixture of sample and reagents are pumped through the mixing coil into the detector. Figure 2.7.3.1 shows the schematic diagram of flow injection analysis methods.

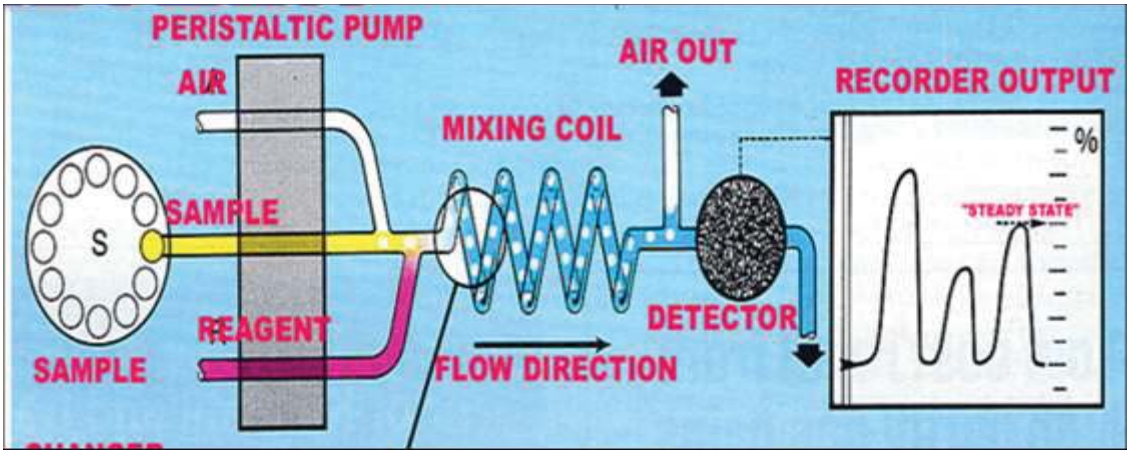

Figure 2.7.3.1: Technicon Auto-Analyzer working diagram [87]

An automated system for monitoring multi-parameter was developed based on the sequential injection analysis [88]. The nitrate was detected by reducing to nitrite using the Griess-Ilovsvay method. It provides the detection limit of 0.0022 mg N/L for nitrate. The detection limit is depends on the machine/setup. In our lab, it has a detection limit of only 0.25 mg/L.

As the next generation system of sequential injection analysis, the flow injection analysis is widely used for nitrate detection. A micro-potentiometric sensor is fabricated in a plasticized PVC membrane with bathophenanthroline nitrate to detect the nitrate concentration using flow injection analysis [89]. The developed sensor can detect the nitrate concentration in the range of 1.0×10^{-1} to 1.0×10^{-6} mol/L with the limitation of low detection at 0.05 µg/mL. It can be used for determination of nitrate

in fertilizers, industrial wastewaters and pharmaceuticals. Research on the detection of nitrate in seawater based on flow injection analysis is also studied. The accuracy and sensitivity of the measurement are improved by using dual-wavelength spectrophotometry at low nitrate concentrations [90]. The flow injection analysis is also used to detect the nitrate and nitrite simultaneously. Luminol is used as a chemiluminescent reaction to detect the nitrite after oxidation and the nitrate is detected by non-toxic photolytic UV reduction. From this research, the nitrate can be detected from the range of 8×10^{-9} to 1×10^{-3} M NO_3^- [91]. A conventional flow injection system can only use one or more reagents are pumped into the stream of the sample which minimizing reagent consumption [92] and support the online monitoring [93].

The advantages of flow injection analysis include [90-93]:

- The high accuracy and sensitivity for measurement
- Low use of the toxic materials
- Low the reagent consumption
- Supports online monitoring

However, there are some limitations of flow injection analysis method like:

- Very expensive equipment usually restricted to lab
- Limited life of mechanical part such as valve and pump
- Interference with other ions in the water sample

The spectrophotometric method is widely used to detect the NO_3-N by using specific chemical reagents. For example, sulfanilic acid is used as reagent and nitrate concentration is determined by diazotization [94, 95]. In other research, Vanadium has been used for the reduction of nitrate ions by acidic Griess reaction [96]. Other detection methods include amperometric based biosensor [97], colorimetric [98, 99] and so on.

2.8 Market Survey

Hach is well-known as suppliers of an analytical instrument and chemical reagents for the laboratory-based purpose, especially for water quality and other liquid

solutions. Take IntelliCal ISENO3181 Nitrate Ion Selective Electrode (ISE) for nitrate detection as an example, it is designed by the solid-state PVC membrane with epoxy and solid gel ion exchange eliminates the frequency of replacing membrane. The ISE can only be used periodically in the lab or field and is not suited to continual measurement. It can detect the nitrate-nitrogen concentration from 0.1 to 14000 mg/L. It has an integrated temperature sensor which can measure the temperature range from 0-50^{o}C. The price is at $2100. Hach Nitratax sc tank sensor is being used extensively internationally and in New Zealand. It uses the UV absorption measurement with reagent-free technique. There are three different models with the different detection range: 0.1 - 100 mg/L by Nitratax plus sc; 1.0 - 20 mg/L by Nitratax exo sc; and 0.5 - 20 mg/L by Nitratax clear sc. These models cost around $40k to 60k.

“S::can” is Austria-based Company which provides varied product range for water and environmental monitoring. All “s::can” instruments are operated followed by the “plug & measure” principle, so all of them are ready to use with pre-calibrated works. The “spectro::lyser” UV monitors can be used to NO_3-N detection. It is measured based on the UV-Vis spectrometry with the nitrate detection range from 0 - 20 mg/L. This instrument is also being used extensively internationally and in New Zealand. However, the whole set of the system is very expensive (around $60-70k).

Hanna Instruments is focused on developing electro-analytical instrumentation. They provide the products like nitrate portable/benchtop photometer and nitrate ion selective electrode. For example, Hanna HI96728 is a portable checker to detect nitrate in freshwater based on the colorimetric method. A special Tungsten lamp is used as the light source and silicon photocell with narrow band interference filter at the wavelength of 525 nm used to detect the light. It uses the cadmium reduction method to determine the nitrate-nitrogen concentration range from 0.0 to 30.0 mg/L. The price is at around $350 NZD.

Xylem is a world leader in providing compact instruments for water technology. It has a broad range of products under different brands. YSI is one of Xylem brand, which providing the environmental monitoring products. IQ SensorNet 182 is a modular water quality terminal which allowed connecting additional sensors such as 6884 Nitrate ISE sensor and it provides a continuously measurement of water quality parameters like pH, Dissolved oxygen, temperature, conductivity, ammonium, nitrate,

potassium, TOC (total organic carbon), COD (chemical oxygen demand), DOC (dissolved organic carbon share of TOC), BOD (biochemical oxygen demand) and SAC (spectral absorption coefficient). It has an easy-to-read digital display and wireless connection via radio transmission with a range of 100 meters. However, when it uses the nitrate sensor such as NitraLyt, the function of real-time monitoring is disabled. Another Xylem brand - WTW, it provides online measurement system - TresCon Analyzer which can monitor Ammonium, Nitrate, and Nitrite continuously. A continuous water sample supply with low solids contents is required for operating this system. For nitrate detection, the UV light is absorbed by the nitrate ions and determines the nitrate concentration at a wavelength of 254 nm.

ABB is a multinational corporation which mainly designs and manufactures power and automation products, including flow measurement, gas and liquid analyzer and environmental monitoring systems. For example, UV Nitrate Monitor AV455 provides a continuous analysis without chemical reagents. It can detect the nitrate concentration at the range of 0 to 100 mg/L at a wavelength of 220 nm. It requires low-maintenance and simple calibration with auto cleaning for the optical component. It uses de-nitrification as a process to reduce the nitrate concentrations for nitrate monitoring.

ASA Analytics Inc. specializes in the manufacture of the automatic chemical analysis system. ChemScan 6101 Process Analyzer can monitor Ammonia, Phosphate, Nitrate-Nitrite and Phosphate in surface water based on the UV-spectrometric method. The light is absorbed by nitrate ions and into 256 wavelengths of 200 to 450 nm. The detection range of nitrate is from 0.5 - 20 mg/L.

Dionex Ion Chromatography with a UV/Visible absorbance detector is one product from Thermo Scientific. It is used to detect the nitrate and nitrite in drinking water with the detection limit of 10 ppb for nitrite and 15 ppb for nitrate. It is free from most ionic interferences due to the specificity of UV detection. The eluent is prepared by 1.8 mM sodium carbonate and 1.7 mM sodium bicarbonate for 1 L of eluent, diluting 10 mL of eluent concentration into 1000 mL of deionized water.

Table 2.8.1: Summary of Commercial Nitrate Detection Products

Model	Method of Detection	Detection range (Nitrate)
IntelliCal ISENO3181	Ion Selective Electrode	0.1 to 14000 mg/L
Nitratax plus sc	UV-photometric	0.1 to 100 mg/L
S::can	UV-spectrometric	0 - 20 mg/L
Hanna HI96728	Colorimetric	0 to 30 mg/L
YSI 6884 Nitrate Sensor	Ion Selective Electrode	0.0 - 200.0 mg/L
TresCon Analyzer	UV-spectrophotometric	0.1 - 60 mg/L
UV Nitrate Monitor AV455	Ion Exchange	0 to 100 mg/L
ChemScan 6101 Process Analyzer	UV-spectrometric	0.5 - 20 mg/L
Dionex	Ion Chromatography	Detection limit: 10 ppb

Table 2.8.1 summarizes the commercially available nitrate detection product/system in the market. Most of these products are used for the laboratory-based measurement. Hanna HI 96728 is a portable device, but it still needs to collect the sample and require the reagent for measurement of nitrate. The YSI IQ SensorNet 182 terminal provides the continuous monitoring, but it calls for a additional sensor for nitrate measurement.

Chapter 3: Design and Development of Nitrate Sensing System

3.1 Introduction

The objective of this chapter is to discuss the design and development of a low-cost sensing system for nitrate detection in natural waters using the interdigital sensor. The whole system consisted of a hardware circuit interfaced to microcontroller and data collection through wireless communication based on ZigBee protocol. It also included the microcontroller programming for data acquisition and control of pumps and the computer programming for Graphic User Interface (GUI), storage and analysis of data.

3.2 System Overview

The sensing system was developed for in-situ measurement of nitrate concentration. The developed system consists of a sensor and power supply, the signal processing circuit and control circuit, microcontroller. The functional block diagram of the system is illustrated in Figure 3.2.1.

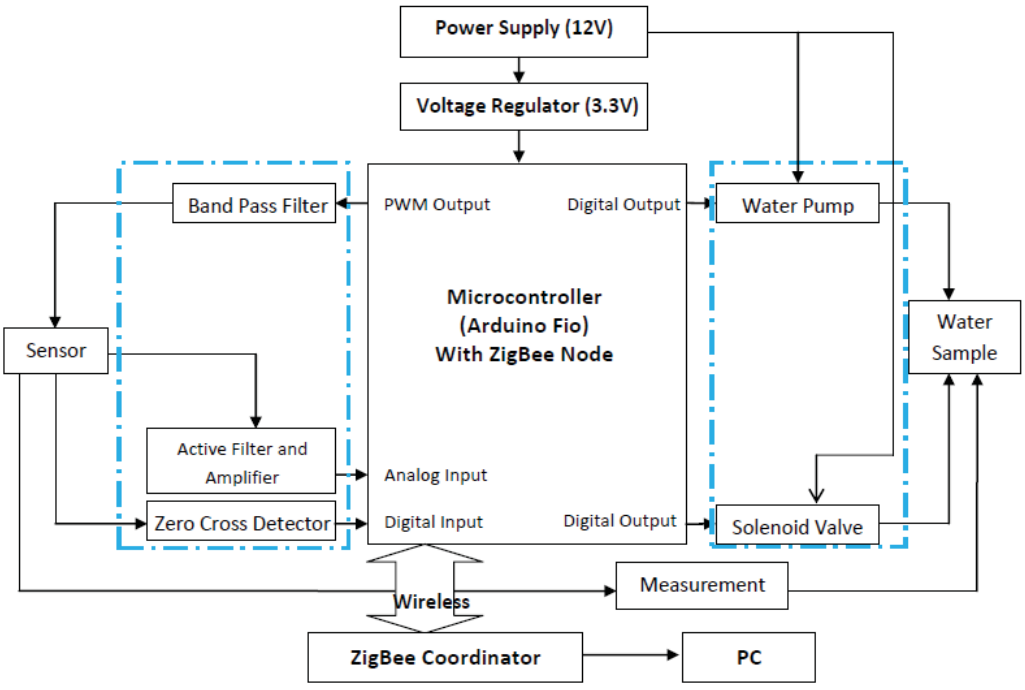

Figure 3.2.1: Functional Block Diagram of the Sensing System

The solar panel with the chargeable battery was used to supply the power to all components such as LM324, LM339, microcontroller, water pump with motor and solenoid valve. The water pump was used to take the water sample into the measurement container and to discharge the water sample. The solenoid valve was used to drain off the water sample from the container on the field.

The microcontroller generated the PWM waveform which was filtered to get the excitation sinusoidal signal (input signal) at a frequency of 120 Hz (frequency selection was based on the experimental results). This excitation signal was applied to an interdigital sensor and output was fed into the signal smoothing circuit to eliminate the noise and amplify the signal. Both the input and output signals were fed into zero cross detector to get the phase difference between them and feed back to the microcontroller. The microcontroller also controlled the time interval to switch on/off the water pump and valve. All measured data were communicated to the main computer based on ZigBee protocol.

3.3 Interfacing to Microcontroller

The microcontroller board used in the project was Arduino Fio (Figure 3.3.1(a)) which is based on the ATmega328P to perform the signal generation, data acquisition and switch control of water pump and solenoid valve.

(a) Arduino Fio Board

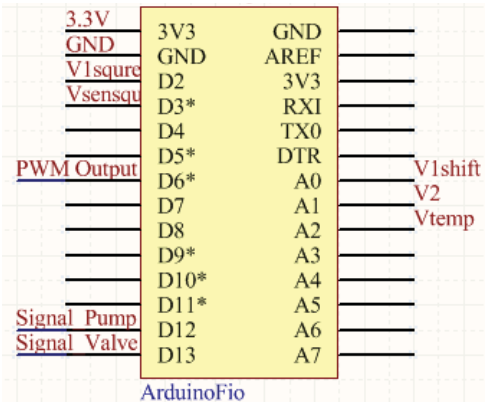

(b) Arduino Fio Pins Mapping

Figure 3.3.1: Arduino Fio Board

Arduino Fio operates at 3.3 volts, and it has 14 digital pins and 8 analog pins which are used as input or outputs. It has two external interrupts pins (D2 and D3) and specific pins (D3, D5, D6, D9, D10, D11) for PWM output and controller by corresponding timers. Figure 3.3.1 (b) indicates the pins mapping between the

hardware circuit and microcontroller board. The summary of ATmega328P is provided in Table 3.3.1.

Table 3.3.1: Summary of ATmega328P

Operating Voltage	3.3V
Input Voltage	3.35 - 12V
Input Voltage for Charge	3.7 - 7 V
Digital I/O Pins	14 (of which 6 provide PWM output)
Analog Input Pins	8
DC Current per I/O Pin	40 mA
Flash Memory	32 KB (of which 2KB used by bootloader)
SRAM	2 KB
EEPROM	1 KB
Clock Speed	8 MHz
Width	28 mm
Length	65 mm
Weight	9 g
PWM output pins and Timers	Timer 0: Pins 5 and 6 Timer 1: Pins 9 and 10 Timer 2: Pins 3 and 11

The objective of the interfacing sensor to the microcontroller is to measure the impedance of the sensor. In order to measure both the resistance and reactive part of the impedance, the input voltage (V1) and the voltage across the series resistance (V2) as shown in figure 3.3.2 were interfaced to the microcontroller via ADC inputs A0 and A1 respectively. To measure the phase difference between these two signals, the sinusoidal signals were first converted to square wave using zero-crossing

detectors (ZCD) and the waveforms from ZCD and then fed into digital inputs D2 and D3 respectively. With the help of the microcontroller, the time difference was measured and converted into phase angle in degree.

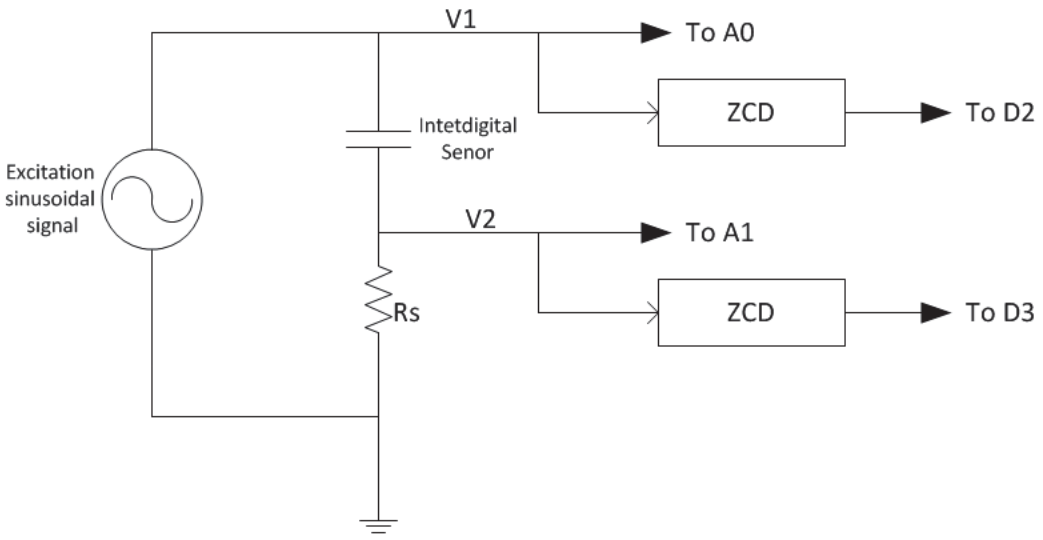

Figure 3.3.2: The interfacing of the sensor to the microcontroller

Figure 3.3.3 shows the picture of Printed Circuit Board (PCB) that involves voltage regulator, TLC555IP, the microcontroller, band-pass filter, LM324, LM338, MOSFET for control of pump and valve.

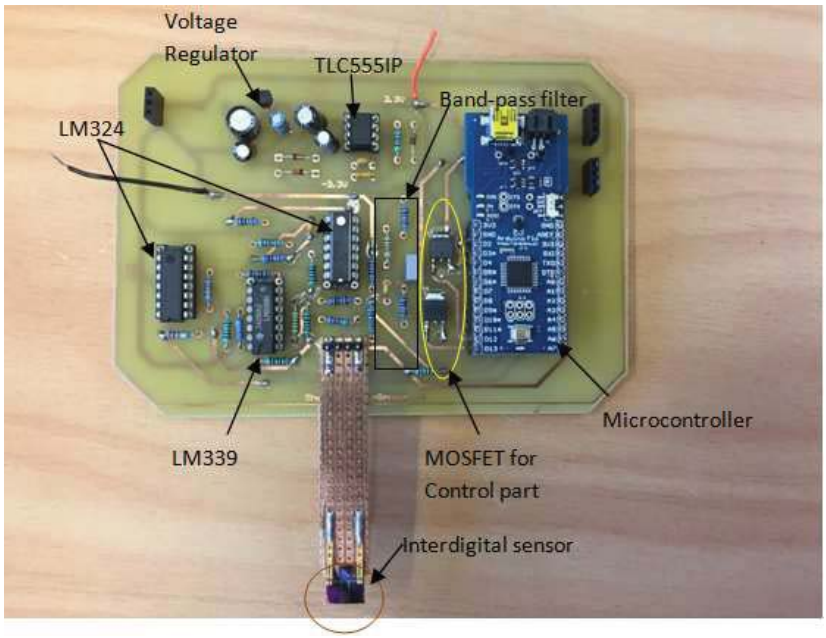

Figure 3.3.3: Picture of the system prototype based on the microcontroller

The sinusoidal signal was produced using PWM output and a band-pass filter. Pin 6 of the microcontroller was used to generate the PWM output which was passed through a band-pass filter to reduce the noise and produce a smooth sinusoidal wave. The sinusoidal wave was used as the exciting source of the sensor.

The sensor was not continuously dipped into the water as the water was pumped into a container at an interval of every 15 minutes. When the measurement was completed, the water was discharged from the container. The pumping in and out of the water was done through the pump and solenoid valve which were controlled by digital pin D12 and D13 respectively.

Arduino Fio can communicate with a computer, another Arduino or other microcontroller [100]. The FTDI Basic was used for serial communication between Arduino Fio and computer which the Arduino software provided. The serial monitor showed the textual data sent from the microcontroller board. One of the advantages of using Arduino Fio is that there is an integrated socket for ZigBee (XBee). Digital pins D0 (RXI) and D1 (TXO) are used for serial communication between microcontroller and XBee. They receive and transmit TTL serial data and internally connect with DOUT and DIN pins respectively of Xbee (as shown in Figure 3.3.4).

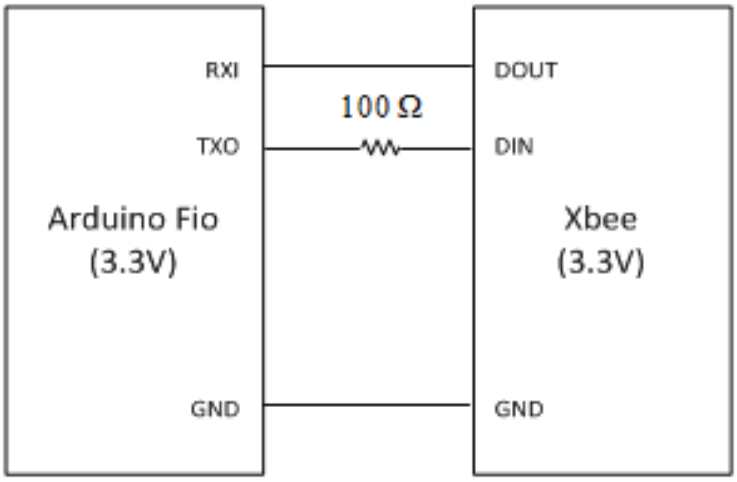

Figure 3.3.4: Serial Communication by Arduino Fio with XBee

3.4 Power Supply Circuits

The solar panel with a rechargeable battery will be the main power source for the system but one 12-volt rechargeable battery was employed for the off-site experiment. The microcontroller, operational amplifier (LM324) and differential

comparator (LM339) were required to supply power at a voltage level at 3.3V which was necessary to reduce the voltage down to 3.3V by using a voltage regulator.

There are different types of voltage regulators used for different purposes. The linear voltage regulator is the easiest type to use, and it can be divided into fixed and adjustable value voltage regulator. The advantages of linear regulator include low noise, low output voltage ripple, fast transient response and low cost but the excessive power dissipation is a major limitation [101]. The L78L33 is a linear fixed voltage regulator with the output voltage of 3.3V and output current up to 100mA which is sufficient for those components so it was employed for the experiment. Figure 3.4.1 shows the circuit for the voltage down from 12V to 3.3V by using L78L33 combined with a diode and capacitors. The diode (D1) was used to nullify the inverse voltage in the circuit and allow the current to flow in one direction. Capacitors (C3, C4, and C5) were used as decoupling capacitors to reduce the effect of noise.

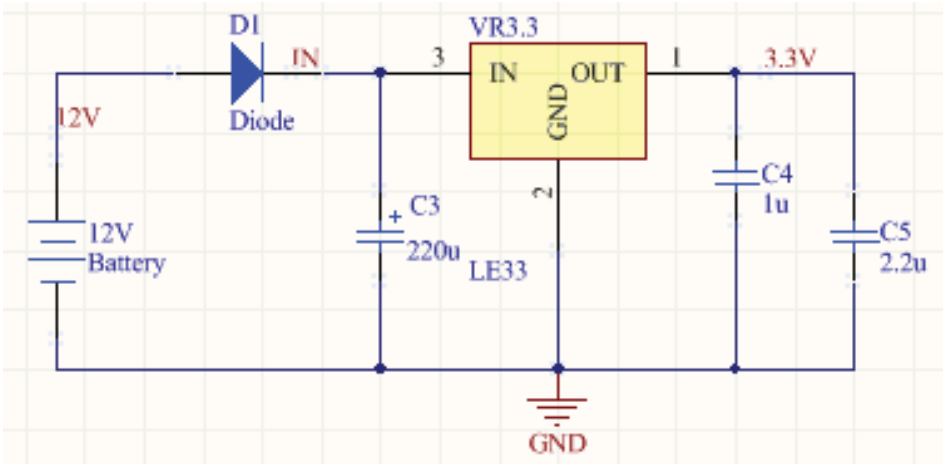

Figure 3.4.1: Circuit for 3.3V voltage regulator application

On the other hand, the switch-mode power supply (SMPS) is also widely used for the application which requires high efficiency, high power density and low power dissipation [101]. SMPS is able to generate not only step-down output voltage but also step-up and reverse output voltage. The input signal applied to the sensor requires both the positive and negative magnitude of the alternating source, so the TLC555IP is employed to provide the negative power supply. The 555 IC is used in a variety of electronic applications such as a timer, pulse generation, and oscillators.

Figure 3.4.2 shows the circuit that converted the positive input voltage to negative output voltage by using TCL55IP and other essential components. R17 is the pull-up resistor which was connected between VDD and discharging signal to make sure that the discharging signal is in either high or low state. R17, R18 and C6 made up a loop to generate the oscillatory output signal through charging and discharging of C6. When the output signal is high, C8 was charging, and D2 conducted the current to the ground but D3 was cut off. When the output signal went to low, the voltage across C8 went to zero as well. In this case, the polarity of D3 was changed so it could conduct the current and C9 started charging. Due to this opposite polarity, it generated the negative voltage.

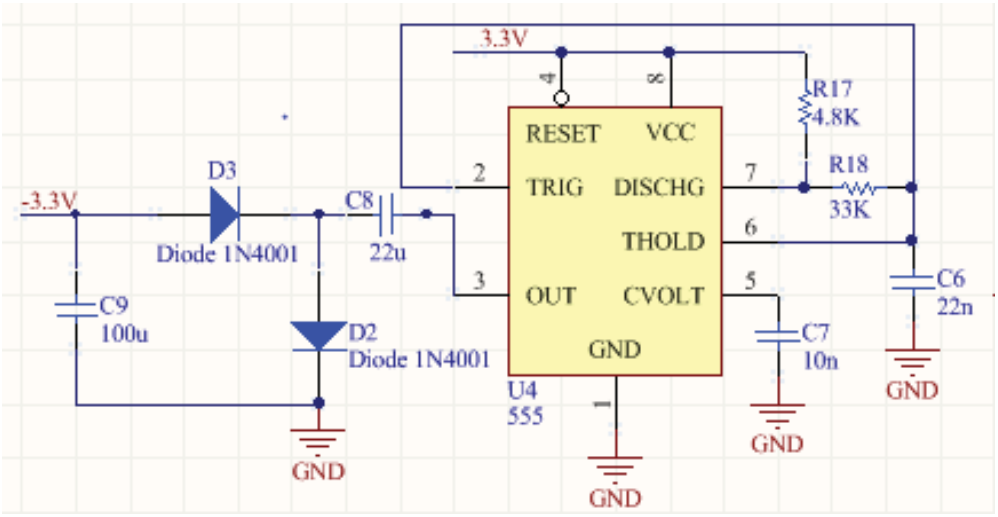

Figure 3.4.2: Use of 555 to generate negative voltage

3.5 Generation of Excitation Supply of the Sensor

The direct digital synthesis (DDS) method is popularly used to generate wanted output at precise frequencies. DDS is implemented by breaking an analog waveform into discrete digital points which are stored in an array as a lookup table (LUT), and the use of phase accumulator is done to calculate a phase angle for LUT and then generate the digital value at different amplitude [102]. Figure 3.5.1 shows the microcontroller code that stored the hexadecimal value of sine waveform in the array as LUT.

```
//---------PROGMEM is a variable modifier, store data in flash (program) memory instead of SRAM.
const unsigned char sine[] PROGMEM={
  0x80, 0x83, 0x86, 0x89, 0x8c, 0x8f, 0x92, 0x95, 0x98, 0x9c, 0x9f, 0xa2, 0xa5, 0xa8, 0xab, 0xae,
  0xb0, 0xb3, 0xb6, 0xb9, 0xbc, 0xbf, 0xc1, 0xc4, 0xc7, 0xc9, 0xcc, 0xce, 0xd1, 0xd3, 0xd5, 0xd8,
  0xda, 0xdc, 0xde, 0xe0, 0xe2, 0xe4, 0xe6, 0xe8, 0xea, 0xec, 0xed, 0xef, 0xf0, 0xf2, 0xf3, 0xf5,
  0xf6, 0xf7, 0xf8, 0xf9, 0xfa, 0xfb, 0xfc, 0xfc, 0xfd, 0xfe, 0xfe, 0xff, 0xff, 0xff, 0xff, 0xff,
  0xff, 0xff, 0xff, 0xff, 0xff, 0xff, 0xfe, 0xfe, 0xfd, 0xfc, 0xfc, 0xfb, 0xfa, 0xf9, 0xf8, 0xf7,
  0xf6, 0xf5, 0xf3, 0xf2, 0xf0, 0xef, 0xed, 0xec, 0xea, 0xe8, 0xe6, 0xe4, 0xe2, 0xe0, 0xde, 0xdc,
  0xda, 0xd8, 0xd5, 0xd3, 0xd1, 0xce, 0xcc, 0xc9, 0xc7, 0xc4, 0xc1, 0xbf, 0xbc, 0xb9, 0xb6, 0xb3,
  0xb0, 0xae, 0xab, 0xa8, 0xa5, 0xa2, 0x9f, 0x9c, 0x98, 0x95, 0x92, 0x8f, 0x8c, 0x89, 0x86, 0x83,
  0x80, 0x7c, 0x79, 0x76, 0x73, 0x70, 0x6d, 0x6a, 0x67, 0x63, 0x60, 0x5d, 0x5a, 0x57, 0x54, 0x51,
  0x4f, 0x4c, 0x49, 0x46, 0x43, 0x40, 0x3e, 0x3b, 0x38, 0x36, 0x33, 0x31, 0x2e, 0x2c, 0x2a, 0x27,
  0x25, 0x23, 0x21, 0x1f, 0x1d, 0x1b, 0x19, 0x17, 0x15, 0x13, 0x12, 0x10, 0x0f, 0x0d, 0x0c, 0x0a,
  0x09, 0x08, 0x07, 0x06, 0x05, 0x04, 0x03, 0x03, 0x02, 0x01, 0x01, 0x00, 0x00, 0x00, 0x00, 0x00,
  0x00, 0x00, 0x00, 0x00, 0x00, 0x00, 0x01, 0x01, 0x02, 0x03, 0x03, 0x04, 0x05, 0x06, 0x07, 0x08,
  0x09, 0x0a, 0x0c, 0x0d, 0x0f, 0x10, 0x12, 0x13, 0x15, 0x17, 0x19, 0x1b, 0x1d, 0x1f, 0x21, 0x23,
  0x25, 0x27, 0x2a, 0x2c, 0x2e, 0x31, 0x33, 0x36, 0x38, 0x3b, 0x3e, 0x40, 0x43, 0x46, 0x49, 0x4c,
  0x4f, 0x51, 0x54, 0x57, 0x5a, 0x5d, 0x60, 0x63, 0x67, 0x6a, 0x6d, 0x70, 0x73, 0x76, 0x79, 0x7c
};
```

Figure 3.5.1: Arrays for the hexadecimal of sinusoidal waveform

In order to convert the different phase-related digital value to analog output, the digital to analog converter (DAC) is usually required but the Arduino Fio does not have embedded DAC. Therefore, it is necessary to find other solution. There are some ways to build a DAC as a solution such as 10-bits DAC which uses a circuit with an operational amplifier, R-2R ladder DAC, PWM combined with an analog filter as DAC and external DAC chip [103]. The advantage and disadvantage of other solutions are shown in table 3.5.1.

Table 3.5.1: Advantages and disadvantages of different DAC methods

Methods	Advantages	Disadvantages
10-bits DAC	-Easy to make	-Requirement of different precise component value -Long settling time
R-2R DAC	-Requirement of only two types of resistor values -Low cost -Easy to make	-Low conversion rate -Big size
PWM as DAC	-Simple -Nice and smooth output signal -Low power consumption	-Working at low frequency (less than 1 KHz)
External DAC	-High accuracy -Short settling time	-Limited frequency -Cost

To achieve a specified frequency at 120 Hz (selected based on the experiment result), for generating a smooth sinusoidal input signal and minimum board size, the use of PWM combined with a bandpass filter as DAC was a good option.

Arduino Fio uses ATmega328 chip that provides the 6 pins for PWM outputs which is controlled by specific timers. There are only 3 timers and each has 2 output compare registers (OCR) used to control the PWM output pins. For example, OCR0A and OCR0B (output compare registers of Timer 0) are used to control Pin 6 and Pin 5 respectively. There are two PWM modes in Atmega328: Fast PWM and Phase-correct PWM mode. The timer repeatedly counts from bottom to top value in fast PWM mode. In contrast, the timer counts from bottom to top and then from top to bottom repeatedly in phase correct PWM mode [104]. In this project, the output compare pin (Pin 6) of Timer0 was set as output at fast PWM mode and the output compare register (OCR0A) was used to load different pulse width by reading the value of the array (as shown in figure 3.5.1). These 256 (8 bit) points gave a compromise between resolution and frequency, as resolution increased, max frequency achievable decreased. With the full resolution of 255, the maximum PWM frequency was reached [105]. The PWM base frequency was calculated by equation 3.5.1:

$$PWM\ base\ frequency = \frac{System\ clock / prescaler}{2^n} \qquad \text{(Equ. 3.5.1)}$$

Where:

- System clock = 8 MHz
- Prescaler = 1
- n: the bit number of the timer; here is 8

Therefore, the PWM base frequency was 31.25 KHz, which means that the Timer 0 was repeated 31250 times per second. To generate different analog levels, the duty cycle and the pulse width of the digital signal was changed. This was implemented by reloading the whole periodic array using interrupt routine service (ISR). The Timer 1 here was employed to execute the ISR at desired frequency. Figure 3.5.2 shows the compare match output register of Timer 0 goes through the sine waveform table periodically based on the Timer 1 ISR.

```
ISR (TIMER1_COMPA_vect)
{
  if (sample >= 256){
    sample =0;
  }
  else{
   OCR0A = pgm_read_byte(&sine[sample]); //To generate sine wave
  }
  sample++;
}
```

Figure 3.5.2: Timer 1 ISR code

The desired frequency was calculated by equation 3.5.2:

$$Desired\ frequency * sample\ number = \frac{System\ clock}{Prescaler * (Compare\ match\ output\ register + 1)} \quad \text{(Equ. 3.5.2)}$$

Here, using the compare match output register (OCR1A) to reload the sine wave so rearranging the formula into the OCR1A as shown in equation 3.5.3:

$$OCR1A = \frac{System\ clock}{prescaler * desired\ frequency * sample\ number} - 1 \quad \text{(Equ. 3.5.3)}$$

Where:

- desired frequency is 120 Hz
- sample number is 256

Therefore, OCR1A = 8000000/30720 - 1 = 259. Figure 3.5.3 illustrates that the analog amplitude increases with the increase in duty cycle and pulse width.

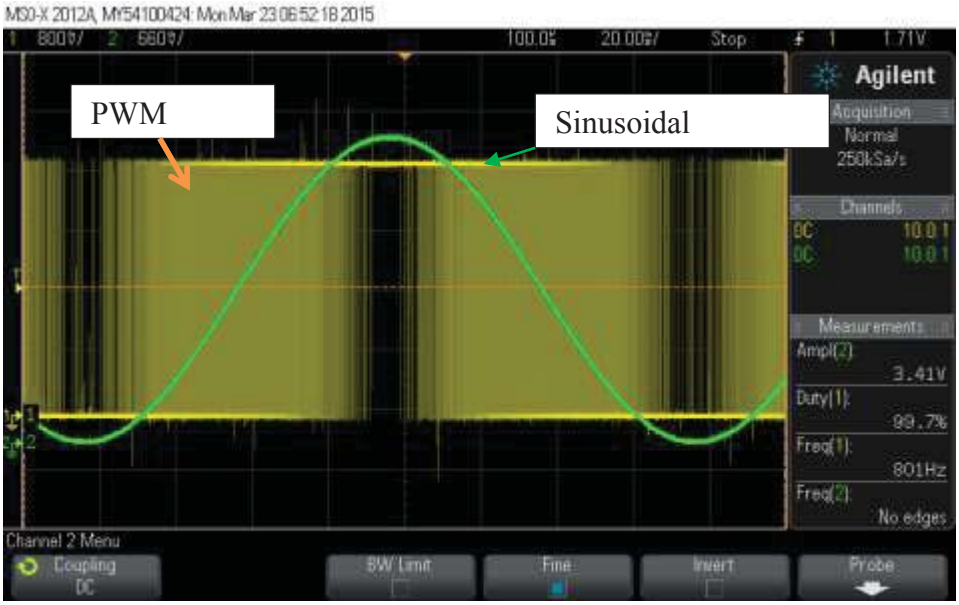

Figure 3.5.3: PWM output

In order to generate the smooth sinewave, the band pass filter (Figure 3.5.4) was used only to pass the frequency range between 106 Hz and 338 Hz. The cut-off frequency (f_c) was calculated based on the value of capacitor and resistor, shown in equation 3.5.4:

$$f_c = \frac{1}{2\pi RC} \qquad \text{(Equ. 3.5.4)}$$

The band pass filter was combined with a high pass filter (C1 and R1) and a low pass filter (R2 and C2). The capacitor C1 connected to PWM output removed the DC offset from this input signal and combined with R1 only allowed the frequency (f_H) above 106 Hz to pass. The capacitor (C1) value was computed based on rearranged equation 3.5.5 using the resistor at a value of 10 KΩ:

$$C1 = \frac{1}{2\pi R f_H} = \frac{1}{2 * \pi * 10000 * 106} = 150\ nF \qquad \text{(Equ. 3.5.5)}$$

The low pass filter part consisted of R2 and C2, assuming the R2 was also fixed at value of 10 KΩ and cut-off frequency (f_L) is at 338 Hz, the C2 value was calculated using equation 3.5.6:

$$C2 = \frac{1}{2\pi R f_L} = \frac{1}{2 * \pi * 10000 * 338} = 47\ nF \qquad \text{(Equ. 3.5.6)}$$

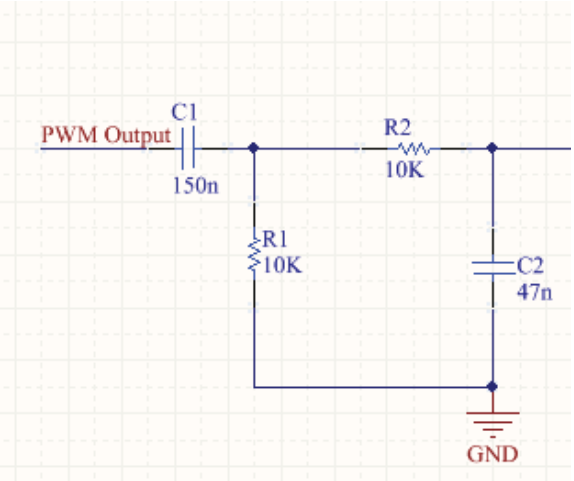

Figure 3.5.4: Bandpass filter for generating smooth sinusoidal waveform

After filtering, the smooth sinusoidal waveform which had positive and negative analog amplitude was generated as shown in Figure 3.5.5 with a frequency of 120 Hz.

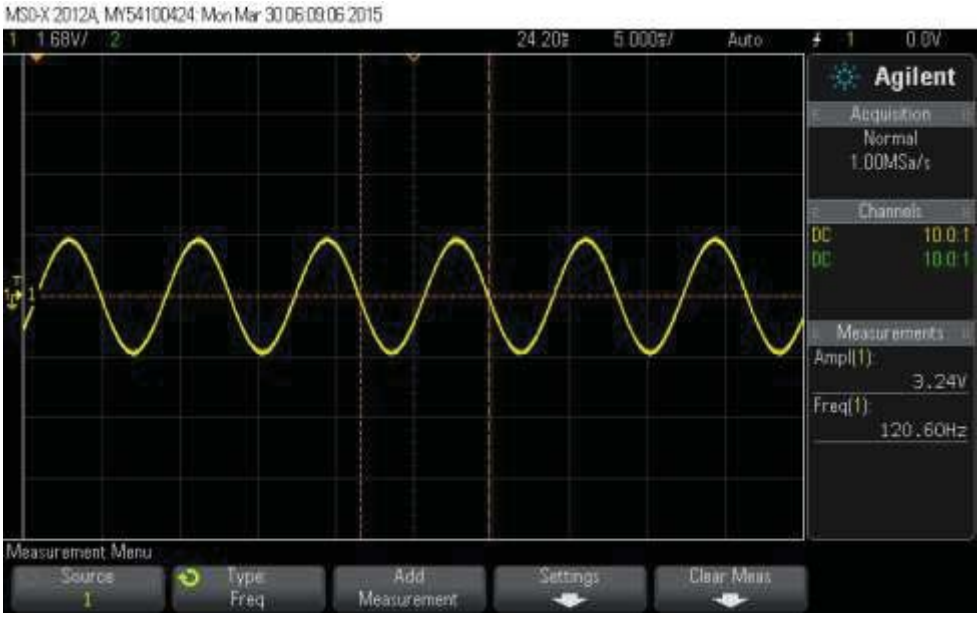

Figure 3.5.5: Smooth sinusoidal waveform generated by combined PWM output and band pass filter

The amplitude of generated input signal was at 3.24V. A small excitation signal usually applied for the electrochemical impedance spectroscopy (EIS) technique [24]. Usually, EIS technique needs a small signal to operate the sensor in a pseudo-linear region. Figure 3.5.6 illustrates how pseudo-linear was done with the EIS technique. When a small signal was applied to this cell, the current changed linearly with the change in voltage.

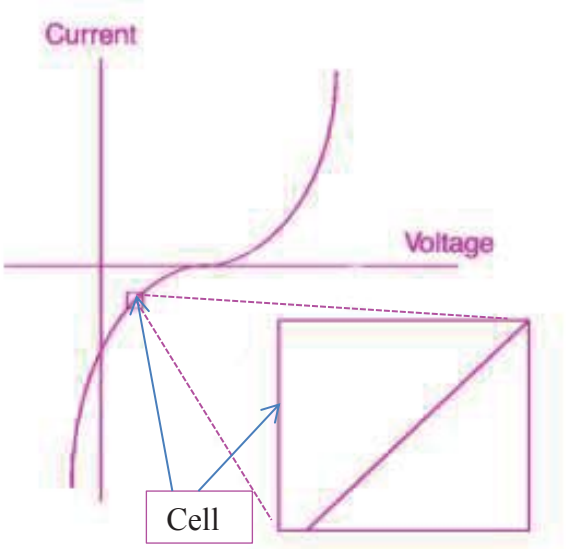

Figure 3.5.6: Pseudo-linearity between current and voltage [24]

Therefore, the applied voltage to the sensor was reduced by adding a resistor, R3 (8.2 KΩ) after the band-pass filter, as shown in figure 3.5.7, to keep the linear relationship between the current and voltage. The equivalent resistance of the filter along with R3 formed a potential divider and reduced the voltage to 860 mV which was suitable fo the operation. One amplifier served as the unity gain buffer or voltage follower to reduce any current drawn from the input voltage, and it also played a role in the impedance matching that minimizing the load effect.

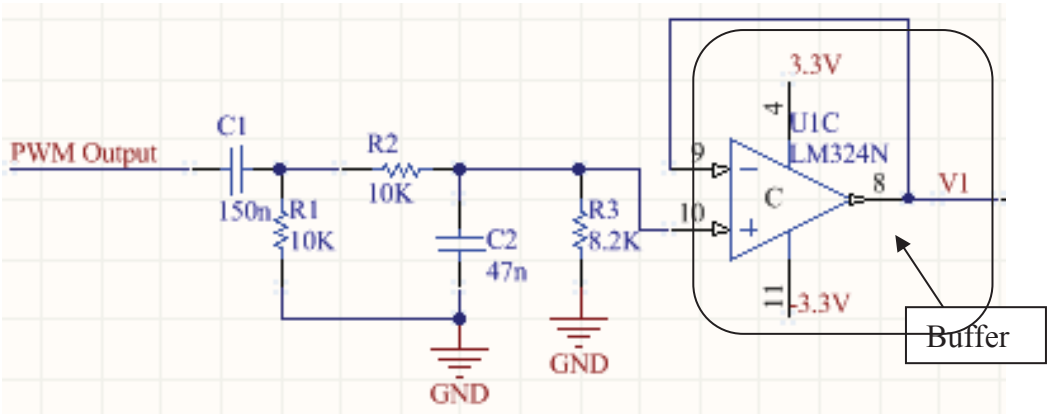

Figure 3.5.7: Circuit for generated input signal fed into sensor

Figure 3.5.8 shows the reduced excitation voltage (V1) after potential divider and buffer was added which was applied to the sensor.

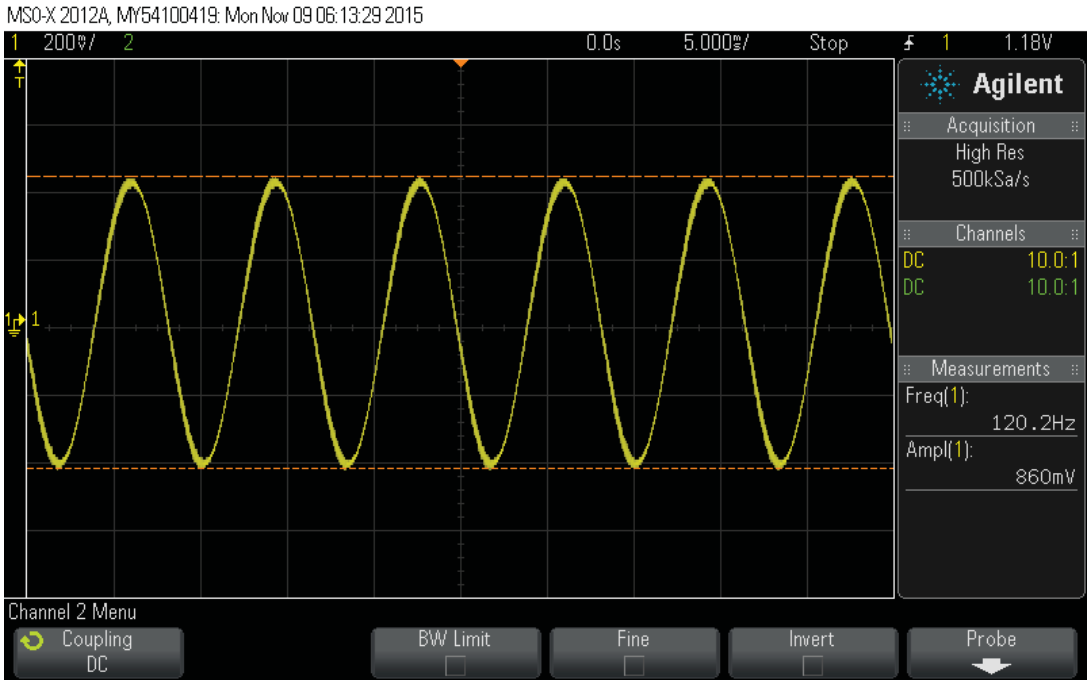

Figure 3.5.8: Input (excitation) signal applied to sensor after voltage divider

3.6 Measurement of the Sensing Voltage

To measure the impedance of the sensor, the voltage applied to the sensor and the current through the sensor was needed to be measured by the system. The excitation voltage to the sensor is bipolar in nature, so it could not be fed directly to the microcontroller. To avoid the negative excitation voltage, a level shift-up circuit is used as shown in figure 3.6.1. Figure 3.6.2 shows the excitation signal before and after level shift.

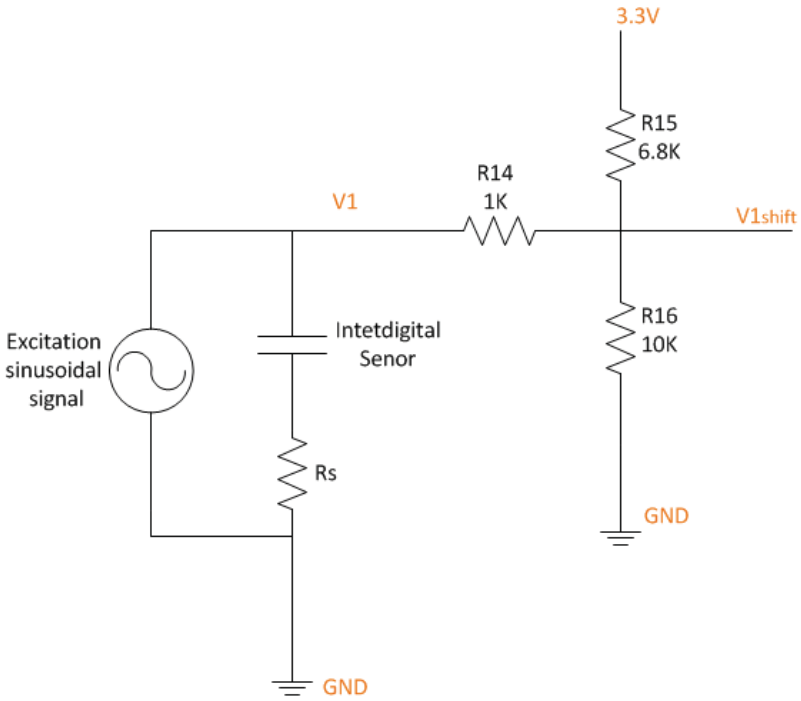

Figure 3.6.1: Circuit for level shifting

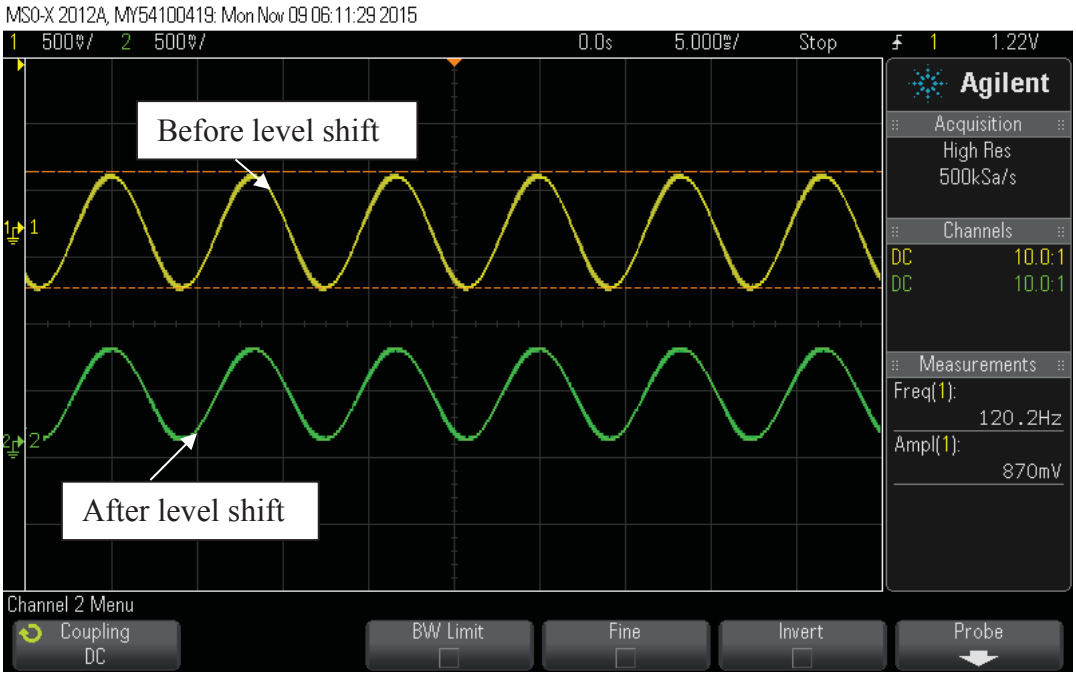

Figure 3.6.2: Excitation signal after shifting up

A resistor, Rs was connected to the sensor in series to determine current flowing through the sensor as shown in figure 3.6.1. The value of Rs was significantly small so that the effect of it was negligible.

Based on the Ohm's law, the current (I_s) flows through the sensor was calculated by equation 3.6.1:

$$I_s = \frac{V_{in}}{Z} \qquad \text{(Equ. 3.6.1)}$$

Where:

- V_{in}: the voltage applied to the sensor
- Z: the total impedance of the circuit

Therefore, the voltage across the sensor V_s is rearranged into equation 3.6.2:

$$V_s = I_s * R_s = \frac{V_{in}}{Z} * R_s \qquad \text{(Equ. 3.6.2)}$$

Where:

- R_s: series resistance, used for measurement of sensing voltage

In figure 3.6.3, another buffer had been connected to the output of V_s in order to reduce the signal reflection from the load and transfer max power from the input. In addition, the active low-pass filter was employed in order to reduce the noise and amplify the signal with a gain of 11 by using R20 and R21.

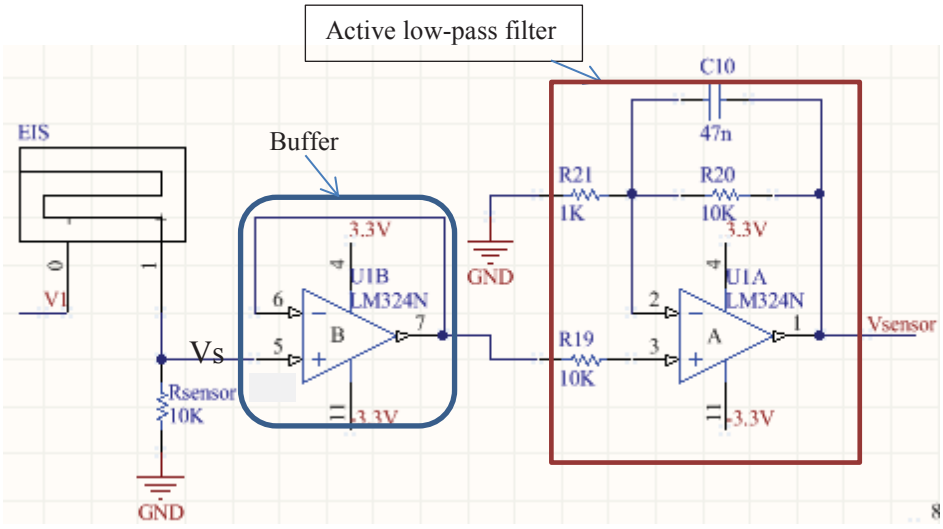

Figure 3.6.3: Circuit for processing the sensing voltage

The reason to use an active low-pass filter was that the amplitude of the output signal in pass low-pass filter is lower than the amplitude of its input signal [106] and the gain is less than 1. In addition, the voltage across the sensor (V_s) is slight (the peak

voltage is around 80 mV) because the total impedance of the sensor was very larger which resulted in a very small current going through the circuit. The resistor value was picked at any value and gain was changed but the value of 10 KΩ and 1 KΩ is a standard resistor value which is available. However, it resulted in the distortion of the sinusoidal waveform as shown in figure 3.6.4 which affected the accurate measurement of V_s.

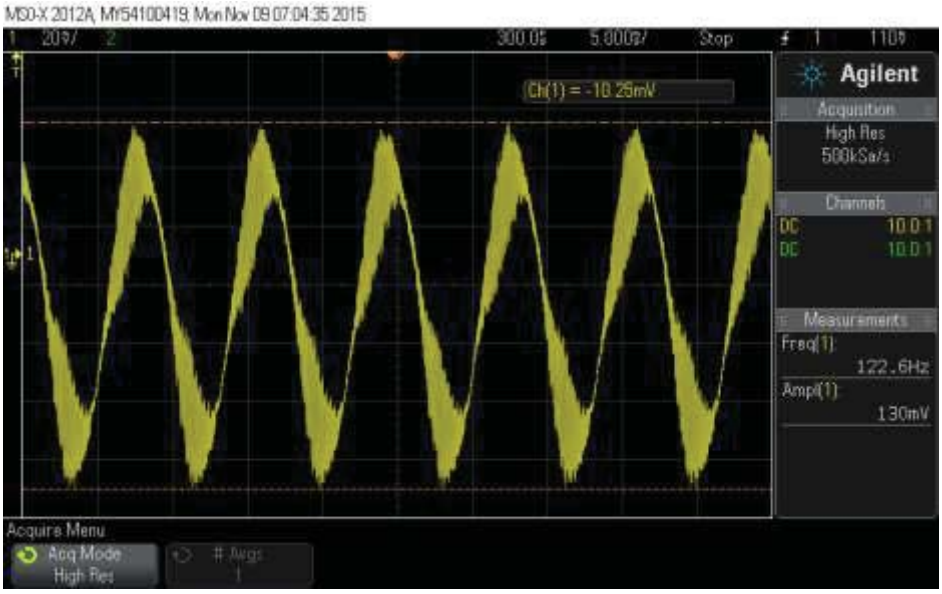

Figure 3.6.4: Distorted sensing voltage output

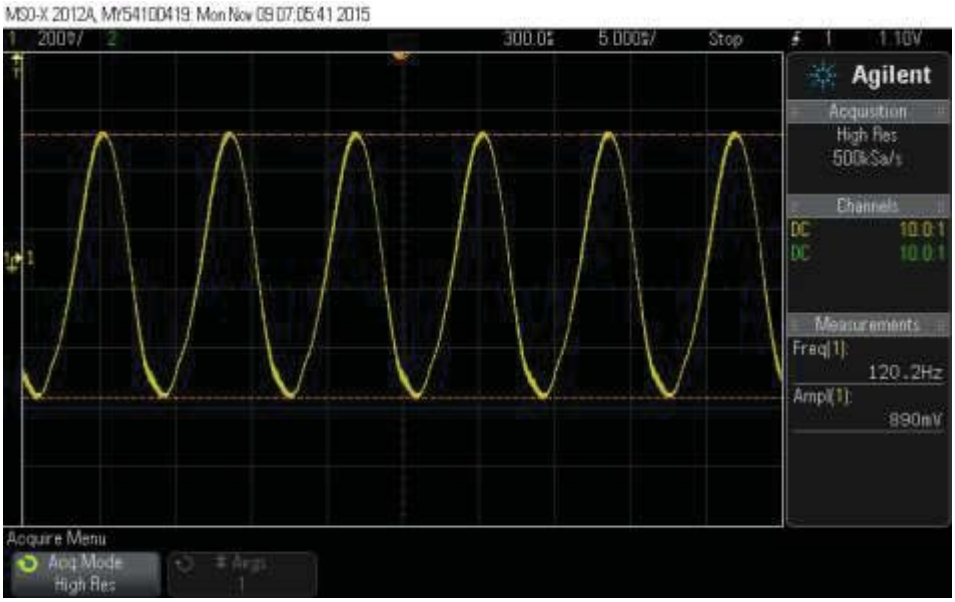

Figure 3.6.5: Sensing voltage (V_{sensor}) after filtering and amplifying

Therefore, using the active low-pass filter with gain control reduced the noise across the signal and amplified the V_s. Figure 3.6.5 showed the amplified and filtered sinusoidal signal across the sensor (V_{sensor}).

Rearranging the equation (8) into the term of Z, this was computed by equation 3.6.3:

$$Z = \frac{V_{in}}{I_s} = \frac{V_{in}}{V_s} * R_s \qquad \text{(Equ. 3.6.3)}$$

The voltage applied to the sensor (V_{in}) and the voltage across the sensor (V_s) were measured and Z was calculated by the microcontroller. Series Resistor (R_s) was given at 10 KΩ (Figure 3.6.4 R_s).

Figure 3.6.6 shows the precision rectifier circuit which was composed of two operational amplifiers for reducing the voltage loss because the V_{sensor} is very small. The output of voltage (V_{sensor}) from the sensor was full sine wave which was fed into the first operational amplifier. When $V_{sensor} > 0$, only positive half wave (V_{pos}) was generated from the first op-amp (Figure 3.6.7) and $V_{pos} = V_{sensor}/2$. The second op-amp worked as a subtractor, $V_{pos} = V_{full}/2$ (where $V_{sensor} = V_{full}$) when $V_{sensor} > 0$, $V_{inmicro} = V_{full} - V_{pos} = V_{full}/2$; when $V_{sensor} < 0$, $V_{inmicro} = 0-(-V_{full}) = V_{pos}$; Therefore the output of $V_{inmicro}$ was a full wave rectified wave (Figure 3.6.8). The $V_{inmicro}$ was then fed into the analogue input pin of the microcontroller.

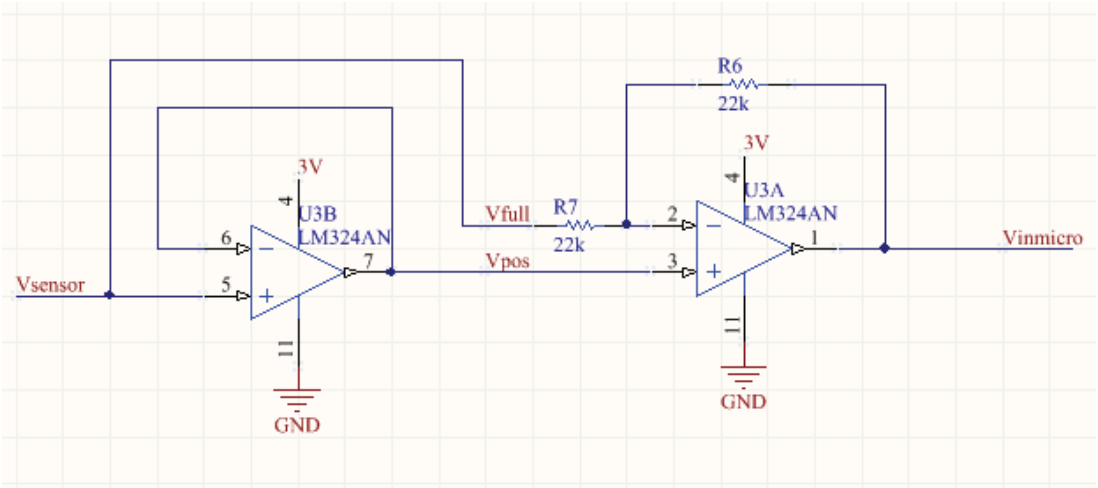

Figure 3.6.6: Precision rectifier circuit

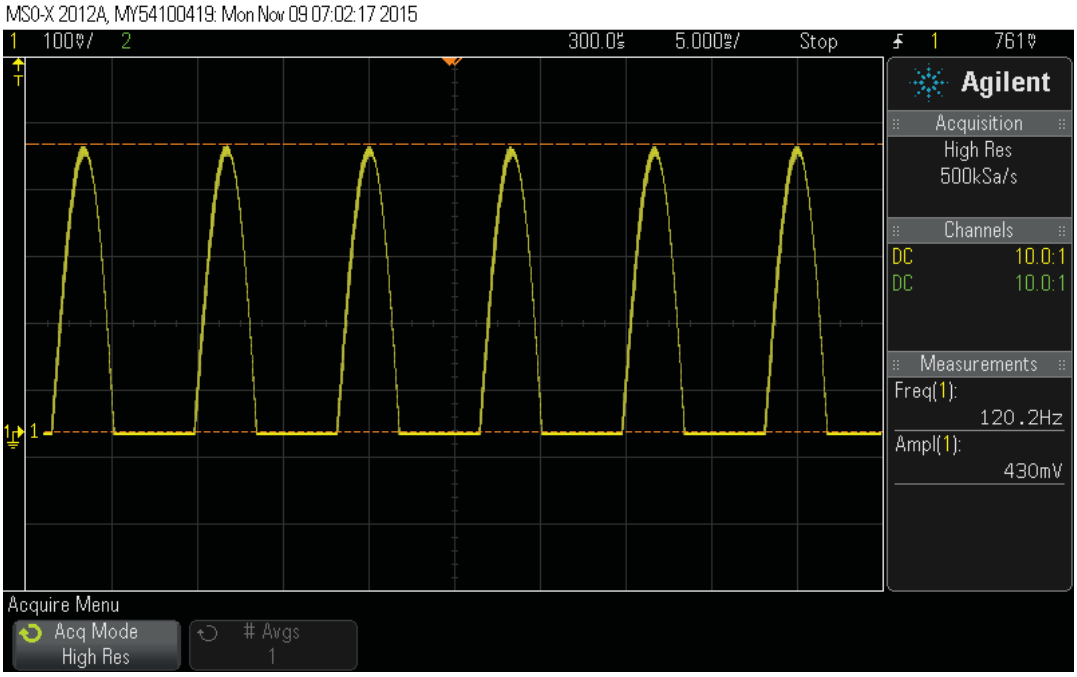

Figure 3.6.7: Output signal of half wave rectifier from V_{pos}

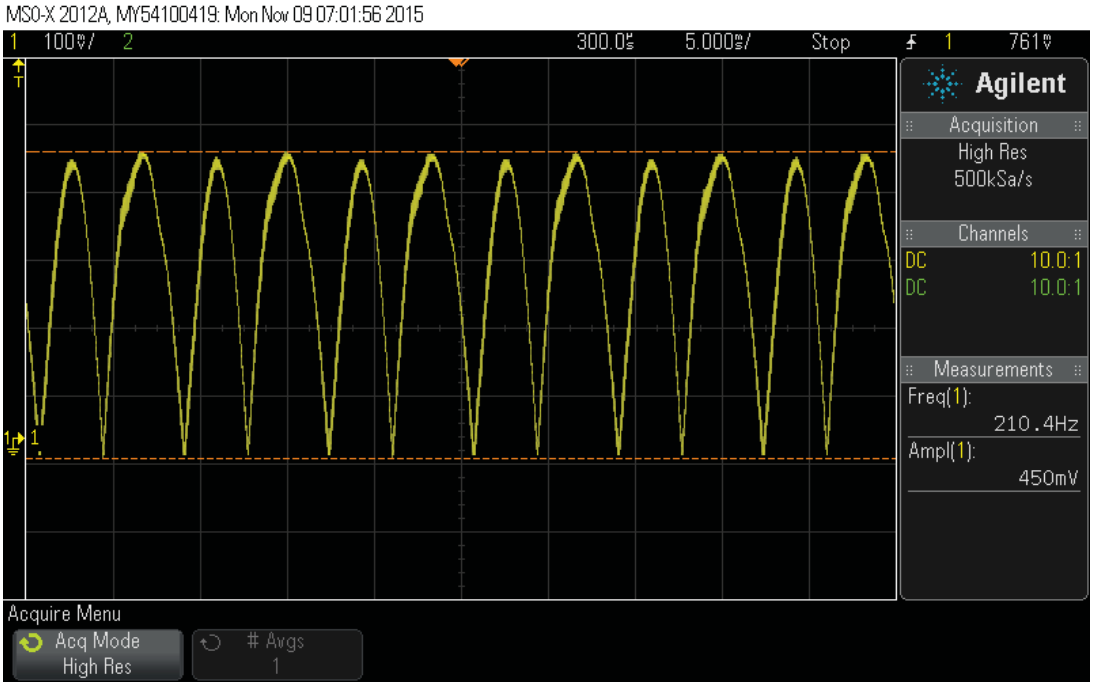

Figure 3.6.8: Output signal of full wave rectifier from $V_{inmicro}$

The voltage applied to the sensor (V_{in}) and the voltage across the sensor (V_s) were all fed into microcontroller ADC input pins for calculation of total impedance. The compare output B register of Timer 1 was used as the trigger source for ADC conversion. The 160 sample points of the whole sinusoidal waveform were taken with the sample rate at 19.2 KHz and each point was compared to get the maximum and minimum of the value. Figure 3.6.9 illustrates the microcontroller code for

collecting and storing 160 sample values into an array. Figure 3.6.10 indicates how to obtain the amplitude of voltage.

```
ISR(ADC_vect)
{
  TIFR1 = (1<<OCF1B);     //clear Timer compare match flag
  if (adcon ==1)
  {
    array[i] = ADCW;     //ADCW takes care of ADCL and ADCH
    i++;
  }
}
void check()
{
  i = 0;
  while(i<160)
  {
    SMCR |=0x02;          //SMCR - Sleep Mode Control Register
                          //bit 3:1, 001, ADC Noise Reduction Mode
                          //ADC noise reduction mode
    adcon = 1;
  }
  adcon = 0;
  SMCR &= 0xFD;           //idle mode
}
```

Figure 3.6.9: Microcontroller code for ADC data collection

```
void collect()
{
  i=0;
  Max = 0;               //Peak value after level shifter
  Min = array[0];
  for(i=0;i<160;i++)
  {
    if(Max<array[i])
    {
      Max = array[i];
    }
    if(Min>array[i])
    {
      Min=array[i];
    }
  }
  Vmax = ((Max-Min)/2)+Min;        //To collect the Peak value before level shifter
}
```

Figure 3.6.10: Microcontroller code for calculating the amplitude of voltage

3.7 Measurement of the Sensor Impedance

The total impedance has two parts: real part (R) and imaginary part (X) of impedance. They can be calculated by following equations 3.7.1 and 3.7.2:

$$R = Z * cos\,\emptyset \qquad \text{(Equ. 3.7.1)}$$

$$X = Z * sin\,\emptyset \qquad \text{(Equ. 3.7.2)}$$

Where:

- R and X are the resistance and reactance of the circuit.
- ϕ: phase angle between V_{in} and I_s

Therefore, the resistive part of the sensor (R_{sensor}) was calculated by equation 3.7.3:

$$R_{sensor} = R - R_s \qquad \text{(Equ. 3.7.3)}$$

To measure the phase angle (ϕ) between V_{in} and I_s, the Schmitt Trigger was used as zero crossing detector (ZCD). The Schmitt Trigger is based on the hysteresis comparator with zero reference voltage is shown in figure 3.7.1. The purpose of employing Schmitt Trigger was to convert the sinusoidal waveform to square waveform which can be easily read by the microcontroller and can reduce undesirable transitions caused by the noisy input signal.

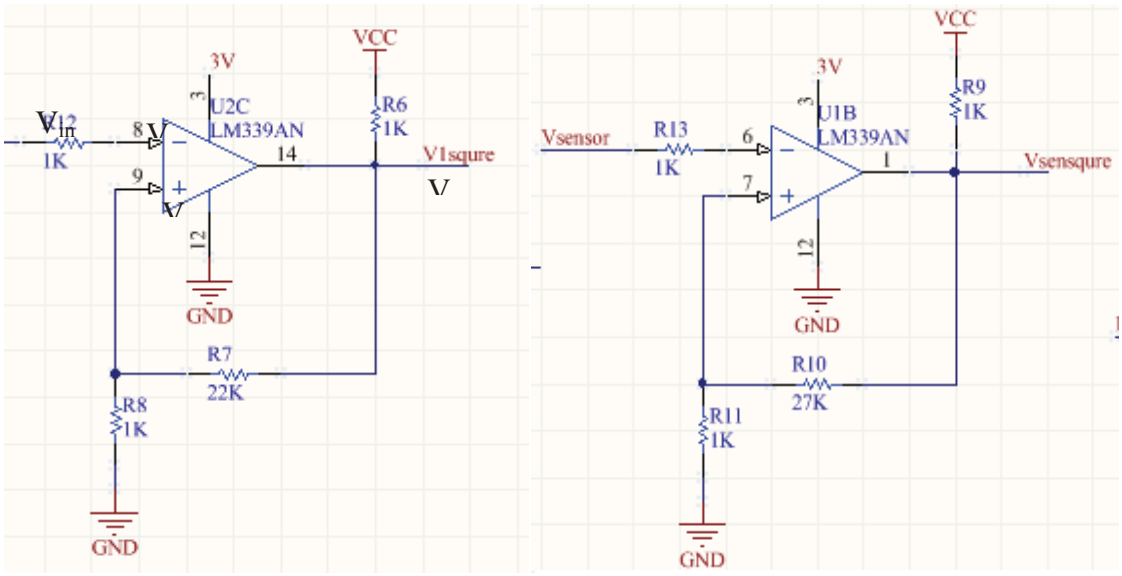

(a) Measurement of the input signal (b) Measurement of the output signal

Figure 3.7.1: Zero cross detector circuit

Figure 3.7.2 shows the time delay between the input signal and output signal. The time delay depends on the nature of the impedance of the sensor. From the time difference (T_d) and the period of one square wave (Period), the phase angle can be calculated by equation 3.7.4:

$$phase\ angle = \frac{T_d}{Period} * 360^o \qquad \text{(Equ. 3.7.4)}$$

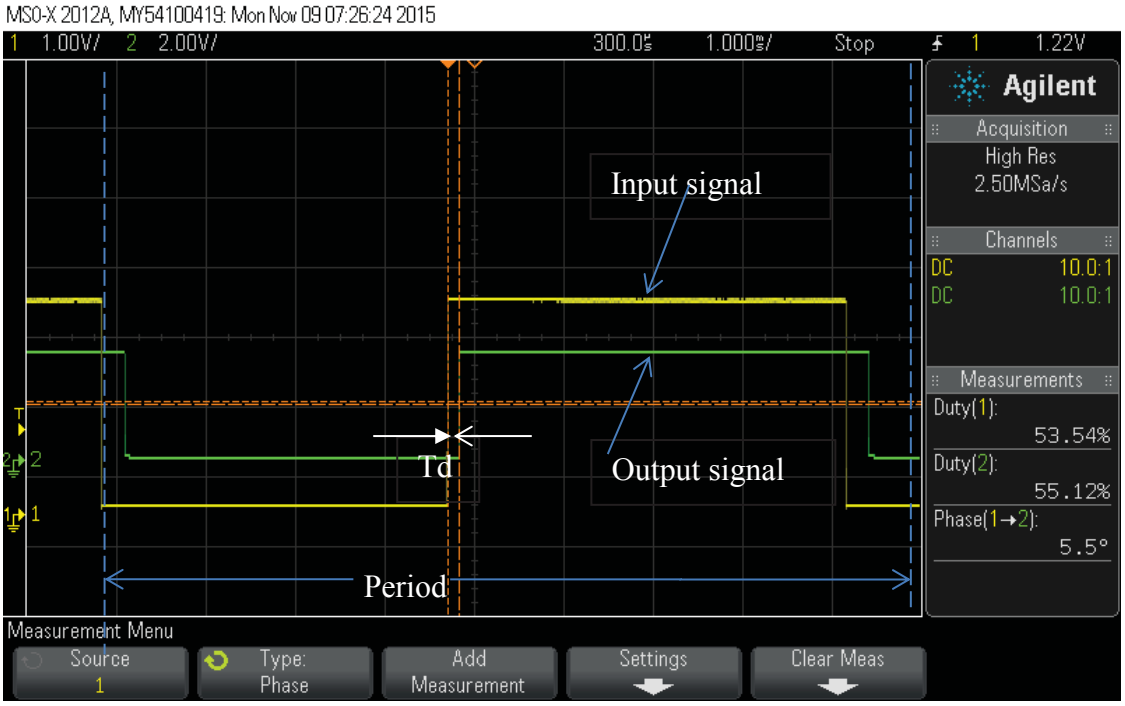

Figure 3.7.2: Outputs of zero cross detectors

To implement the calculation, two external interrupts were used to capture the rising edge of input and output square wave, and Timer 2 was used as a normal counter to get the period of the signal. Figure 3.7.3 illustrates the detailed code to capture the signal.

```
ISR (TIMER2_COMPA_vect)
{
  count++;
}

ISR(INT0_vect)
{
  TIMSK2 = 0x02;
  period = count;
  count = 0;
}

ISR(INT1_vect)
{
  Td = count;     //collect time difference between two rising edge
}
```

Figure 3.7.3: Microcontroller code for capturing signals

3.8 Control of Water Pump

For the field trial, stream water should be pumped into container and measurement of sensor impedance will be carried out. The water then will be pumped out of the container after the measurement is complete. This was done to avoid the sensor being continuously dipped in water as this would cause changing the impedance of the sensor. The water pump and solenoid valve were switched by two MOSFETs which were controlled by microcontroller signals as shown in figure 3.8.1 at appropriate time intervals. The pump required 12V and 2A and the solenoid valve also required 12V and 1A as working conditions, so the MOSFET (model IRLR/U2703) was used having the parameters: V_{DSS} = 30V and I_D = 23A.

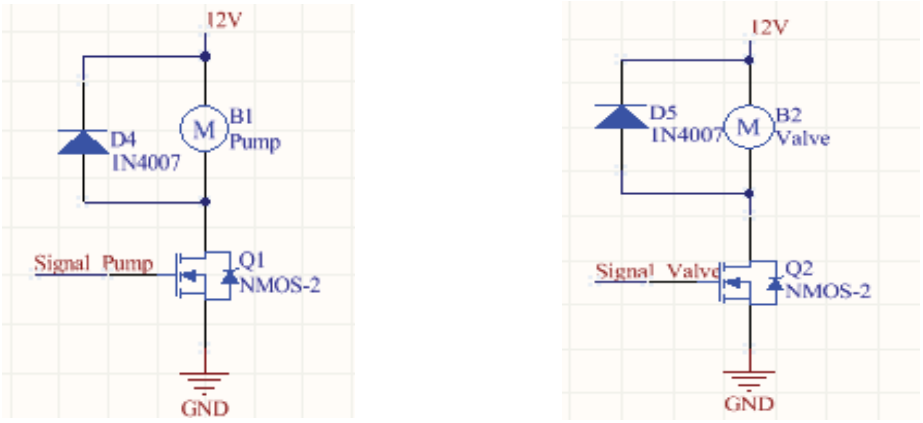

(a) pump control (b) valve control

Figure 3.8.1: Control circuit for pump and solenoid valve

The water sample was planned to collect every 15 minutes which used the software counter to count the time as all timers of the microcontroller were used for other purposes. Figure 3.8.2 shows the microcontroller code for controlling the time interval for the pump and valve switching on/off.

```
if (period>=580)
{
  a++;
  //Take sample every 15 Mins
  if ((a >= 180)&&(a<182))
  {
    PORTB |= 0x10;     //PortB4(pin 12) set to high, Motor on
  }
  if ((a>=182)&&(a<194)) //Time for measurement 1min = 12
  {
    PORTB &=0xCF;     //the Motor and valve all off (take measurement for 1 min)
  }
  if((a>=192)&&(a<204))
  {
    PORTB |= 0x20;     //PORTB5(pin 13) set to high, valve on  for 1 min
  }
  if(a>=204)
  {
    PORTB &=0xCF;     //the Motor and valve all off
    a = 36;           //preload 3 min (16*3-1)
  }
 }
```

Figure 3.8.2: Microcontroller code for controlling time interval of pump and valve

3.9 Temperature Measurement

The interdigital sensor is sensitive to the temperature so it is important to measure the temperature of the ambient environment for temperature compensation. The TMP36 temperature sensor was used in the project. The power supply range of TMP36 was between 2.7V to 5.5V, so the 3.3V output from the voltage regulator was also suitable for it. It can measure the temperature from -40^{o}C to +125^{o}C and it provides very low self-heating. Figure 3.9.1 shows that the V_{out} pin from TMP36 was connected to the ADC input pin of microcontroller directly.

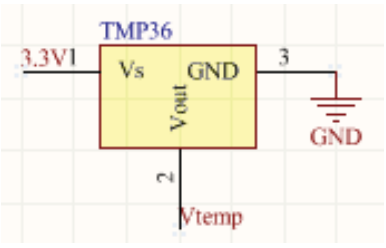

Figure 3.9.1: TMP36 connection

The voltage output of TMP36 in microcontroller is the ADC, where the digital value was converted to real voltage reading by equation 3.9.1:

$$V_{out} = \frac{ADC\_Value * V_{refrence}}{1023} \qquad \text{(Equ. 3.9.1)}$$

Where:

- $V_{reference}$ is 3.3 V (input voltage); this was configured at the ADC register
- 1023: ADC of Arduino Fio is 10 bits, so it is 2^{10} -1

According to the datasheet, the temperature was calculated by equation 3.9.2:

$$Temperaute\ (^{o}C) = \frac{(V_{out} - V_{offset})}{Scale\ factor} \qquad \text{(Equ. 3.9.2)}$$

Where:

- V_{out}: Output voltage from the measurement.
- V_{offset}: 500 mV for TMP36.
- The scale factor is 10.

Therefore, substituting equation 14 into equation 15, the temperature was obtained by equation 3.9.3:

$$Temperaute\ (^{o}C) = \frac{\left(\frac{ADC_{Value} * 3.3 * 1000}{1023} - 500\right)}{10} \qquad \text{(Equ. 3.9.3)}$$

3.10 Data Collection and Monitoring

The measured data were sent via the internal serial port to ZigBee node from the microcontroller and these data were received by ZigBee coordinator through wireless communication, and then stored in the computer. Figure 3.10 shows the functional block diagram for data collection.

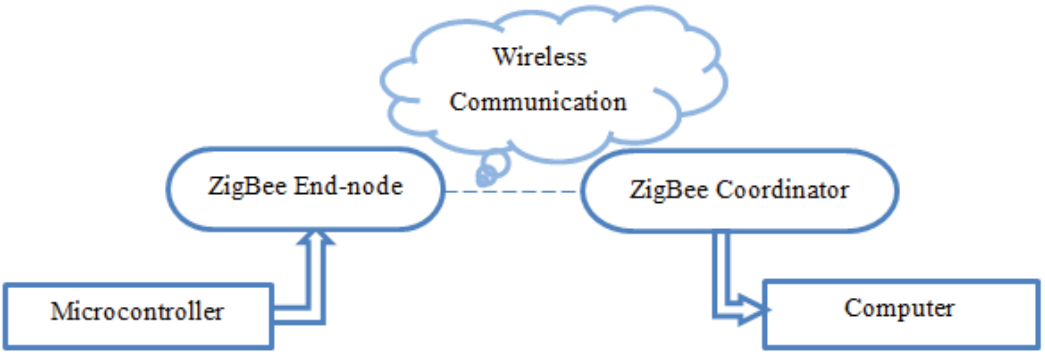

Figure 3.10: Functional block diagram for data collect

3.10.1 Serial Communication

Serial communication is the process of sending data one bit at one time sequentially. It has different serial communication methods such as Universal Asynchronous Receiver Transmitter (UART), Universal Synchronous and Asynchronous serial Receiver and Transmitter (USART), Serial Peripheral Interface (SPI), Inter-Integrated Circuit (I2C) and so on. For Arduino Fio, it communicates with other devices through serial port (USART). The serial communication between the microcontroller board and XBee is implemented through RXI and TXO pins as shown in figure 3.3.4. Figure 3.10.1.1 displays the structure of the sending data in a byte. It starts with a start bit and sends the data from the least significant bit (LSB) to most significant bit (MSB) sequentially followed by the parity bit and stop bit.

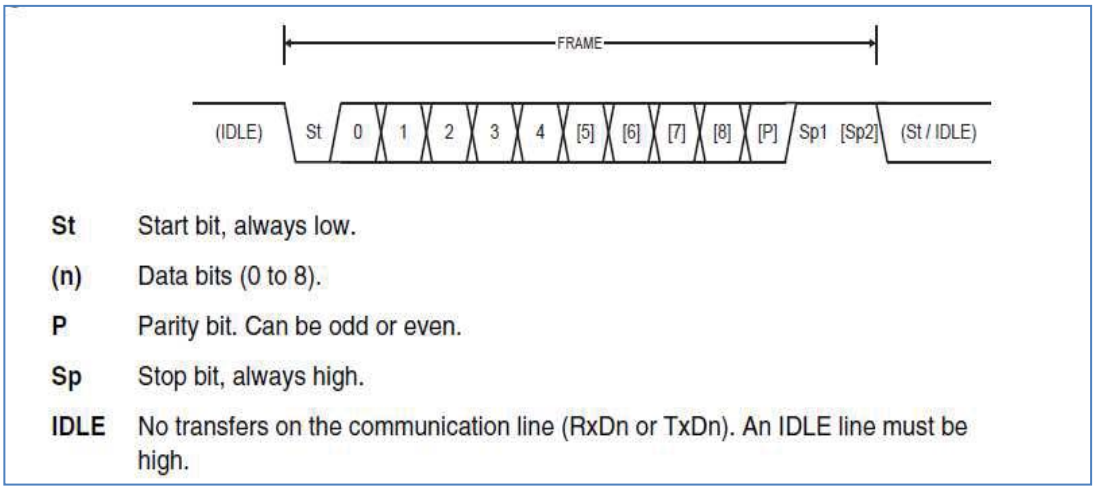

Figure 3.10.1.1: Serial communication frame formats

3.10.2 Wireless Communication

Wireless communication can implement transmission of information without any wires and cables from one device to another, such as Wi-Fi, Bluetooth, ZigBee and so on. Wi-Fi has the security issue for data transmission due to free access, and Bluetooth can only transmit data within the short distance (around 10m), also consuming a lot of power [107]. ZigBee has some advantages such as low cost, low power consumption, and flexible integration with the sensor node. Therefore, the ZigBee protocol is widely used in the energy monitoring and control system [108], environment monitoring [109, 110], industrial automation [111], smart home monitoring [112, 113]. Table 3.10.2.1 lists some features of ZigBee protocol.

Table 3.10.2.1: Feature of ZigBee Protocol

IEEE Standard	802.15.4
Frequency Band	868 Hz / 915 MHz / 2.4 GHz
Rate	20-250 K/Bps
Power Consumption	40 mA - 50 mA
Security	High
Coverage	100 m
Network Topology	Star / Mesh / Cluster Trees

Figure 3.10.2.1 shows the ZigBee node which was integrated with the Arduino Fio board in the sensor node and the ZigBee coordinator was connected to the computer through ZigBee explorer. In addition, each ZigBee has a unique address. The ZigBee node passes all data received via RX (D0) pin and transmits out from TX (D1) pin. The software X_CTU was used here to configure ZigBee and test radio frequency mode.

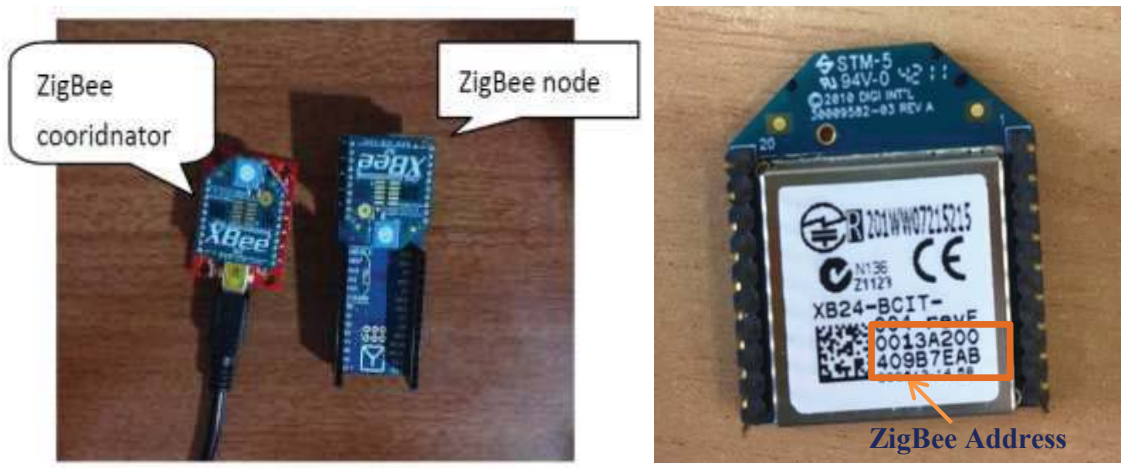

Figure 3.10.2.1: XBees used in the experimental system

There are two modes in the ZigBee configuration: API mode and AT mode. In API mode, the data is assembled into a packet which includes the destination address. This mode is useful for large networks for communicating with the individual node by changing the destination address, and it can implement the configuration in remote module [114]. However, the user can receive the serial data from remote end and send the command back from the coordinator but there is no solution to change the destination address in coordinator side so far. In this project, AT mode is used for monitoring nitrate concentration.

Figure 3.10.2.2 shows the configuration of ZigBee Coordinator (a) and End device (b). Both of the coordinator and end device are selected in AT mode. The purple rectangle circles the Personal Area Network (PAN) ID which is unique for each network. Both coordinator and end device should have the same PAN ID, and then they are recognized in the same network. Destination Address is 0xFFFFFFFF in coordinator configuration because it works as broadcast to receive data from all end-device in this network. However, the end device only sends the data to coordinator so it need indicate its destination address is coordinator address. The Baud rate of ZigBee should be configured as the same as the value used in the microcontroller for serial communication.

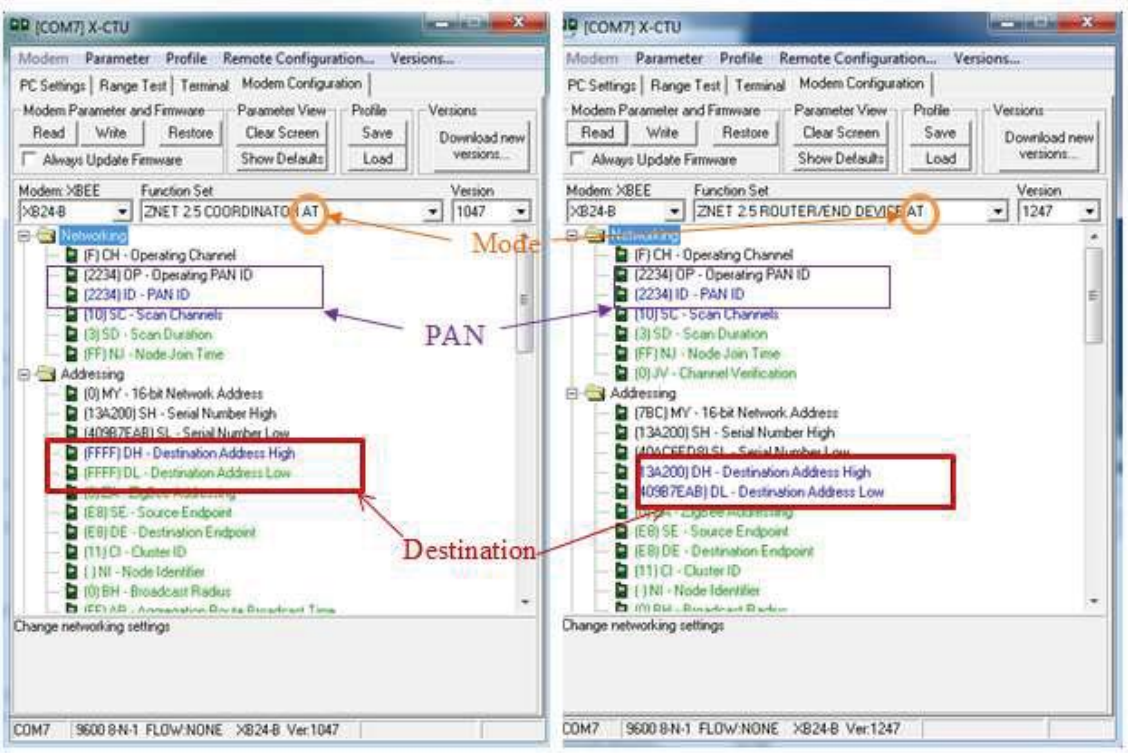

(a) Configuration of coordinator (b) Configuration of end device

Figure 3.10.2.2: Configuration of ZigBee coordinator

From the sensor node, the microcontroller transmits the data to ZigBee node through serial port as shown in figure 3.10.2.3. The whole packet of data which includes the delimiters and measured values is sent from microcontroller to the ZigBee node. In order to distinguish the different end-device, the delimiter can be used to determine the sensor node number and end of the data packets. For example, '#1' for end device ID at 1, followed by '*' to indicate starting reading data, '$$' used for indicating the end of the packet. As the fraction number can be transmitted from microcontroller so that all ADC value multiplies 100 (on the computer side, it will divide for calculation) for measurement of more accurate data. The ADC in the microcontroller is 10 bits so the maximum value it can transmit is $2^{10} = 1024$, and the measured value sent at higher 8 bits first and sent lower 8 bits so total 16 bits of data are sent ($2^{16} = 65536$ is the maximum value can be transmitted). Therefore, the 11 bytes data package was transmitted to ZigBee node (end device).

```
//Sent parameters to ZigBee/GUI
Serial.write('#1');       //Device_ID[0][1]  Device #1
Serial.write('*');        //Start sign
Serial.write(PA);         //Send ADC valuephase angle (degree);
PA = PA>>8;               //right  shift 8 bits (one byte)
Serial.write(PA);

Serial.write(Vlmax);      //Send ADC value of excitation voltage applied to sensor
Vlmax = Vlmax >>8;
Serial.write(Vlmax);

Serial.write(V2max);      //send ADC value of oltage across the sensor
V2max = V2max >>8;
Serial.write(V2max);

Serial.write(Vtemp);     //Send ADC value of measured temperature
Vtemp = Vtemp>>8;
Serial.write(Vtemp);

Serial.write('$$');       //End sign
delay(10);
```

Figure 3.10.2.3: Transmit data from microcontroller to ZigBee node

Figure 3.10.2.4 shows the terminal window in X-CTU that is displaying the received data from one sensor node. The blue rectangle circles the data received by ZigBee coordinator. It includes the device ID, start symbol, phase angle, input and output voltage of the sensor, ambient temperature and end symbol.

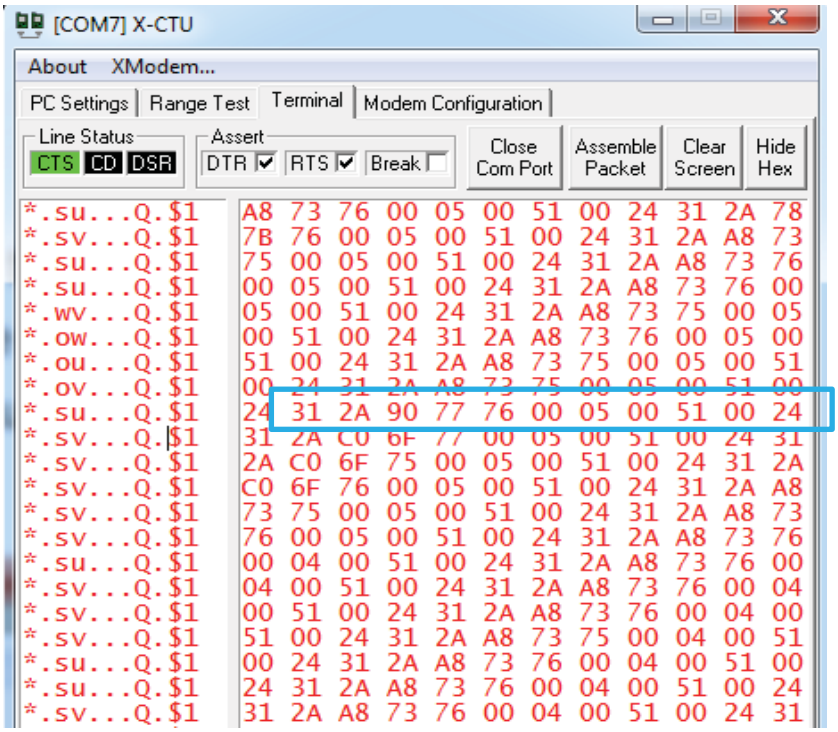

Figure 3.10.2.4: Data received in X-CTU terminal

All the data received in the terminal are a hexadecimal value. Figure 3.10.2.5 shows the description of received data.

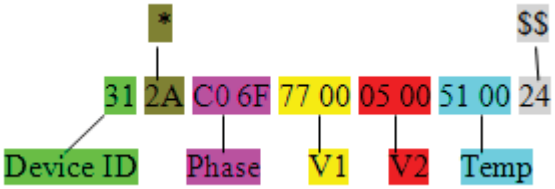

Figure 3.10.2.5: Description of received data

2A represents the symbol '*' of starting reading data

24 is represented '$$' as the end of packet

3.10.3 Graphic User Interface

The Microsoft Visual Studio C sharp programming was used to develop the graphic user interface and store the data. C sharp has inbuilt serial port class which can eliminate the setup for threads and overlapped I/O to make the serial communication much easier. Figure 3.10.3.1 illustrates the steps for receiving sensor data through the serial port in C sharp programming.

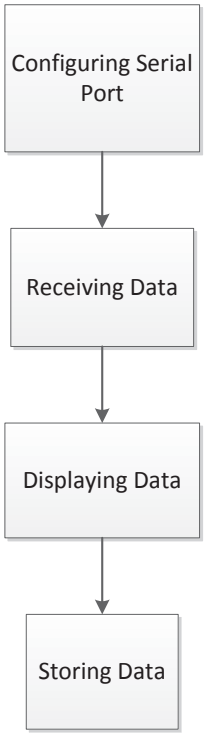

Figure 3.10.3.1: Steps for receiving sensor data

In the first step, the options of serial port name and baud rate are available in the combo box so the user can choose it. When the serial port is opened, the data is ready to send, and the DataReceived event of serial port should be handled (more details in the appendix of C# coding). For the displaying data step, the hexadecimal value is converted to decimal value and the calculation is done by applied formulas. The received data can be stored in the txt file finally.

Figure 3.10.3.2 shows the graphic user interface developed by C# programming. To implement the serial communication, the serial port component (serialPort1) needs to add into the design form.

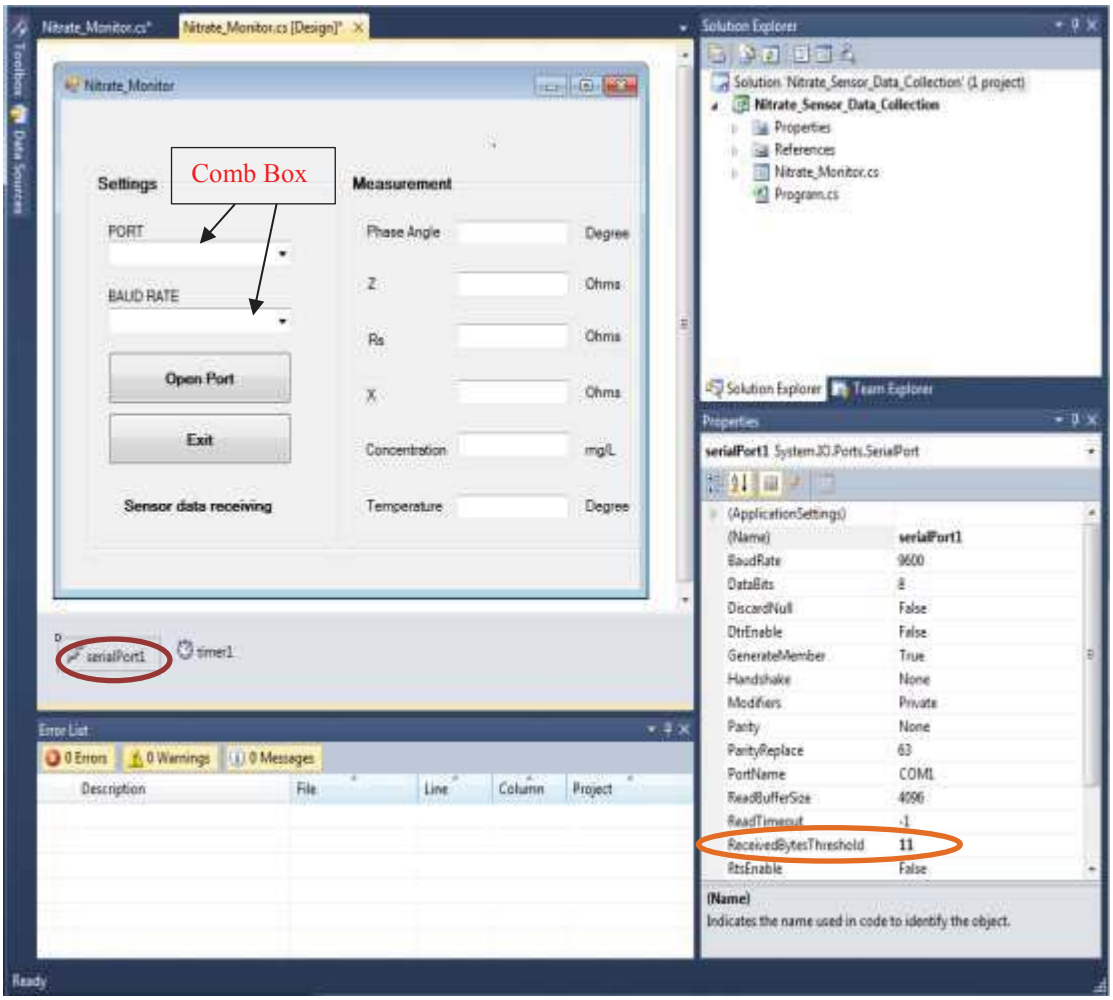

Figure 3.10.3.2: GUI Design by C#

Then the user can select the serial port which connected to ZigBee coordinator and the baud rate from the comb box respectively. The coordinator starts to receive the data when clicking the open port button. It can display the phase angle, impedance value, calculated concentration and temperature. The timer1 used here to control the

time interval to update the data in the texture box for measurement section. One thing needs to pay attention is the 'ReceivedBytesThreshold' (shown in figure 3.10.3.2) in the properties of serialPort1. This byte number must match the input byte number in order to ensure that receiving all bytes arrived at the serial port at the same time without missing any incoming bytes. For example, the data packets sent 11 bytes from the microcontroller so the number of ReceivedBytesThreshold should be 11 as well.

The data received from the serial port was the byte value sent from the microcontroller so it was converted to hexadecimal value by the method 'ByteToHex' [115] as shown in figure 3.10.3.3.

```
private string ByteToHex(byte[] comByte)
{
    StringBuilder builder = new StringBuilder(comByte.Length * 3);
    foreach (byte data in comByte)
        builder.Append(Convert.ToString(data, 16).PadLeft(2, '0').PadRight(3, ' '));
    return builder.ToString().ToUpper();
}
```

Figure 3.10.3.3: Method for converting bytes to hexadecimal value

The calculations in the C# can be done only in decimal values, so it was needed to convert hexadecimal values to decimal values by the code shown in Figure 3.10.3.4.

```
PA = Int32.Parse(hex[6].ToString() + hex[7].ToString() + hex[4].ToString()
     + hex[5].ToString(), System.Globalization.NumberStyles.HexNumber);
V1 = Int32.Parse(hex[10].ToString() + hex[11].ToString() + hex[8].ToString()
     + hex[9].ToString(), System.Globalization.NumberStyles.HexNumber);
V2 = Int32.Parse(hex[14].ToString() + hex[15].ToString() + hex[12].ToString()
     + hex[13].ToString(), System.Globalization.NumberStyles.HexNumber);
Vtemp = Int32.Parse(hex[18].ToString() + hex[19].ToString() + hex[16].ToString()
     + hex[17].ToString(), System.Globalization.NumberStyles.HexNumber);
```

Figure 3.10.3.4: Code for converting hexadecimal value to decimal value

The collected data was stored in the text file by fileStream.write as illustrated in figure 3.10.3.5.

```
//To write data in a file
StreamWriter fileStream = new StreamWriter(@"h:\nitrate_reading_test0.2.txt", true);
fileStream.Write(dt);
fileStream.Write(",  ");
fileStream.Write("Phase Angle: ");
fileStream.Write(textBox2.Text);
fileStream.Write(",  ");
fileStream.Write("Impedance: ");
fileStream.Write(textBox3.Text);
fileStream.Write(",  ");
fileStream.Write("Real Part: ");
fileStream.Write(textBox4.Text);
fileStream.Write(",  ");
fileStream.Write("Imaginary Part: ");
fileStream.Write(textBox5.Text);
fileStream.Write(",  ");
fileStream.Write("Concentration: ");
fileStream.WriteLine(textBox6.Text);
fileStream.Write(",  ");
fileStream.Write("Temperature: ");
fileStream.WriteLine(textBox7.Text);
fileStream.Close();
```

Figure 3.10.3.5: C# code for storing data in txt file

As the data is transmitted wirelessly through ZigBee protocol, the measured information displayed in the GUI is changing by every 10 seconds (this is determined by timer 1 component) so it can implement the real-time monitoring.

3.11 Conclusion

In this chapter, a low-cost sensing system for nitrate detection based on planar interdigital sensor immersed in the water sample was developed. The microcontroller was used to generate the excitation signal applied to the sensor, process the data and control the time interval for the pump and valve. In order to calculate the impedance, the voltage applied to the sensor and the voltage across the series resistance were fed back to the microcontroller via ADC input, and phase difference was implemented by capturing the rising of input and output voltage (This required to convert the sinusoidal waveform convert to square waveform) by an external interrupt. The measurement was conducted in every 15 minutes interval. As the microcontroller has integrated with ZigBee end node, the data collected by the microcontroller can be transmitted wirelessly to the computer where all information was stored in the txt file and database to implement a real-time monitoring condition.

Chapter 4: Experiments, Results and Discussion

4.1 Introduction

The objective of this chapter is to investigate the capability of the designed sensors and sensing system. The aim is to measure the characteristics (total impedance) of the sensor for the detection of nitrate concentration. The interdigital sensor is very sensitive to ambient temperature and humidity. In this chapter, the first experiment was conducted to measure the impedance characterization in a temperature range between 10^{o}C to 40^{o}C and obtain the linear relationship between temperature and impedance. The second experiment was performed to get the relationship between temperature and impedance by varying the humidity in different thermal condition. Then, the sensor was tested to observe the impedance response in prepared diluted water samples from two nitrates forms: sodium nitrates ($NaNO_3$) and ammonium nitrates (NH_4NO_3) by commercial equipment-LCR meter and designed system. For each case, the concentration level was varied from 0.02 mg/L to 10 mg/L. In addition, the sensor was also tested to detect the nitrate concentration in samples collected from streams flowing through the Massey University Agricultural Experiment Station called Tuapaka, located near Palmerston North, New Zealand and the results were compared between by the designed system and the colorimeter method using the Technicon Auto Analyzer discussed in Chapter 1.

4.2 Description of the Selected Sensor

Two sensors based on 1-5-50 configuration were used: a bared sensor and a Parylene coated sensor. Figure 4.2.1 shows the uncoated sensor employed in the project.

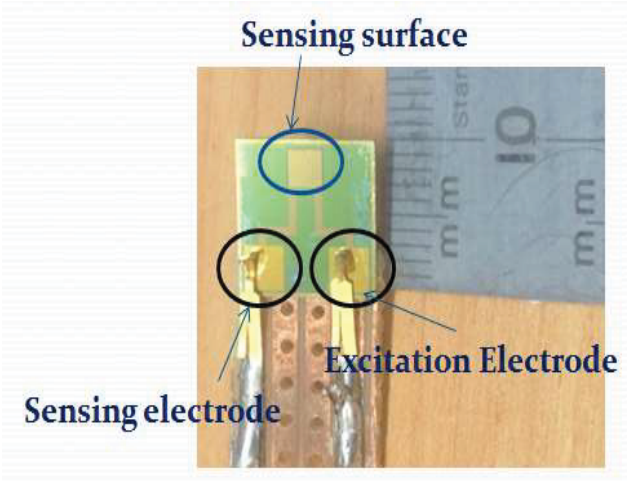

Figure 4.2.1: Uncoated sensor employed in the project

Bared sensor is the one without any protective layer, so the electrode of the sensor may be damaged by the ions in the water. The sensor with Parylene coating provides the waterproof coat [116, 117] to protect the sensing surface from oxidation. However, the selectivity of the coated sensor must be done carefully as the selective material may react with the coated material which will result in a change in the profile of the sensor.

Bared sensor is used to determine the impedance response in the Milli-Q water (deionized water) in varying range of temperature (10 to 40 ^{o}C) and humidity by LCR meter. Both of these two sensors were used in the experiment to observe the impedance changing in different nitrate concentration by LCR meter and designed system.

4.3 Temperature Measurement

The sensor was tested in the Milli-Q water in the temperature range from 10^{o}C to 40^{o}C. The characteristics of the sensor can be extended to accommodate the behavior of it outside the range. The objective of this experiment was to observe the impedance response of the sensor to different temperatures.

4.3.1 Experimental Setup

Figure 4.3.1.1 shows the experimental setup and it involved high precision Hioki 3522-50 LCR meter, Hioki 4-terminal probe 9140, mercury thermometer, SCILOGEX MS 7-H550 Digital Hotplate and computer for data acquisition. The

hotplate had the maximum limit from ambient temperature to 550^{o}C. In order to measure the water sample at a lower temperature (below room temperature), the water sample was stored in the freezer initially to let its temperature fall close to 0^{o}C and then taken out for testing at room temperature. The mercury thermometer was immersed in the water to obtain a continuous temperature reading. Meanwhile, the sensing surface was also immersed in the water and starts to collect data when the temperature reached to a certain degree. The heating plate was used to heat the water sample to reach the desired temperature. The Parylene coated sensor (1-5-50A) was used for this experiment.

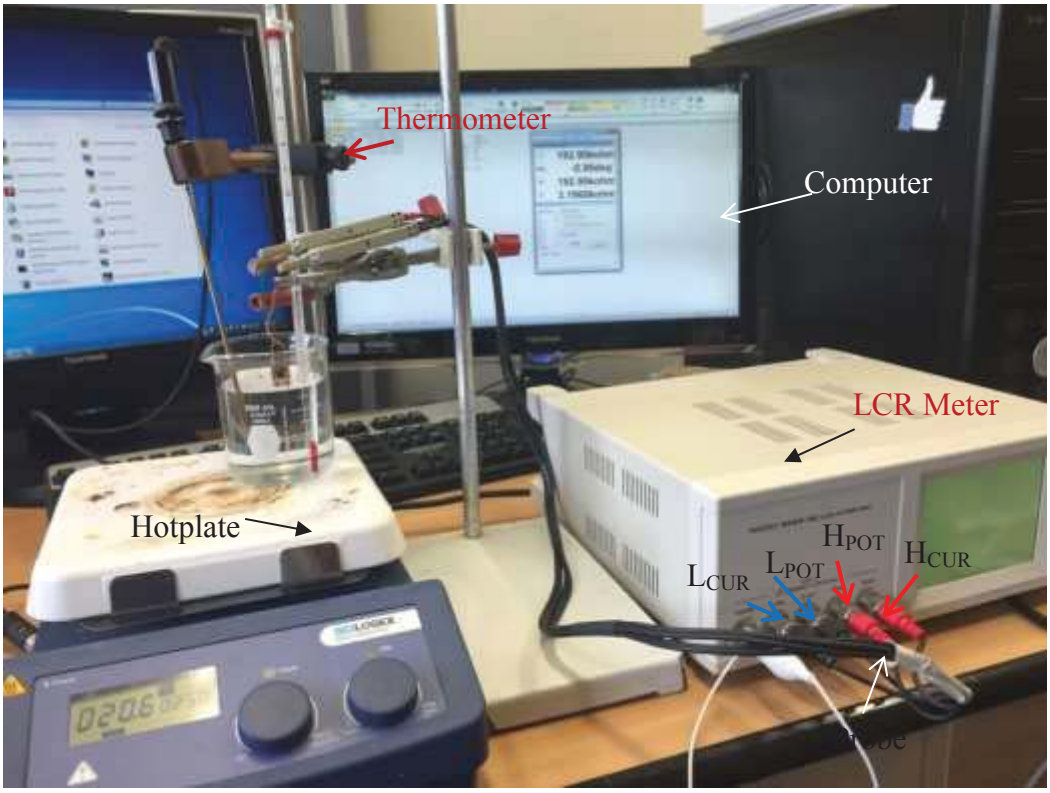

Figure 4.3.1.1: Lab setup for sensor response at different temperature

The Hioki 3522-50 was used to obtain the measured parameters for investigating the impedance values in the frequency range between 1 Hz to 100 KHz. The probe 9140 had two sets of terminals connected between the sensor and LCR meter. The H_{CUR} and L_{CUR} were used to measure the current flowing through the sensor and H_{POT} and L_{POT} were used to measure the voltage across the sensor. Table 4.4.1.1 illustrates the technical specifications of the Hioki 3522-50 LCR meter [118].

Table 4.3.1.1: Specification of Hioki 3522-50 LCR meter

	3522-50 LCR Meter
Measurement parameters	|Z|, |Y|, Θ, R_p (DCR), R_S (ESR,DCR), G, X, B, C_p, C_S, L_p, D (tanδ), Q
Measurement ranges |Z|, R, X	10.00 mΩ to 200.00 MΩ (depending on measurement frequency and signal levels)
Θ	-180.00° to +180.00°
C	0.3200 ᵨF to 1.0000 F
L	16.000 nH to 750.00 KH
D	0.00001 to 999.99
Q	0.01 to 999.99
|Y|, G, B	5.0000 nS to 99.999 S
Basic Accuracy	Z: ±0.08% rdg. Θ: ±0.05°
Measurement Frequency	DC, 1 mHz to 100 kHz
Measurement Signal Levels	10 mV to 5 V rms/10 µA to 100 mA RMS
Output Impedance	50Ω

4.3.2 Results and Discussions

The parylene coated 1-5-50A sensor was immersed into the MilliQ water in varying thermal conditions. The resistance (Rs) and reactance (X) part of the impedance were evaluated and plotted in figure 4.3.2.1. The X-axis shows resistance part of impedance in Ω and the Y-axis shows the reactance part of the impedance in Ω. With the increase in temperature, the total impedance is decreased. Each data point on the plot indicates the impedance at a specific frequency.

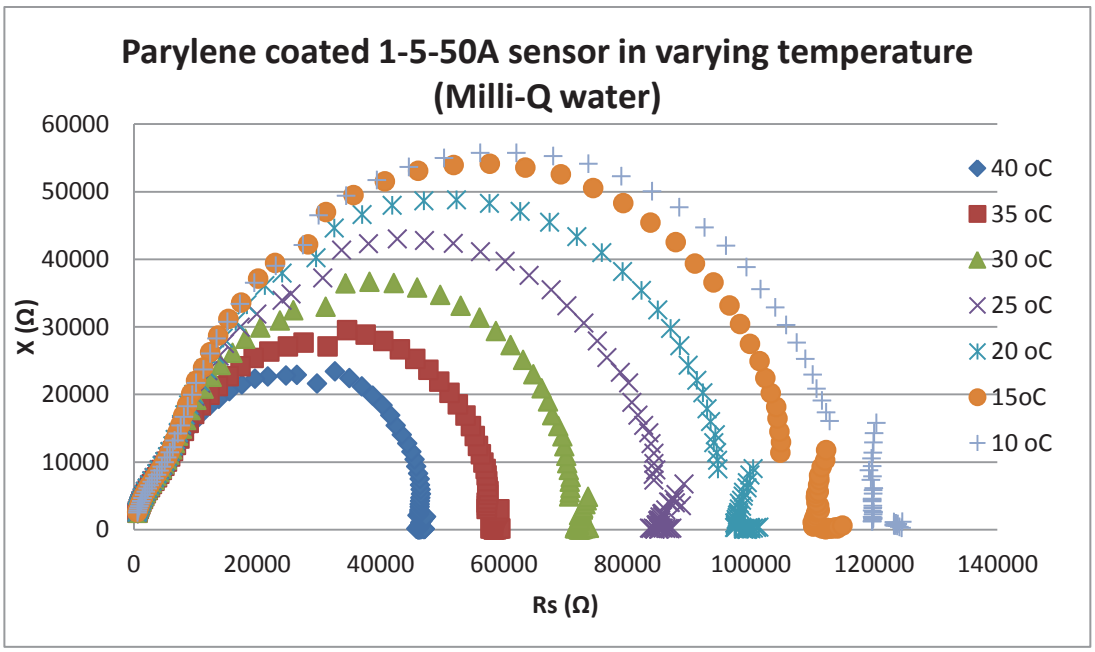

Figure 4.3.2.1: Nyquist plot for testing MilliQ at various temperatures

Figure 4.3.2.2 shows the relationship between the resistance of impedance and the frequency. The resistance is decreased with the increasing in temperature and the sensitive range is significant till 400 Hz.

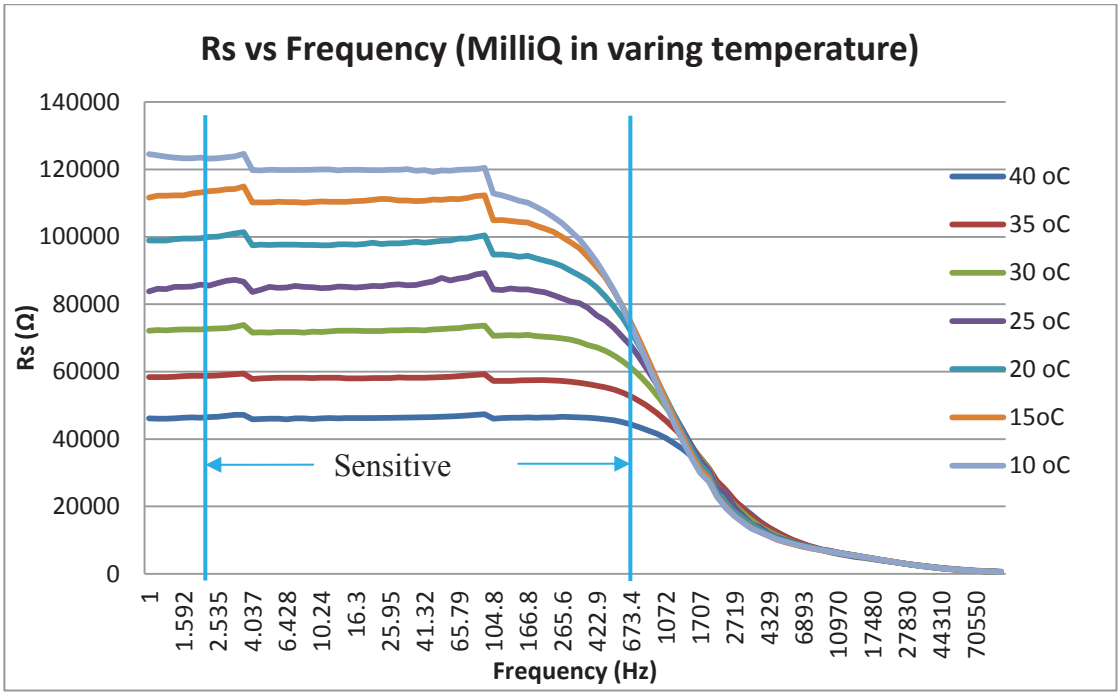

Figure 4.3.2.2: Real part of impedance vs. frequency in varying temperature

Figure 4.3.2.3 shows the reactance (X) of MilliQ to changing temperature plotted against frequency. This parameter is used to measure the dielectric properties of the MilliQ in different temperature.

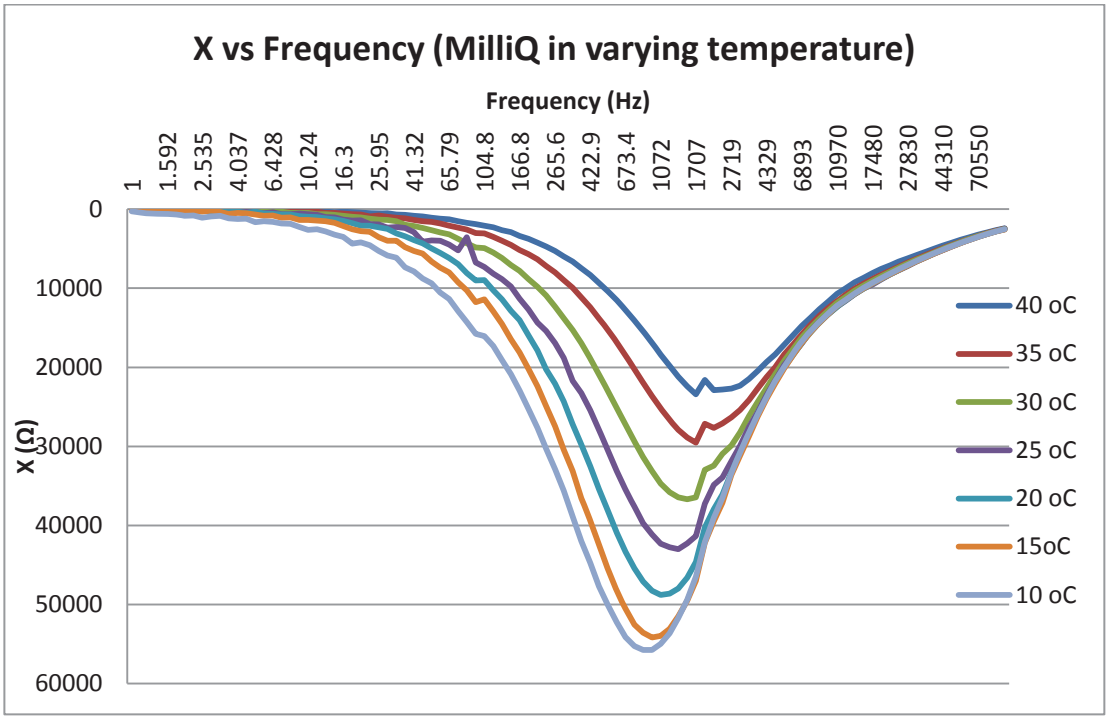

Figure 4.3.2.3: Imaginary part of impedance vs. frequency in various temperature

Table 4.3.2.1: Temperature Measurement

Actual Temp (°C)	**Ave Rs (Ω)**	**Average calculated Temp by Rs (°C)**	**Ave X (Ω)**	**Average calculated Temp by X (°C)**
10	118037.7617	9.55	47125.9455	9.74
15	104281.2167	15.01	41141.9445	14.54
20	91693.88783	20.00	34318.99883	20.00
25	77142.05667	25.77	26339.72167	26.39
30	64181.38833	30.91	19565.99883	31.81
35	52901.83333	35.84	14054.88283	36.23
40	42392.83333	39.55	9658.2	39.75

The experiment was repeated at different times to observe impedance behavior and to take average results for the measurement of temperature for Parylene coated sensor. Table 4.3.2.1 shows the average measurement results for resistance (R_s) and reactance (X) at a different temperatures. As the linear relationship between the impedance and temperature, the slope can be calculated by the equation 4.3.2.1:

$$Slope = \frac{\Delta R}{\Delta T} = \frac{R_{40} - R_{10}}{T_{40} - T_{10}} \qquad \text{(Equ. 4.3.2.1)}$$

Where:

- R_{40}: Resistance value measured at 40°C
- R_{10}: Resistance value measured at 10°C
- T_{40}: Temperature at 40°C
- T_{10}: Temperature at 10°C

Therefore, the slope for resistance part is (42392.83 - 118037.76)/(40-10) = -2521.498. Similarly, replacing the ΔX with ΔR, the slope for reactance part is (9658.2-47125.95) / (40-10) = -1248.92. Figure 4.3.2.4 shows the relationship between the temperature and Rs. The resistance of impedance drops nearly linearly with the increase in temperature.

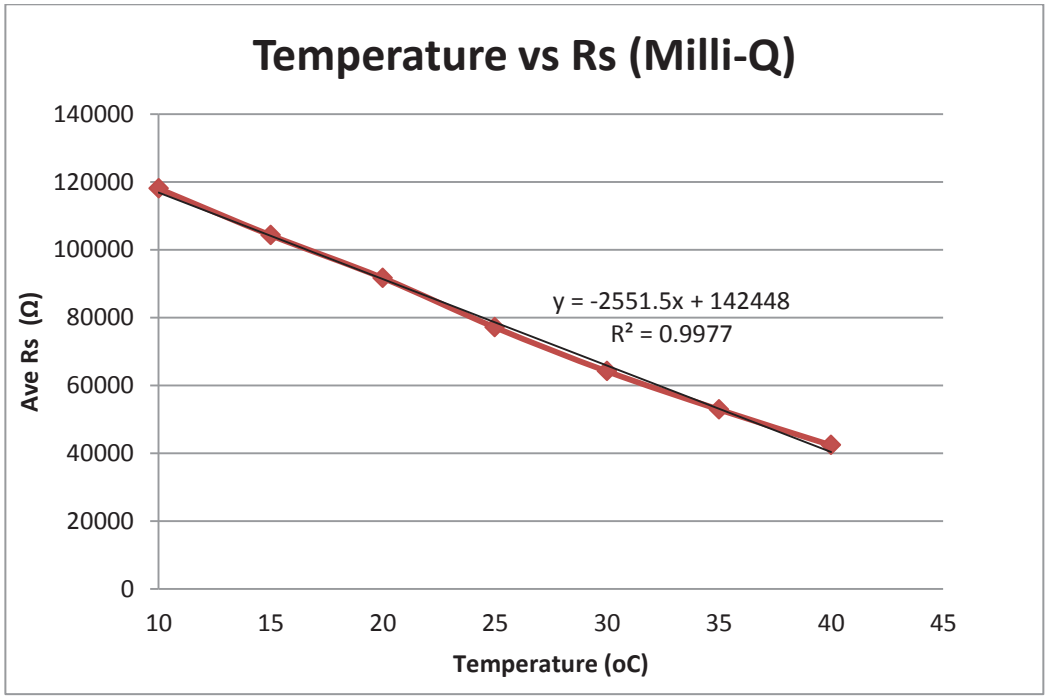

Figure 4.3.2.4: Relationship between the temperature and resistance part of impedance

Therefore, the temperature can be measured by equation 4.3.2.2:

$$T\ (^{o}C) = \frac{R_T - R_{20}}{slope} + T_{20} \qquad \text{(Equ. 4.3.2.2)}$$

Where:

- R_T: Measured resistance value
- R_{20}: Resistance value at 20°C (which is the reference value)
- T_{20}: Reference temperature is at 20°C

The calculated temperature is shown in table 4.3.2.1 and figure 4.3.2.5 displays the correlation between the actual temperature and calculated temperature. The calculated temperature has good correlation with the reactance R^2 = 0.9942 and the resistance (R^2 = 0.9975) for part, respectively.

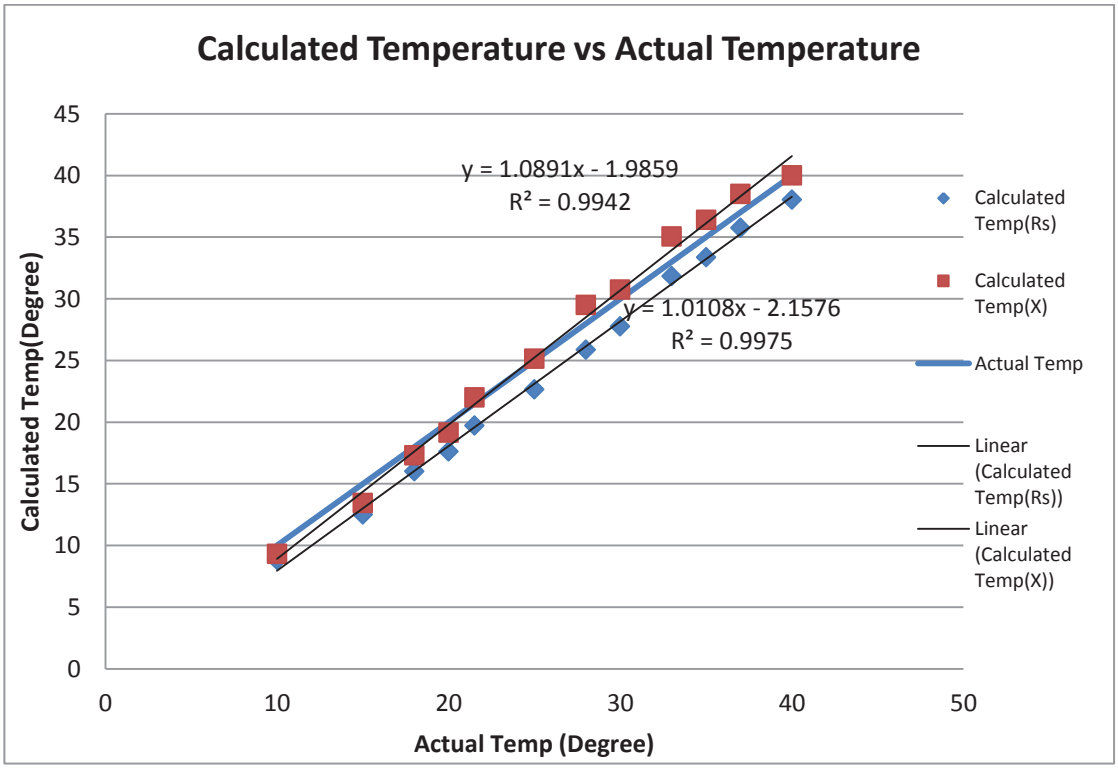

Figure 4.3.2.5: Comparison between the actual temperature and measured temperature

4.4 Humidity Experiment and Results

This experiment observed the impedance characteristics as a function of humidity and temperature. The experiment was tested at a temperature range from 20°C to 40°C with the step of 5°C and the varied humidity was applied.

Figure 4.4.1 shows the experimental setup for obtaining the impedance of sensor in the various temperature and humidity. It used the Thermo Scientific Heratherm Compact Microbiological Incubator, LCR meter, Humidity and temperature portable sensor and computer. The incubator can control the temperature between 17°C to 40°C but it cannot control the humidity. Therefore, to vary the humidity, a small container with the hot water was used to increase the humidity in the incubator. However, this humidity rate could not be controlled exactly, so the humidity range in this experiment depended on the volume of hot water in the container. The LCR meter was used to obtain the parameters' measurement for investigating the impedance value in the frequency range between 1 Hz to 100 KHz, and the computer is used for data acquisition.

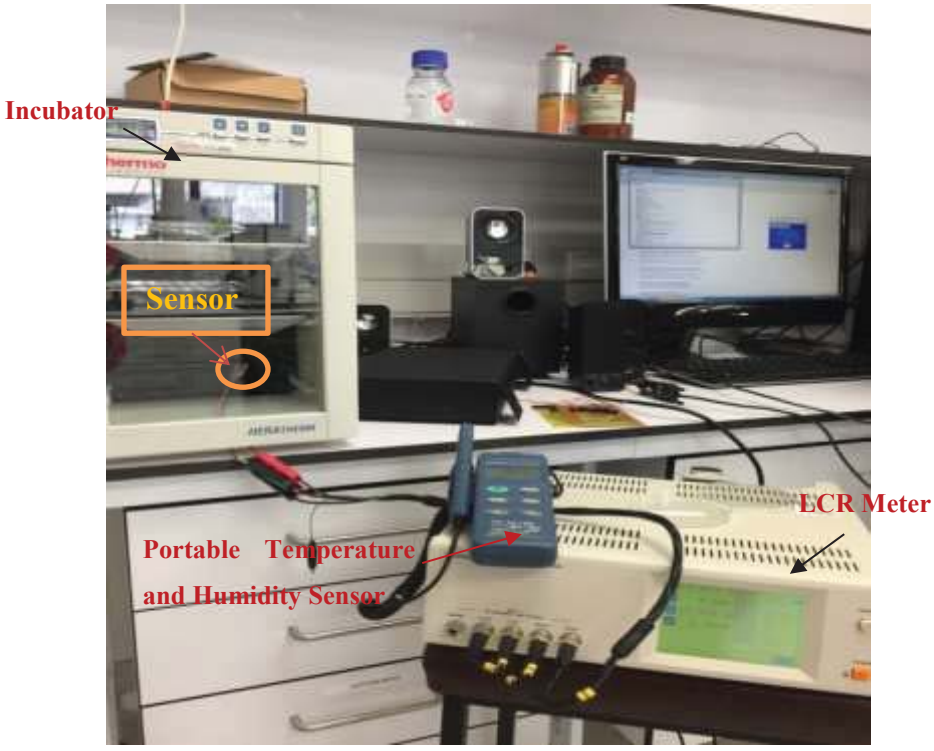

Figure 4.4.1: Experiment setup for temperature and humidity measurement

Figure 4.4.2 shows the Nyquist plot for the Parylene coated sensor test at 25°C with varying humidity. From the figure 4.4.2, the total impedance is reduced with the

increase in humidity. The relationship between the resistive part of impedance and frequency at different humidity is shown in figure 4.4.3. The most sensitive area of the sensor is from 1 Hz to 400 Hz.

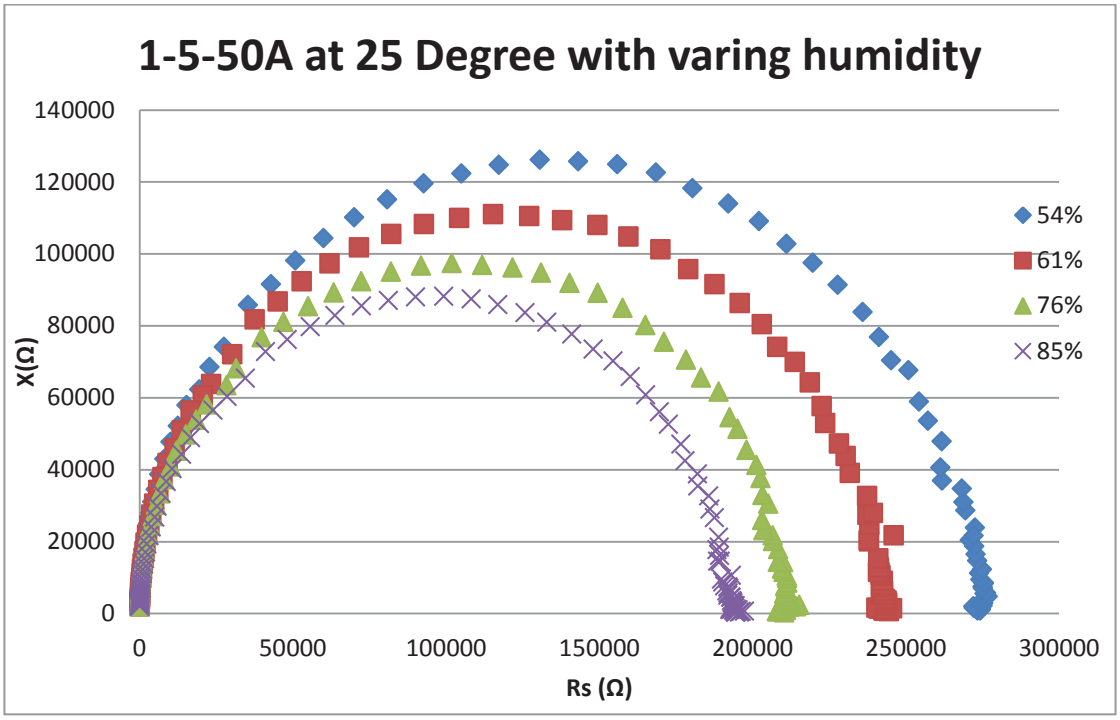

Figure 4.4.2: Nyquist plot for testing varying humidity at 25°C

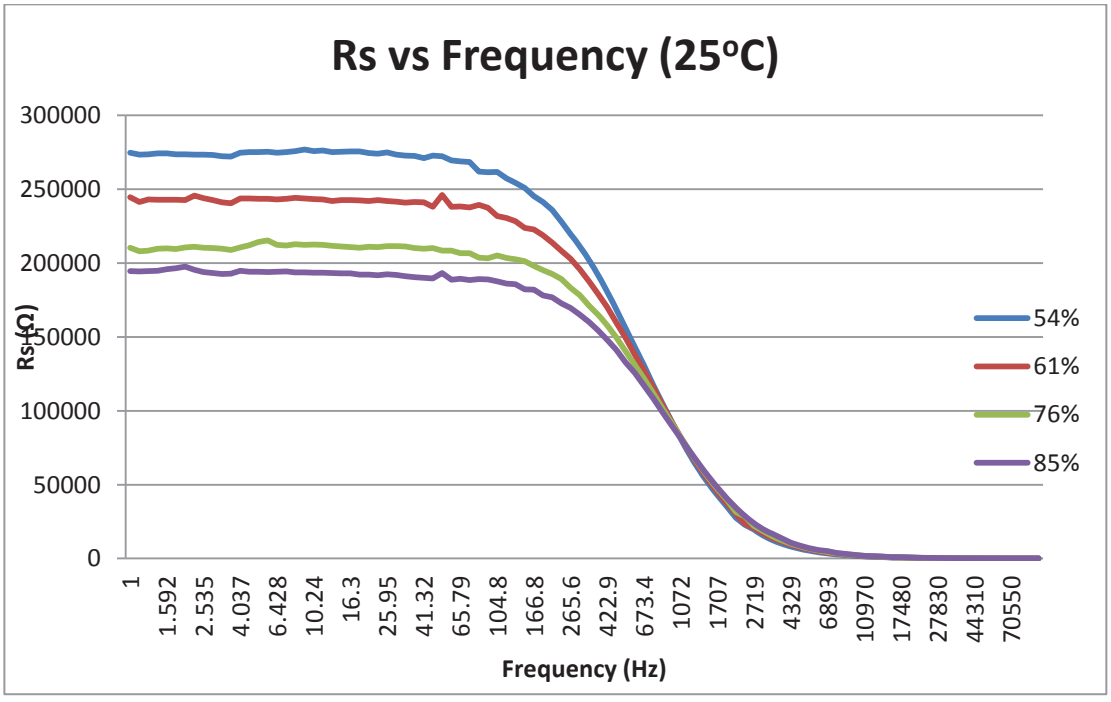

Figure 4.4.3: Resistance part of impedance vs. frequency in varying humidity at 25°C

Figure 4.4.4 illustrates when the increase in humidity, the resistance of impedance reduces and it shows a good correlation with R^2= 0.9833.

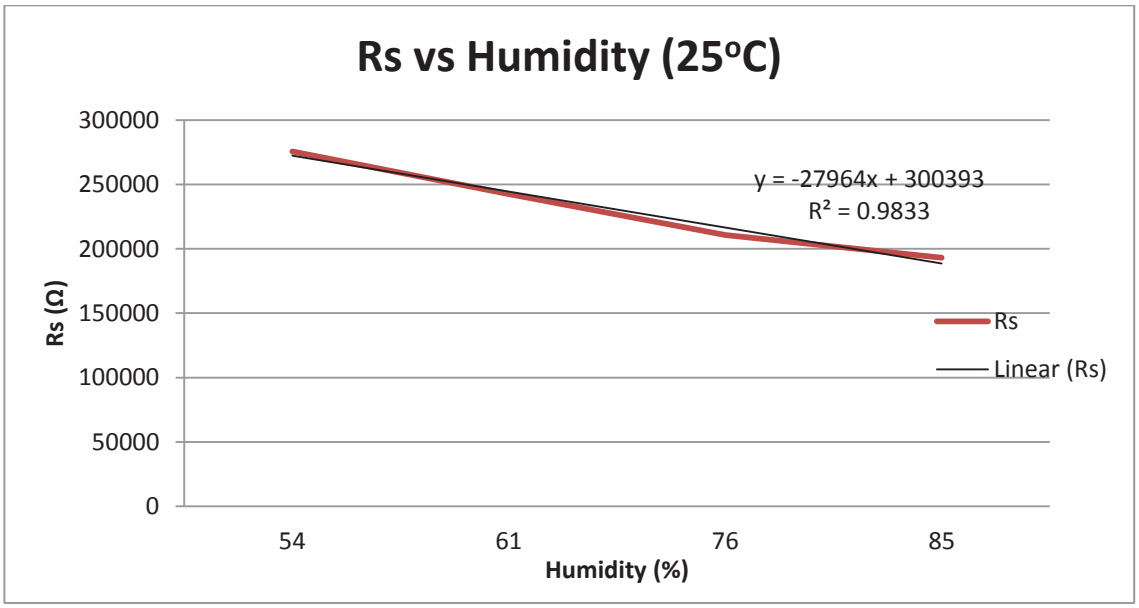

Figure 4.4.4: Resistance of impedance against humidity at 25°C

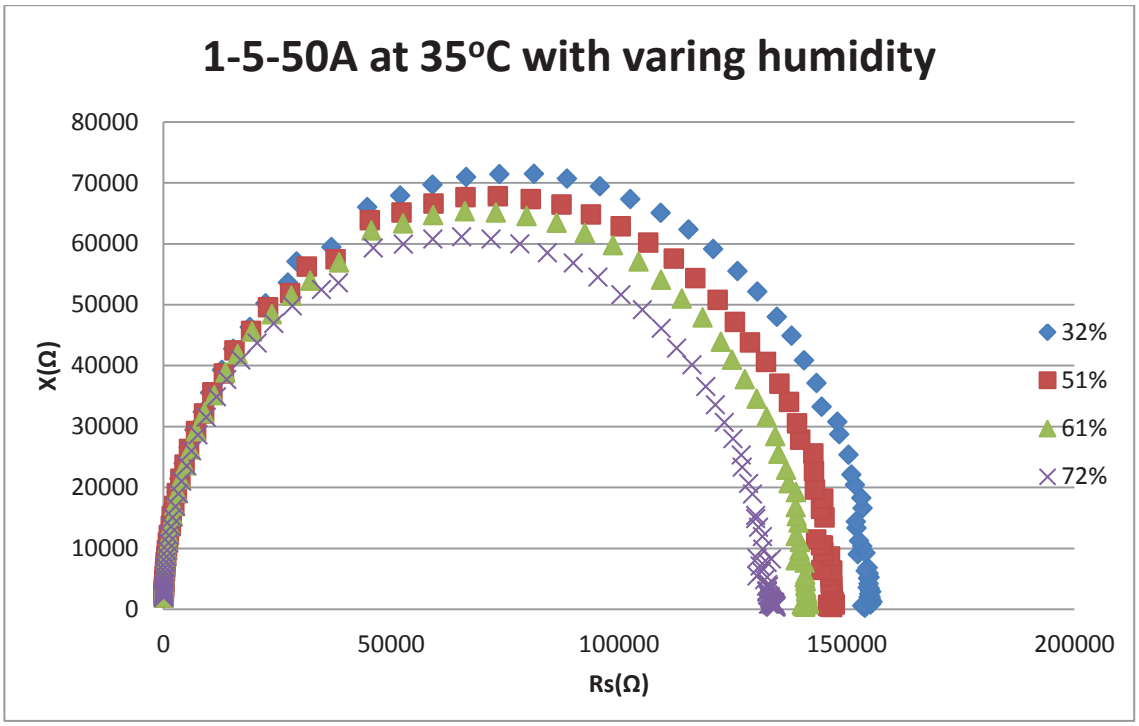

Figure 4.4.5: Nyquist plot for testing varying humidity at 35°C

The humidity experiment also tested at 35°C. Figure 4.4.5 shows the Nyquist plot of impedance in changing humidity and figure 4.4.6 illustrates the sensitive area and the relationship between the resistance and frequency. Figure 4.4.7 indicates the linear relationship between the humidity and resistance.

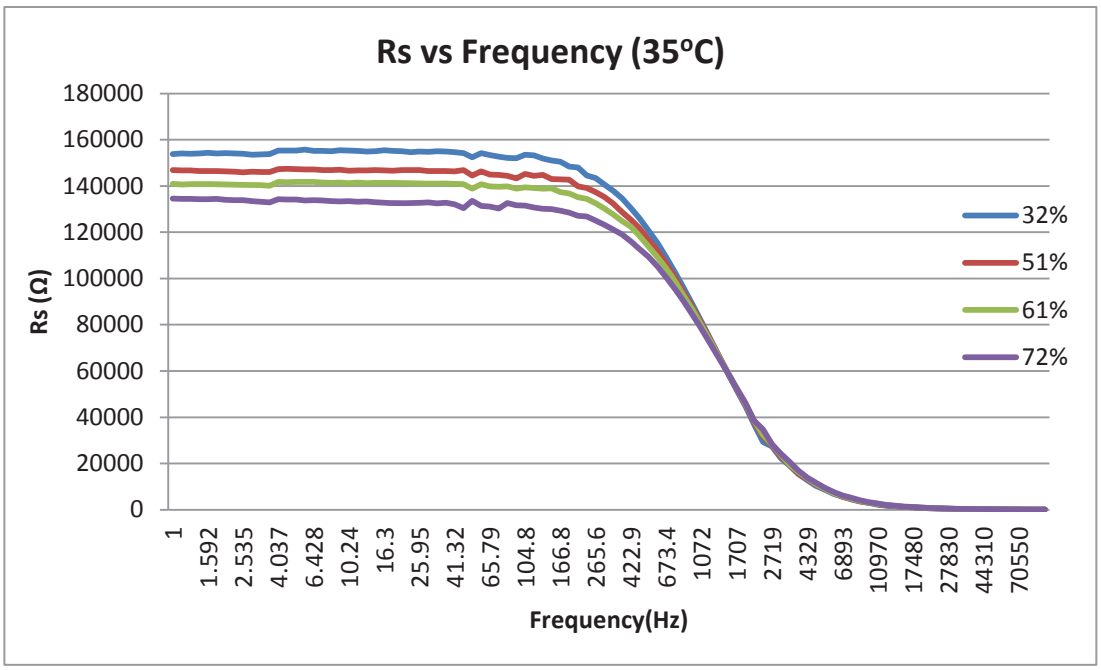

Figure 4.4.6: Resistance part of impedance vs frequency in varying humidity at 35°C

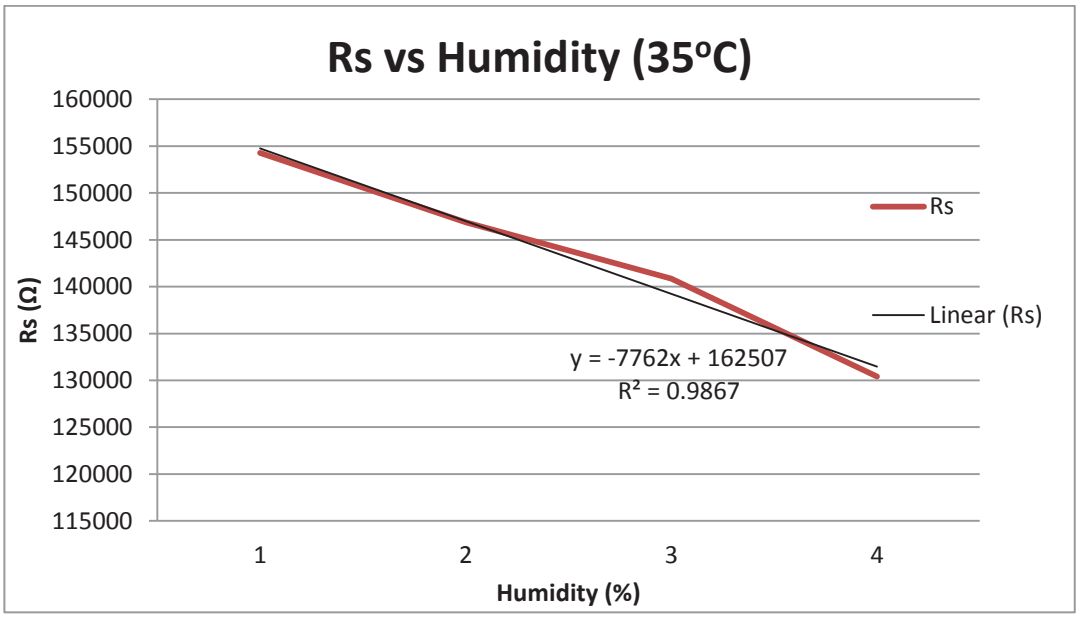

Figure 4.4.7: Resistance of impedance against humidity at 25°C

From figure 4.4.2 to figure 4.4.7, the impedance is reduced with the increase in temperature and humidity. Although the project is to detect the nitrate in the water, the temperature and humidity can play a significant role in the accuracy of the measurement, so a correction factor needs to be introduced.

4.5 Experimental Results with Water

4.5.1 Preparation of Solution

The solutions were prepared using the serial dilution method which is a simple method without making replicated samples [119]. It only needs to prepare one stock solution at a certain concentration and serially diluted to diluent, and it generally uses the same dilution factor. Figure 4.5.1.1 illustrates the working principle of the method [120]. In each tube, it adds 9ml of distilled water and transfer 1ml of the previous solution into it. The different concentration of Sodium Nitrate ($NaNO_3$) and Ammonium Nitrate (NH_4NO_3) solution were prepared.

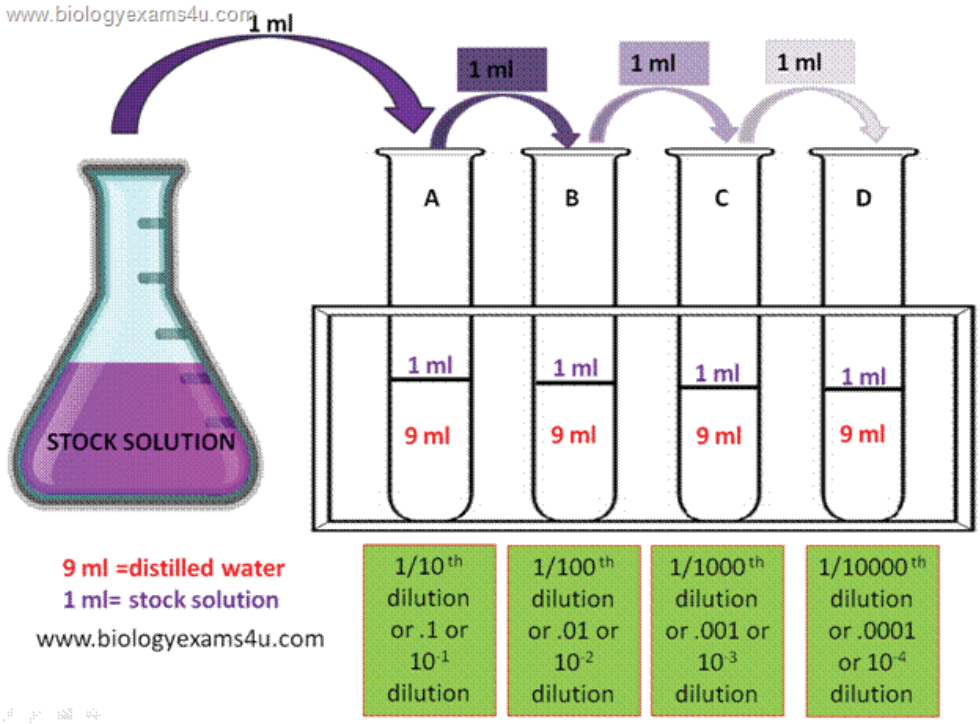

Figure 4.5.1: Serial dilution procedure [120]

The molecular weight of NH_4NO_3 can be calculated by equation 4.5.1:

$$NH_4NO_3 = 14.0067 + 1.00794 * 4 + 14.0067 + 15.9994 * 3$$
$$= 80.043\ {}^{g}/_{mol} \qquad \text{(Equ. 4.5.1)}$$

Equation 4.5.2 can be calculated % N as NH_4NO_3 or $NaNO_3$:

$$\%\ \text{N as } NH_4NO_3 = \frac{14.0067}{80.043} = 17.499\% \qquad \text{(Equ. 4.5.2)}$$

Therefore, for 10 PPM (mg/L) of NH_4NO_3, it requires the amount be in equation 4.5.3:

$$NH_4NO_3(\text{mg}) = \frac{10}{0.17499} = 57.15\ \text{mg} \quad \text{(Equ. 4.5.3)}$$

Similarly, the molecular weight of $NaNO_3$ can be presented as equation 4.5.4:

$$NaNO_3 = 22.98977 + 14.0067 + 15.9994 * 3 = 84.99467\ \text{g/mol} \quad \text{(Equ. 4.5.4)}$$

% N of NaNO3 can be calculated by equation 4.5.5:

$$\%\ \text{N as}\ NaNO_3 = \frac{14.0067}{84.99467} = 16.4795\% \quad \text{(Equ. 4.5.5)}$$

The amount of NaNO3 (mg) for 10 PPM can be computed by equation 4.5.6:

$$NH_4NO_3(\text{mg}) = \frac{10}{0.164795} = 60.7\text{mg/L} \quad \text{(Equ. 4.5.6)}$$

The dilution factor can be calculated by equation 4.5.7:

$$Dilution\ Factor = {Final\ Volume}/{Solute\ Volume} \quad \text{(Equ. 4.5.7)}$$

For example, the stock solution of 10 mg/L was prepared by mixing 60.7 mg of $NaNO_3$ into 1 L MilliQ water. For a 5 mg/L solution, its dilution factor is 5/10 = 1:2 and is prepared by mixing 500 ml of stock solution into 500 ml of MilliQ water. The solution was prepared at a concentration range from 10 mg/L to 0.02 mg/L for $NaNO_3$ and NH_4NO_3. To make a stock solution of NH_4NO_3, it requires mixing 57.15 mg of NH_4NO_3 into 1 L of MilliQ water. All of the prepared solutions were sent to the laboratory to check the concentration. Table 4.5.1.1 shows the dilution factor for preparing solutions and the results of concentration test using the laboratory method.

Table 4.5.1.1: Solution Concentration test result from laboratory and dilution factor

Prepared Solution Concentration (mg/L)	Tested by laboratory (mg/L)	Dilution Factor
10	10.07	1
5	4.85	0.5
1	0.76	0.2
0.5	0.42	0.5
0.4	0.35	0.8
0.3	0.26	0.75
0.2	0.17	0.67
0.1	0.07	0.5
0.02	0.01	0.2

The tested results for solutions are slightly different compared to actual concentration. This could be explained by measurement error as the standard solution was prepared by a technician, using another method.

4.5.2 Results from LCR Measurement

The first experiment was to test different concentration of Ammonium Nitrate (NH_4NO_3) with concentrations ranging between 0.02 mg/L and 0.4 mg/L using a commercial LCR meter. The purpose of this experiment was to observe the impedance characteristic of the Parylene coated sensor and the most sensitive frequency of the sensor under different nitrate concentrations.

Using the frequency response analyzer method and the standard for electrochemical impedance spectroscopy [52], the impedance measurement result is represented in the Nyquist plot as shown in figure 4.5.2.1 with a frequency range from 1 Hz to 100 KHz. It illustrates that the total impedance is reduced when the concentration of the water solution was increased.

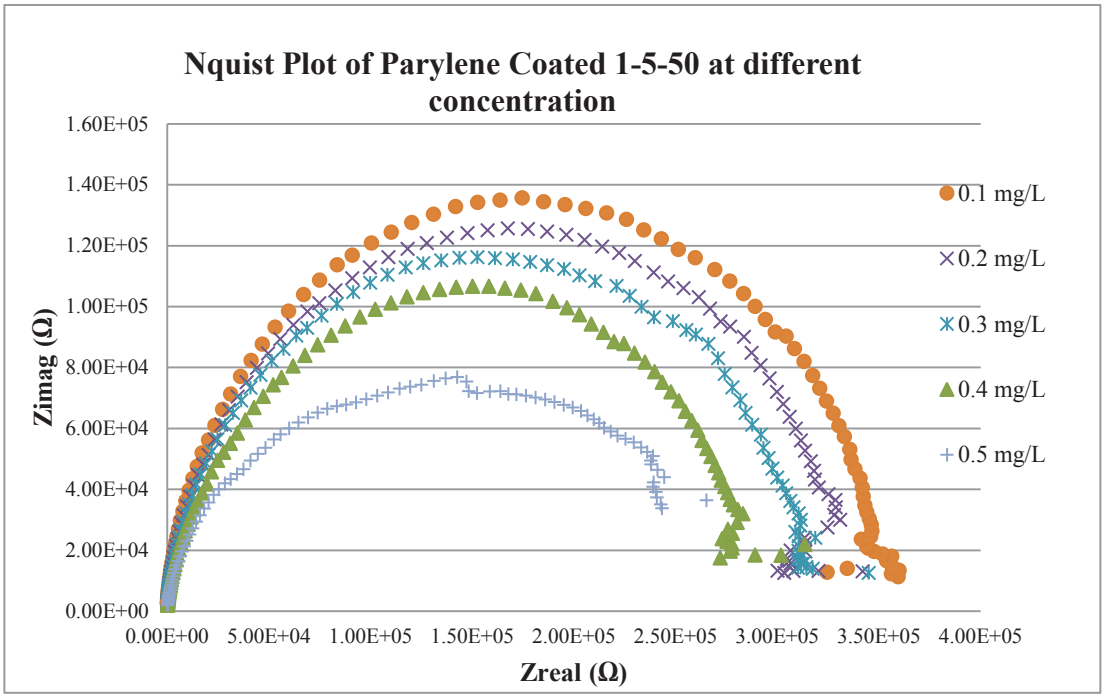

Figure 4.5.2.1: Nyquist plot for NH_4NO_3 at different concentration

Due to the presence of ionic salts in the solution, there was a significant change in the real part of the impedance compared to the imaginary part. From figure 4.5.2.2, it is seen that the real part of the impedance changes with the change in frequency. Different concentrations of solution were considered to determine the sensitive region (from 5 Hz to 150 Hz) of the sensor under consideration (120 Hz is chosen in this case).

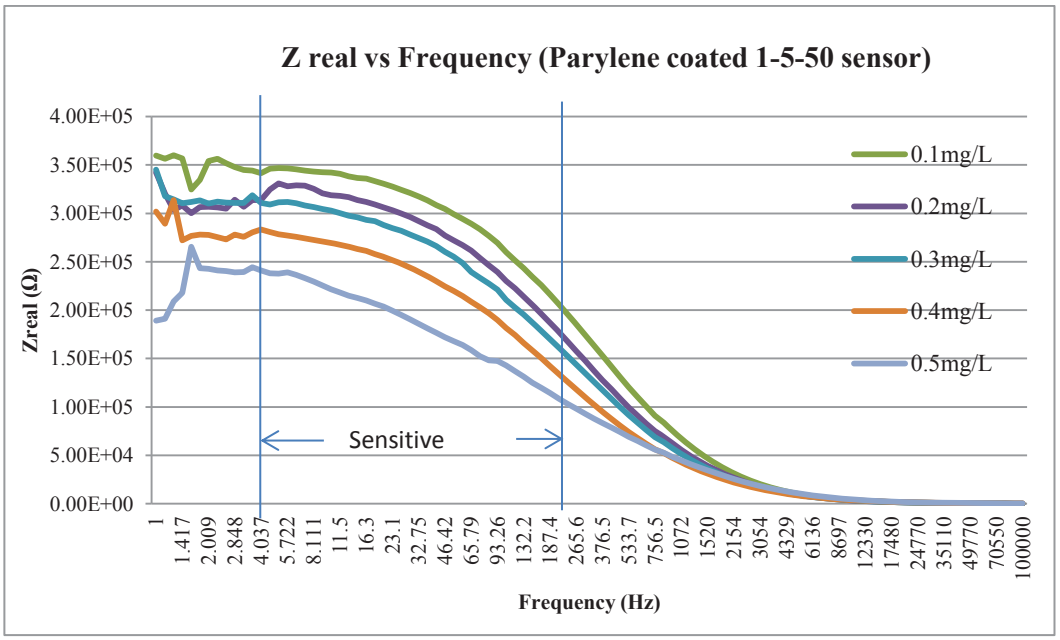

Figure 4.5.2.2: Real part of Impedance vs. Frequency at different concentrations (NH_4NO_3)

Figure 4.5.2.3 shows the corresponding change in the imaginary part of impedance with the change in frequency. It is seen from the figure that there is not much change in the reactance values for the complete frequency range as compared to the change in the resistive (Real part of Impedance) values in figure 4.5.2.2.

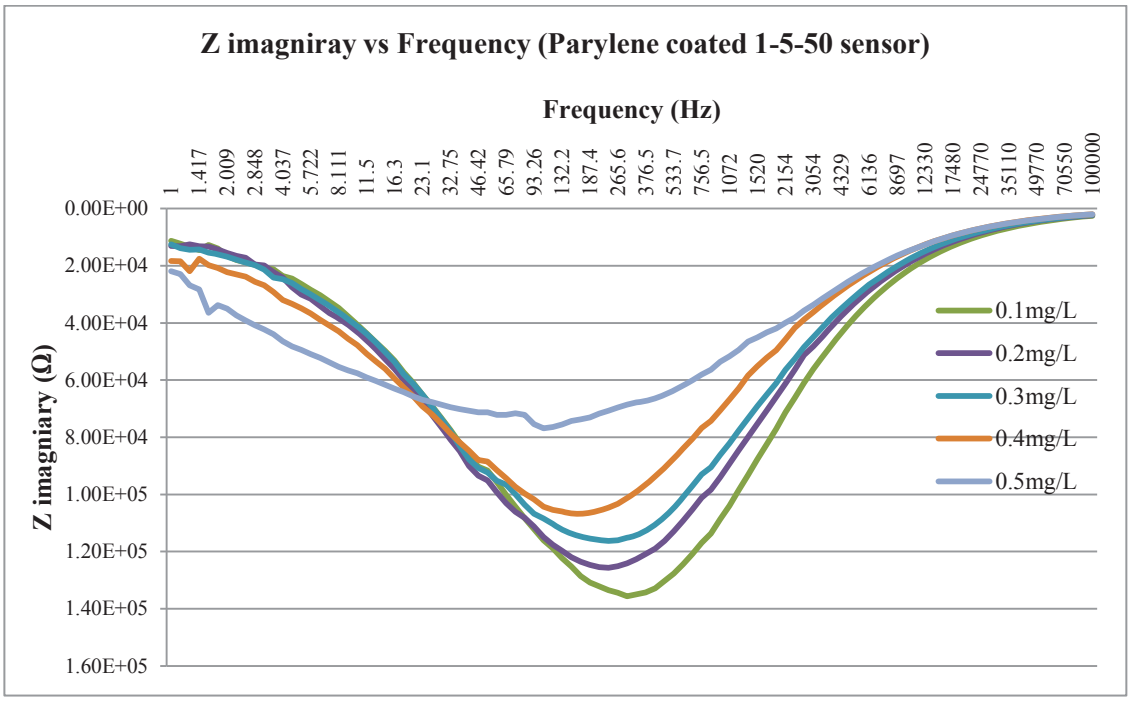

Figure 4.5.2.3: Imaginary part of Impedance vs. Frequency at different concentrations (NH_4NO_3)

Equation 4.5.8 illustrates the chemical formula for the ionic equilibrium state for ammonium nitrate. The purpose is to detect nitrate ions, the real part of the impedance (R) shows a significant change compared to the imaginary part (X), the real part of impedance (R) is chosen as the reference for measurement.

$$NH_4NO_3 \leftrightarrow NH_4^+ + NO_3^- \qquad \text{(Equ. 4.5.8)}$$

4.5.3 Water Solution Tested by Designed Sensing System

Figure 4.5.3.1 shows the experimental setup for NO_3-N concentration measurement. The experiments were performed in ambient conditions. Arduino Fio was used to generate the sinusoidal waveform that was the input signal for the sensor and perform data acquisition. The sensor was immersed into prepared water solution at different NO_3-N concentration. The electronic circuit was designed to get the input and output voltage of the sensor and detect the phase across the sensor. The sensor's

impedance was calculated by the microcontroller. The detailed explanation has described in Chapter 3.

Figure 4.5.3.1: Experimental setup for water solution test by the designed system

Experiments with Uncoated Sensor

This experiment was to test different concentration of $NaNO_3$ and NH_4NO_3 between 0.02 mg/L to 10 mg/L on the bared (uncoated) sensor and Parylene coated sensor respectively by designed system and LCR meter. The purpose of this experiment is to observe the impedance response of the sensor in different nitrate concentrations and derive the formula to calculate the concentration based on the EIS, without selectivity.

Figures 4.5.3.2 and 4.5.3.3 illustrates test results of NH_4NO_3 on the uncoated sensor from the designed system and the LCR meter. When the concentration increased, the real part of impedance is decreased. At the low level, although the designed system had a steeper slope which was around three times than that of the slope on LCR meter, it showed a good linear correlation with $R^2 = 0.9923$.

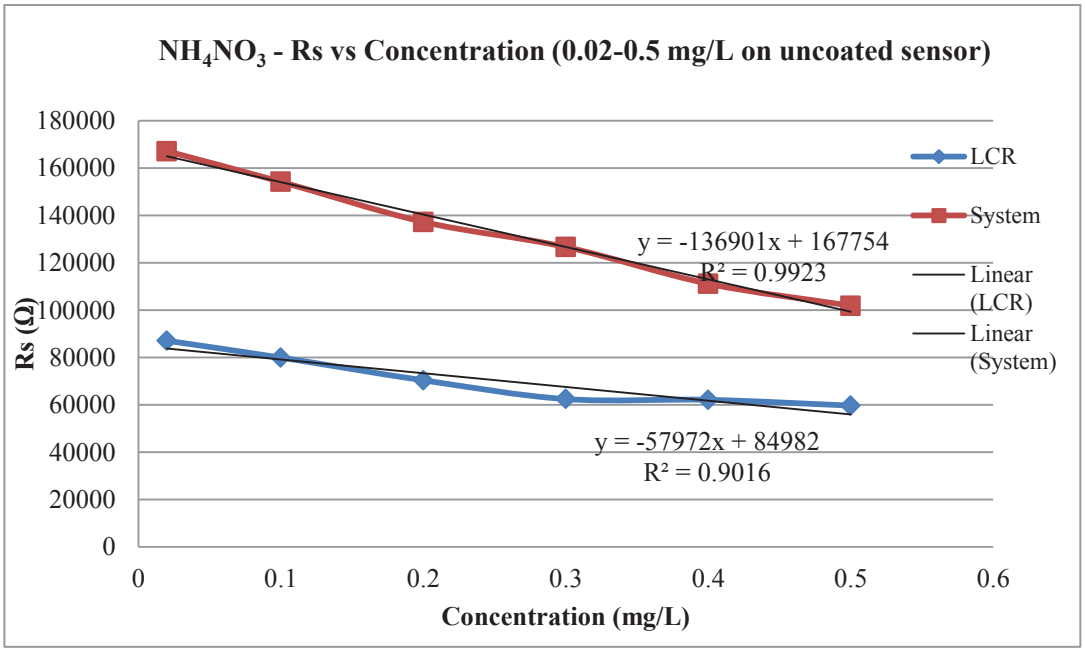

Figure 4.5.3.2: Real part of imaginary comparison between system and LCR at low concentration (NH_4NO_3)

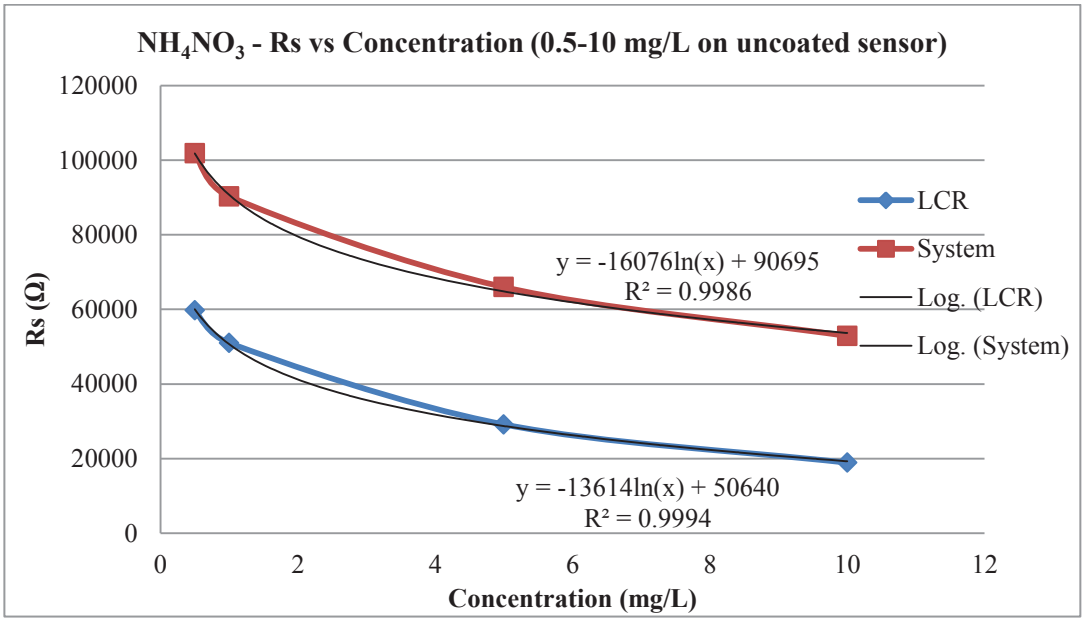

Figure 4.5.3.3: Imaginary part of imaginary comparison between system and LCR at high concentration (NH_4NO_3)

When the concentration was above 0.5 PPM, the relationship between impedance and concentration was more logarithmic rather than linear. Both the results from LCR and designed system showed a high correlation, $R^2 = 0.9986$ and $R^2 = 0.9994$ respectively. Figure 4.5.3.4 and figure 4.5.3.5 display the relationship between concentration and real part (R) of the impedance on $NaNO_3$ water solutions. The Rs values reduced with the increase in the detection of ammonium concentration in the

water samples. The relationship shows the very high correlation R^2 = 0.973 and 0.9997 for low concentration and high concentration, respectively.

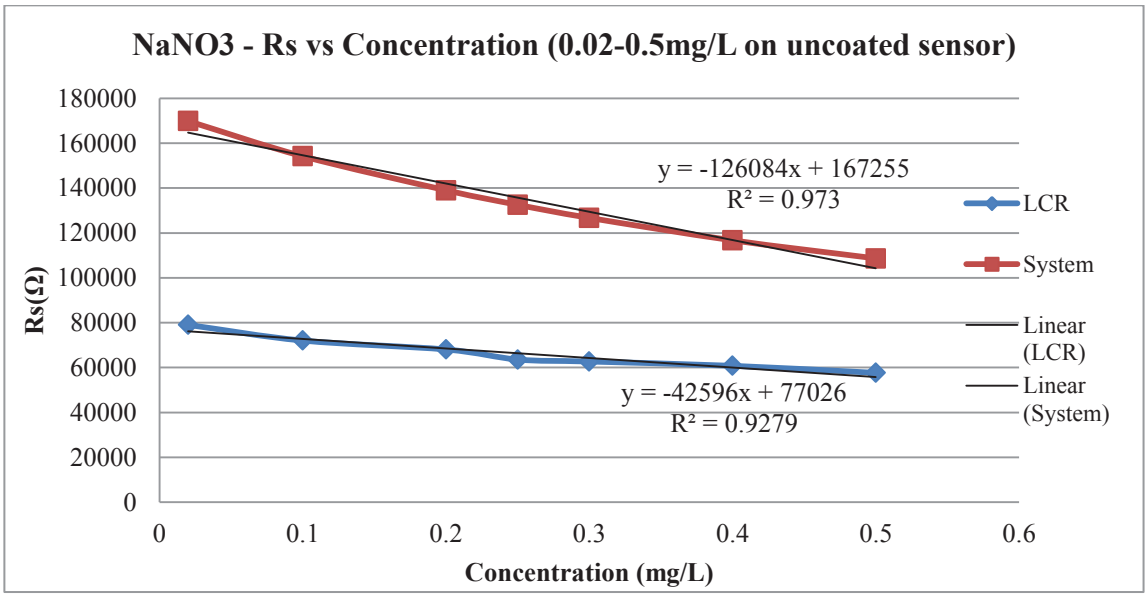

Figure 4.5.3.4: Real part of imaginary comparison between system and LCR at low concentration ($NaNO_3$)

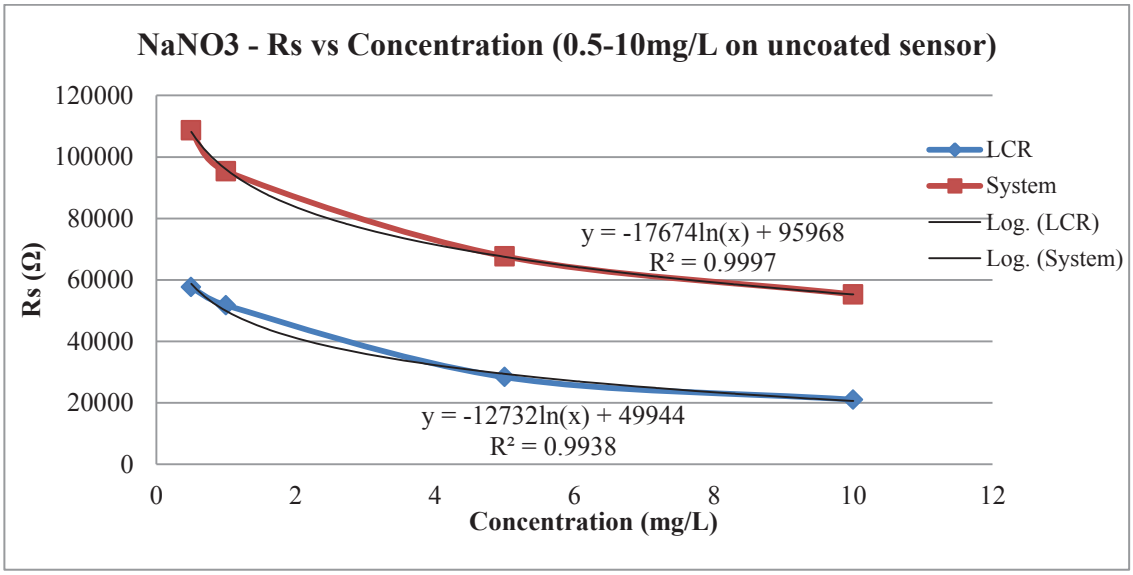

Figure 4.5.3.5: Imaginary part of imaginary comparison between system and LCR at high concentration ($NaNO_3$)

From figure 4.5.3.2 to figure 4.5.3.5, it could be seen from the relationship of real part of impedance and concentration of the water solution based on above results, the system is more linear in NH_4NO3 than $NaNO_3$, so the computational formula of concentration would be as shown in equation 4.5.9:

$$C = \frac{R - R_{0.3}}{-136901} + C_{0.3} \qquad \text{(Equ. 4.5.9)}$$

Where R is the real impedance of water sample, $R_{0.3}$ is the real part of the impedance at 0.3 mg/L of NH_4NO_3, $C_{0.3}$ represent the concentration of 0.3 mg/L, which is a reference. Substituting the value of $R_{0.3}$ and $C_{0.3}$ into equation 4.5.10, the concentration was calculated by:

$$C = \frac{R - 126684.17}{-136901} + 0.3 \qquad \text{(Equ. 4.5.10)}$$

Since the sensor is very sensitive to the temperature change, the relationship between the resistance (R) and the temperature (T) based on the result of the temperature experiment, the correction factor for the changing rate of R on changing T can be represented by equation 4.5.11:

$$\alpha = \frac{\Delta R}{\Delta T} = \frac{R_{40} - R_{10}}{T_{40} - T_{10}} = \frac{42392.83 - 118037.76}{40 - 10} = -2521.49\ \Omega/\ ^oC \quad \text{(Equ. 4.5.11)}$$

Therefore, by using the correction factor, the R_{acutal} is modified by equation 4.5.12:

$$R_{actual} = R + \alpha * (T - T_{20}) \qquad \text{(Equ. 4.5.12)}$$

Where T_{20} is at 20^oC. To replace R with R_{actual} in equation 10, the computational formula of concentration with correct factor for uncoated sensor can be represented as shown in equation 4.5.13:

$$C = \frac{R + \alpha * (T - T_{20}) \quad - 126684.17}{-136901} + 0.3 \qquad \text{(Equ. 4.5.13)}$$

Experiments with Parylene Coated Sensor

This experiment tested different concentrations of NH_4NO_3 between 0.1 mg/L and 0.5 mg/L by the developed system using the same water solutions using a Parylene coated sensor. Figure 4.5.3.6 illustrates the test results from designed the system in comparison to the LCR meter. When the concentration increased in the water solution, the real part of impedance decreased accordingly. The result is similar to the results tested on the uncoated sensor which showed a strong linear correlation with $R^2 = 0.9818$, but the value of resistance is different.

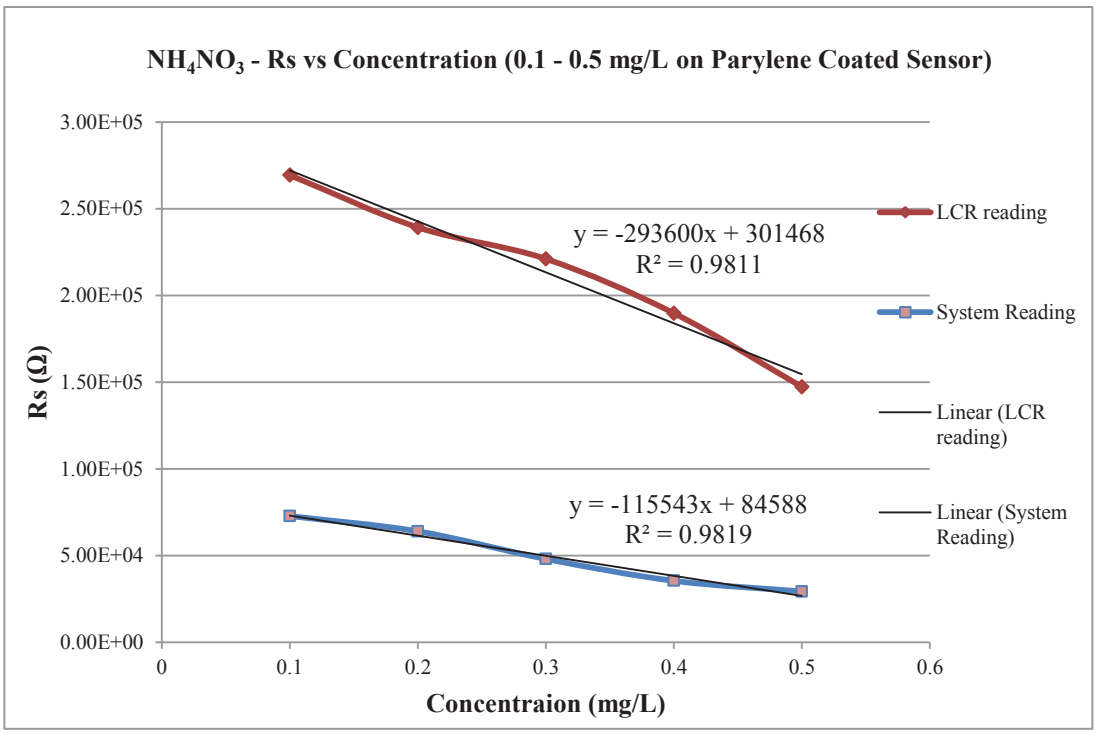

Figure 4.5.3.6: Real part of imaginary comparison between system and LCR at concentration (NH_4NO_3)

Therefore, the computational formula of concentration with correction factor for Parylene coated sensor can be represented by equation 4.5.14:

$$C = \frac{R + \alpha * (T - T_{20}) \quad - 48056.78}{-115543} + 0.3 \qquad \text{(Equ. 4.5.14)}$$

4.6 Stream Water Sample Testing

In this experiment, the water samples collected from different surface water sources were tested by the designed system and Parylene coated sensor. Table 4.6.1 compares the nitrate concentrations measured using the designed system and the laboratory spectrophotometric method. The measurement from the designed system in sample S359 is the same as the result from laboratory. The results from sample numbers S348, S349, S351, S252 and S357 tested by the designed system were very close to the results from laboratory test, with only ±0.01 mg/L difference. The results from sample numbers S350 and S354 were 0.2 mg/L and 0.3 mg/L higher than the laboratory result respectively. Sample numbers S353 and S358 also measured higher test results using the designed system compared to the laboratory method (±0.7 mg/L and ±0.6 mg/L). The largest difference between the two test results was 66.7%,

where the designed system is measured a concentration which was 0.06 mg/L, higher than the laboratory measurement. The Actual Error rate can be calculated by equation 4.6.1:

$$Actual\ error\ \% = \frac{Measured\ Value - Actual\ value}{Actual\ Value} * 100 \qquad (4.6.1)$$

Where:

- Measured Value: is the measured value from designed system
- Actual value: is the measured value from laboratory spectrophotometric method

Table 4.6.1: The compared results between the designed system and laboratory measurement (Stream samples are represented by numbers followed by S and surface runoff samples are identified by their sample name)

Samples for testing nitrate sensor				
Date sampled	Sample name	Laboratory result Nitrate-N (mg/L)	Designed system result Nitrate-N (mg/L)	Actual Error %
6/8/2015	S348	0.19	0.2	5.00
6/8/2015	S349	0.13	0.14	7.14
6/8/2015	S350	0.12	0.1	-20.00
6/8/2015	S351	0.05	0.04	-25.00
6/8/2015	S352	0.07	0.06	-16.67
6/8/2015	S353	0.35	0.42	16.67
6/8/2015	S354	0.10	0.07	-42.86
6/8/2015	S355	0.32	0.28	-14.29
6/12/2015	S356	0.62	0.38	-63.16
6/12/2015	S357	0.60	0.61	1.64
6/12/2015	S358	0.46	0.52	11.54
6/12/2015	S359	0.59	0.59	0.00
7/7/2015	Paddock 9 runoff	0.10	0.16	37.50
7/7/2015	Paddock 12 runoff	0.32	0.41	21.95
7/16/2015	Paddock 9 runoff	0.10	0.06	-66.67
7/20/2015	Paddock 9 runoff	0.09	0.15	40.00

The actual error rate for each sample is also shown in Table 4.6.1. Although there were more stream samples measurd in this comparison compared to surface runofff samples (12 verses 4), the average % error for the stram samples was -7% compared to +29% for surface and runoff samples. The surface runoff samples contrained a higher concentration of suspended soil sediment which may have interfered with the sensing system. In addition to NO_3-N and suspended sediment, the stream water samples also contain phosphates, ammonium, organics and other mineral salts. Without the proper selectivity, our sensor cannot capture the nitrate ions, so there was a difference between two results. However, considering that the sensing system doesn't yet have selective capacity, the majority of low concentrations measured by the designed system were very close to the laboratory measurement.

Figure 4.61 illustrates the correlation between results from laboratory analysis and designed system. Although there is a difference between two results, the correlation coefficient R^2 is at 0.8655 which shows the potential for this new approach.

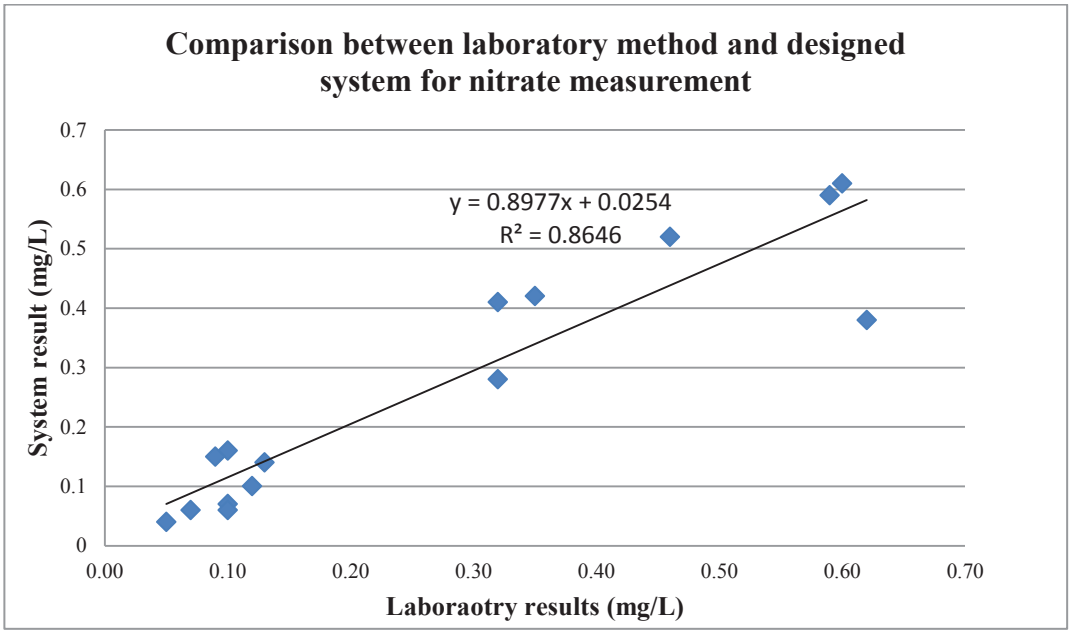

Figure 4.6.1: Comparison between laboratory method and designed system for nitration measurement

4.7 Experimental Test of Complete System

Figure 4.7.1 shows the experimental setup for NO_3-N concentration measurement. Tests were implemented in ambient conditions. The 12-Volt DC battery is used as a power source for the main circuit board, water pump and solenoid valve. Arduino Fio

was used to generate the sinusoidal waveform that was the input signal for the sensor and perform data acquisition. The sensor was immersed into stream samples collected at the Massey University Experimental Research Station, Tuapaka near Palmerston North, New Zealand and standard samples at different NO_3-N concentration. The electronic circuit was designed to get the input and output voltage of the sensor and detect the phase angle across the sensor. The ions in the nitrate get polarized towards the plates according to their charge. These charges generated the electric field which changes the impedance of the sensor [121]. Since the experiments were conducted in laboratory conditions, two water pumps were used. The pumps were connected to the motor with one being used to fetch the water sample into a container for measurement at every 15 minutes and another one was used for discharging the sampled water from the container after 1 minute. The sensor's impedance was calculated by the microcontroller. The data obtained by the microcontroller was transmitted to the computer via ZigBee wireless communication. All information is shown in the Graphic User Interface (GUI) for real-time monitoring.

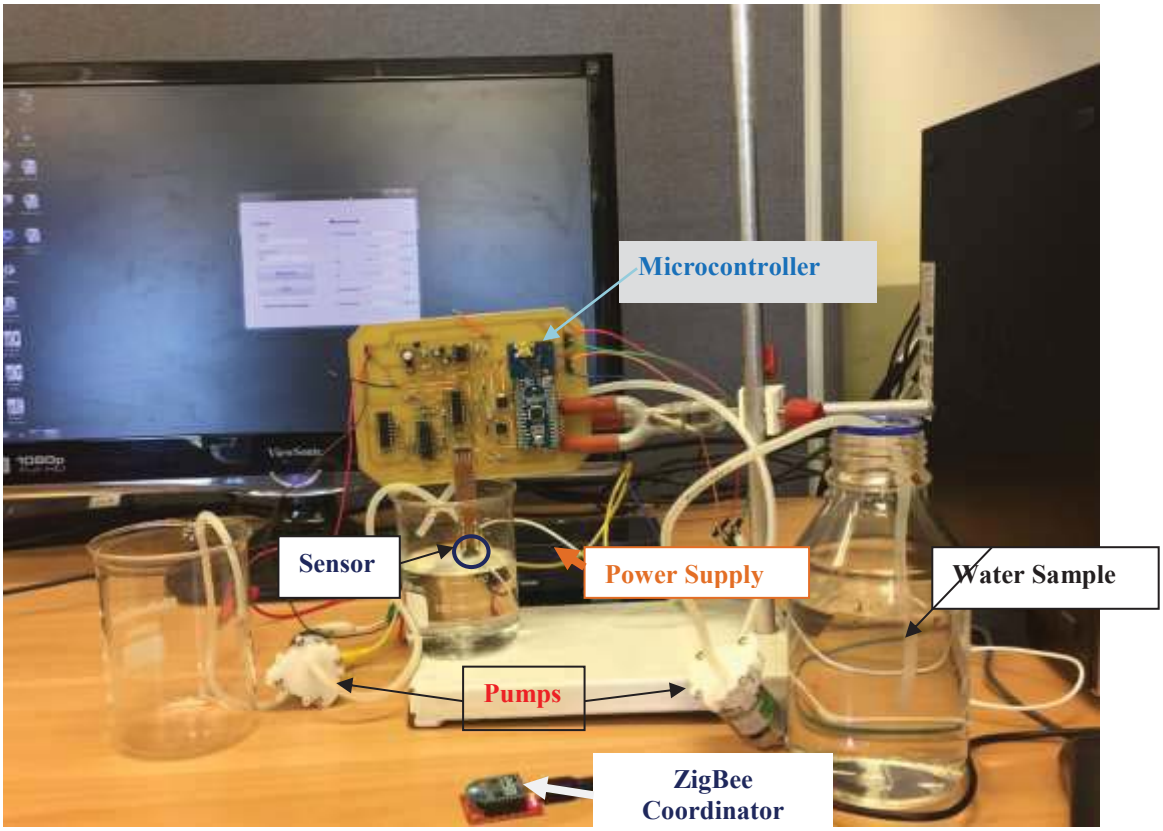

Figure 4.7.1: Experimental setup for system testing

In situ measurement of nitrate concentration will also require the incorporation of a filter to remove soil sediments and organic particles, prior to measurement. This feature would be required for future developments of a nitrate sensor.

Figure 4.7.2 shows the GUI for real-time monitoring when testing water solution of concentration at 0.2 mg/L. The user can choose the port name and Baud rate and start to receive the real-time data by clicking the open port button. It shows parameters of measurement and the calculated concentration. The measured temperature is used for correct factor for concentration calculation.

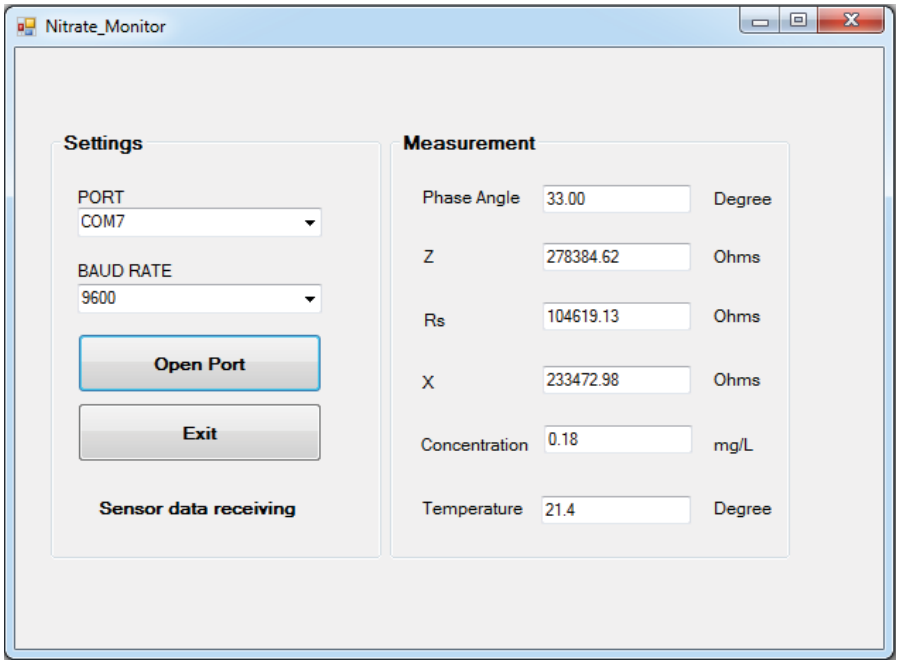

Figure 4.7.2: GUI for real-time monitoring

4.8 Conclusion

In this chapter, temperature and humidity are two factors that cause a change in the impedance of the Parylene coated sensor in the measurement environment. The higher the temperature and humidity in the environment is, the lower the impedance of the sensor will be. Electrochemical Impedance Spectroscopy was employed to detect and display nitrate concentrations by evaluating the impedance change read by interdigital sensors (Parylene coated sensor and bared sensor) immersed in the available water solutions and groundwater samples. The nitrate water solution and water sample collected from stream samples were evaluated by the LCR meter and designed system. The developed system showed a good linear relationship between

the measured nitrate concentrations (ranging from 0.02-0.5 mg/L for the uncoated sensor and 0.1-0.5 mg/L for the Parylene coated sensor) to those measured by the LCR meter. With the temperature correction factor in the calculation of nitrate concentration, the total actual error is around 24% to the measured results from the laboratory spectrophotometric method. The pump and valve controlled by microcontroller work every 15 minutes for measurement. The wireless communication is implemented for the real-time monitoring.

Chapter 5: Conclusions and Future Works

5.1 Conclusions

This thesis contributed to the development of an electrochemical impedance spectroscopy based sensing system for nitrate detection by using the novel interdigital sensor. Agriculture is the primary industry in New Zealand and most of the nitrate contamination sources come from agricultural activities like livestock farming and fertilizer application to pasture and crops. Therefore, the nitrate level is higher than the threshold in some areas in New Zealand. Water quality is routinely monitored by regional councils around New Zealand, and water samples have to be collected manually from the field and tested in the laboratory. This requires not only expensive equipment and professional technicians but is time-consuming. More importantly, the quality of the data collected can be compromised by this approach, as water quality changes rapidly with increasing flow (i.e. storm events) and decreasing flow and monthly sampling approaches are unable to fully capture these changes. Hence, a low-cost portable/in-situ, high frequency nitrate sensor is essential to improve water quality monitoring not only in New Zealand, but for the result for the world. The work done in this thesis includes the system design, characterizing of sensor impedance, testing, data collecting and analyzing. An electrochemical impedance spectroscopy based nitrate sensing system has been developed for nitrate detection. The proposed system is designed to read the nitrate concentration in water and represents a stand-alone, robust, real-time and low-cost system. The microcontroller in the designed system was used to generate the excitation signal applied to the sensor; for data processing and controlling time interval for the switch on/off the automatic sample-intake pump. The data in the microcontroller is transmitted to a computer for data storage and calculation via wireless communication. As the sensor geometry used in the project is the interdigital type which is very sensitive to the temperature, therefore, the sensor was initially tested in the deionized water at variable temperatures. From the results of testing in various temperature ranges, the temperature correction factor was obtained for nitrate measurement. The calibration samples were prepared by the serial dilution of the nitrate stock solution using sodium nitrate ($NaNO_3$) and ammonium nitrate (NH_4NO_3)

with different concentrations. The sensor was immersed in the solution to observe the impedance change at various nitrate concentration. The experimental results showed a good linear relationship between the concentration and real part of the measured impedance and the computational model for nitrate concentration was predicted based on the experimental results achieved. The sensor was also tested in the water samples collected from different stream and surface runoff samples, and the results were validated with the applied laboratory testing results. The experimental result showed that the sensing system is more sensitive to the lower nitrate concentrations in the stream and surface runoff water and serval areas fro future improvement of the system have been identified in section 5.2. The system was prototyped and applied in the field. The real-time low-cost testing system displayed its potential for the in-situ continuous nitrate monitoring in the paddocks.

The literature reviews on different sensors and methods which can be used for nitration detection. The working principle of the interdigital sensor and the electrochemical impedance spectroscopy method were explained. Other types of sensors such as fiber optic sensor, electrochemical biosensor, and microwave sensor and other detection methods are also discussed. In addition, the comparison of currently commercial nitrate detector is done based on their price, detection limit/range, and detection method. However, these commercial systems are either used in the laboratory or require the chemical reagent. The designed system consisted of the power supply, microcontroller, signal processing circuit, a control circuit and data collection via ZigBee protocol. The microcontroller is used to provide PWM output filtered by band pass filter and then generate the oscillated excitation signal. This input signal is the voltage applied to the sensor and the output signal is the voltage across the series resistor. In order to measure the impedance read by the sensor, the input signal is fed into the microcontroller after level shifting because the ADC of microcontroller only can receive the positive value. The active low pass filter and full rectifier were used to amplify the output signal and reduce the noise across the signal. The filtered and amplified output signal was fed into ADC of the microcontroller as well. To get the phase difference between input and output signal, both of these sinusoidal waveforms are firstly converted to a square wave by zero cross detector and using external interrupt function to capture both of their rising edges and fed back to the microcontroller. With the help of a microcontroller, the

phase angle can be calculated in degree. The microcontroller also controls the time interval of an on/off switch for the water pump and valve. Therefore, the water sample can be injected into the container for measurement by immersed sensor and discharging the water after the measurement is done. The total impedance and phase angle collected by the microcontroller are transmitted to the computer via ZigBee protocol. The ZigBee end device is integrated with the microcontroller board, and the coordinator is connected to the computer. C# programming is used here to collect the transmitted data through the serial port and calculate the concentration of nitrate from water samples. This designed system can be applied for nitrate detection with low cost and quick response in continuous real-time monitoring.

The experimental work started from investigating the characterization of sensor impedance when tested in deionized water at temperatures ranging from 10^{o}C to 40^{o}C. This experimental result showed an excellent linear relationship between the temperature and real part of the impedance. With the increase in temperature, the real part of impedance decreased almost linearly. This result is used as temperature correction factor in the calculation of nitrate concentration. Since the interdigital sensor is very sensitive to the temperature and humidity, the next experiment was to test the deionized water at the different combination of temperature and humidity. Although the humidity is not an issue for nitrate detection in water, the result is useful for other application using the sensor in the project. The experimental result indicated the higher temperature and humidity in the environment, the lower the impedance of the sensor. The developed system detected the nitrate using EIS method. A commercial device - hi precision LCR meter was used to measure the impedance based on the EIS as well. The developed system showed a good linear relationship between the measured nitrate concentrations (ranging from 0.02-0.5 mg/L for uncoated sensor and 0.1-0.5 mg/L for Parylene coated sensor) to those measured by the LCR meter. The water sample collected from difference groundwater sources are tested by the designed system. With the help of the temperature correction factor, the calculated concentration was closely correlated with the measured laboratory results for concentrations of between 0.02 to 0.2 mg/L. However, without inducing selectivity to the system, the sensor is not very sensitive to the nitrate ions at high concentrations.

5.2 Future Works

The currently designed sensing system showed potential for the accurate detection of nitrate in stream and surface runoff samples. However, to improve the reliability and accuracy of the sensor, it still requires additional improvements as follows.

1. **Improvement of sensitivity and selectivity:**

   Currently, the area of the sensing surface is 25 mm x 25 mm and gold is used to fabricate electrodes. Increasing the sensing surface area and the use of different materials, may improve sensitivity. In addition, the connection of the sensor is another problem. The sensor is supposed to be immersed in water for measurement, and the impedance of the sensor will be changed if there is any water on the excitation or sensing electrodes. The impedance of the sensor could also be modified if solder heat damages the excitation and sensing electrodes. Therefore, these problems may be avoided by increasing the distance between the sensing surface and excitation/sensing electrode (increase the length of the sensor).

   The precise selectivity is required to capture the nitrate ions to improve the accuracy of the measurement. Synthesis of molecular imprinted polymer (MIP) for recognition of nitrate ions using precipitation polymerization method. It involves polymerization of long chain polymers using initiator and crosslinker. The synthesized polymer called ionophores, could be functionalized on the sensing surface to capture the nitrate ions present in the sample selectively. The molecular imprinted polymer and non-imprinted polymer (NIP) coated transducer can read the nitrate concentration in the sample that could be characterized using impedance spectroscopy. HPLC and Spectrophotometry could be used for the validation of the achieved results.

2. **Increase in the capability of sensing system:**

   The array of the sensor can be used in the sensing system for the detection of other major ions in the water such as phosphate, ammonium, pH, chloride and so on. The developed system based on the interdigital sensor is capable of detecting any material under test. Therefore, it can help to develop a multi-sensing system.

3. **Implement the real-time in-situ monitoring:**

A robust box which includes the circuit board, pumps, battery, measurement container and other system components inside should be made and installed in the field for the in-situ testing purpose. The filter with pore-size of 0.22 μm should be added to the system in order to protect the sensor and reduce soil and sediment interference with the measurement.

The shortcoming of the ZigBee protocol is that the maximum coverage of transmission is 100 meters. This means that this approach is not practical to achieve real-time, in-situ monitoring in remote areas. The other microcontroller integrated with Wi-Fi can be used and using Wi-Fi to upload the data to the cloud server. The data can be stored in the cloud server directly so that user can access the data remotely.

References

[1] C. E. McMichael, "Freshwater," in *The Encyclopedia of Earth*, A. Al-Rawajfeh, Ed., ed.

[2] N. Geographic. *A Freshwater Story*. Available: http://environment.nationalgeographic.com/environment/freshwater/freshwater-101-interactive/

[3] B. Oram. (2014). *Nitrates and Nitrites in Drinking Water and Surfacewaters*. Available: http://www.water-research.net/index.php/nitrate

[4] P. C. f. t. Envrionment. (2013). *Water quality in New Zealand: Land use and nutrient pollution*. Available: http://www.pce.parliament.nz/assets/Uploads/PCE-Water-quality-land-use-web-amended.pdf

[5] L. Kellman and C. Hillaire-Marcel, "Evaluation of nitrogen isotopes as indicators of nitrate contamination sources in an agricultural watershed," *Agriculture, ecosystems & environment,* vol. 95, pp. 87-102, 2003.

[6] P. J. Thorburn, J. S. Biggs, K. L. Weier, and B. A. Keating, "Nitrate in groundwaters of intensive agricultural areas in coastal Northeastern Australia," *Agriculture, ecosystems & environment,* vol. 94, pp. 49-58, 2003.

[7] M. f. t. Enviroment. (2010). *Nitrate in groundwater*. Available: http://www.mfe.govt.nz/more/environmental-reporting/fresh-water/groundwater-quality-indicator/nitrate-groundwater

[8] M. f. t. Envrionment. (2013). *River condition indicator: Summary*. Available: http://www.mfe.govt.nz/more/environmental-reporting/fresh-water/river-condition-indicator/summary

[9] U. N. E. Programme, *Global environment outlook 2000*: Routledge, 2013.

[10] P. C. f. t. Environment, "Water Quality in New Zealand: Understanding the science " 2013.

[11] R. Haynes and P. Williams, "Nutrient cycling and soil fertility in the grazed pasture ecosystem," *Advances in agronomy (USA),* 1993.

[12] P. M. Lee Haller, Terrence O'Brien, Joe Riehle, and Thomas Stuhldreher. *NITRATE POLLUTION OF GROUNDWATER*. Available: http://www.reopure.com/nitratinfo.html

[13] A. Mahvi, J. Nouri, A. Babaei, and R. Nabizadeh, "Agricultural activities impact on groundwater nitrate pollution," *International Journal of Environmental Science & Technology,* vol. 2, pp. 41-47, 2005.

[14] W. H. Organization, "Nitrate and nitrite in drinking-water: Background document for development of WHO Guidelines for Drinking-water Quality," 2011.

[15] M. A. M. Yunus and S. Mukhopdhyay, "A new method for monitoring ammonium nitrate contamination in natural water sources based on independent component analysis," in *Sensors, 2011 IEEE*, 2011, pp. 1066-1069.

[16] D. L. Pfost, C. D. Fulhage, and S. W. Casteel, "Water quality for livestock drinking," *Extension publications (MU),* 2001.

[17] L. Kamphake, S. Hannah, and J. Cohen, "Automated analysis for nitrate by hydrazine reduction," *Water research,* vol. 1, pp. 205-216, 1967.

[18] M. S. Abdul Rahman, S. C. Mukhopadhyay, P.-L. Yu, J. Goicoechea, I. R. Matias, C. P. Gooneratne*, et al.*, "Detection of bacterial endotoxin in food: New planar interdigital sensors based approach," *Journal of Food Engineering,* vol. 114, pp. 346-360, 2013.

[19] C. Valero Vidal and A. Igual Muñoz, "Effect of physico-chemical properties of simulated body fluids on the electrochemical behaviour of CoCrMo alloy," *Electrochimica Acta,* vol. 56, pp. 8239-8248, 2011.

[20] C. Xhoffer, K. Van den Bergh, and H. Dillen, "Electrochemistry: a powerful analytical tool in steel research," *Electrochimica Acta,* vol. 49, pp. 2825-2831, 2004.
[21] X. Li, K. Toyoda, and I. Ihara, "Coagulation process of soymilk characterized by electrical impedance spectroscopy," *Journal of Food Engineering,* vol. 105, pp. 563-568, 2011.
[22] A. I. Zia, A. R. Mohd Syaifudin, S. C. Mukhopadhyay, I. H. Al-Bahadly, P. L. Yu, C. P. Gooneratne*, et al.*, "MEMS based impedimetric sensing of phthalates," in *Instrumentation and Measurement Technology Conference (I2MTC), 2013 IEEE International*, 2013, pp. 855-860.
[23] B.-Y. Chang and S.-M. Park, "Electrochemical impedance spectroscopy," *Annual Review of Analytical Chemistry,* vol. 3, pp. 207-229, 2010.
[24] G. Instruments. Basics of Electrochemical Impedance Spectroscopy. Available: http://www.gamry.com/application-notes/EIS/basics-of-electrochemical-impedance-spectroscopy/
[25] E. Udd and W. B. Spillman Jr, *Fiber optic sensors: an introduction for engineers and scientists*: John Wiley & Sons, 2011.
[26] A. A. Ensafi and M. Amini, "Highly selective optical nitrite sensor for food analysis based on Lauth's violet–triacetyl cellulose membrane film," *Food Chemistry,* vol. 132, pp. 1600-1606, 2012.
[27] B. Mahieuxe, M. Carré, M. Viriot, J. André, and M. Donner, "Fiber-optic fluorescing sensors for nitrate and nitrite detection," *Journal of fluorescence,* vol. 4, pp. 7-10, 1994.
[28] J. Camas-Anzueto, A. Aguilar-Castillejos, J. Castañón-González, M. Lujpán-Hidalgo, H. H. de León, and R. M. Grajales, "Fiber sensor based on Lophine sensitive layer for nitrate detection in drinking water," *Optics and Lasers in Engineering,* vol. 60, pp. 38-43, 2014.
[29] M. Y. Chong, M. Z. M. Jafri, L. H. San, and T. C. Ho, "Detection of nitrate ions in water by optical fiber," in *Computer and Communication Engineering (ICCCE), 2012 International Conference on*, 2012, pp. 271-273.
[30] A. Lalasangi, J. Akki, K. Manohar, T. Srinivas, P. Radhakrishnan, S. Kher*, et al.*, "Fiber Bragg grating sensor for detection of nitrate concentration in water," *Sensors & Transducers,* vol. 125, p. 187, 2011.
[31] C. Munkholm, D. R. Walt, and F. P. Milanovich, "A fiber-optic sensor for CO 2 measurement," *Talanta,* vol. 35, pp. 109-112, 1988.
[32] Y. Zhu and A. Wang, "Miniature fiber-optic pressure sensor," *Photonics Technology Letters, IEEE,* vol. 17, pp. 447-449, 2005.
[33] S. Zhang, H. Chen, and H. Fu, "Fiber-optic temperature sensor using an optoelectronic oscillator," in *Optical Communications and Networks (ICOCN), 2015 14th International Conference on*, 2015, pp. 1-3.
[34] F. Delport, J. Pollet, K. Janssen, B. Verbruggen, K. Knez, D. Spasic*, et al.*, "Real-time monitoring of DNA hybridization and melting processes using a fiber optic sensor," *Nanotechnology,* vol. 23, p. 065503, 2012.
[35] P. Bhatia and B. D. Gupta, "Fabrication and characterization of a surface plasmon resonance based fiber optic urea sensor for biomedical applications," *Sensors and Actuators B: Chemical,* vol. 161, pp. 434-438, 2012.
[36] R. Lalauze, *Chemical sensors and biosensors*: John Wiley & Sons, 2012.
[37] C. J. Taylor, L. A. Bain, D. J. Richardson, S. Spiro, and D. A. Russell, "Construction of a whole-cell gene reporter for the fluorescent bioassay of nitrate," *Analytical biochemistry,* vol. 328, pp. 60-66, 2004.

[38] N. Plumeré, J. r. Henig, and W. H. Campbell, "Enzyme-catalyzed O2 removal system for electrochemical analysis under ambient air: Application in an amperometric nitrate biosensor," *Analytical chemistry,* vol. 84, pp. 2141-2146, 2012.

[39] A. A. Gokhale, J. Lu, R. R. Weerasiri, J. Yu, and I. Lee, "Amperometric Detection and Quantification of Nitrate Ions Using a Highly Sensitive Nanostructured Membrane Electrocodeposited Biosensor Array," *Electroanalysis,* vol. 27, pp. 1127-1137, 2015.

[40] T. Wang, K. T. Schlueter, B. L. Riehl, J. M. Johnson, and W. R. Heineman, "Simplified Nitrate-Reductase-Based Nitrate Detection by a Hybrid Thin-Layer Controlled Potential Coulometry/Spectroscopy Technique," *Analytical chemistry,* vol. 85, pp. 9486-9492, 2013.

[41] C. Bernou, D. Rebière, and J. Pistré, "Microwave sensors: a new sensing principle. Application to humidity detection," *Sensors and Actuators B: Chemical,* vol. 68, pp. 88-93, 2000.

[42] B. Kapilevich and B. Litvak, "Microwave sensor for accurate measurements of water solution concentrations," in *Microwave Conference, 2007. APMC 2007. Asia-Pacific*, 2007, pp. 1-4.

[43] B. Jackson and T. Jayanthy, "A novel method for water impurity concentration using microstrip resonator sensor," in *Recent Advances in Space Technology Services and Climate Change (RSTSCC), 2010*, 2010, pp. 376-379.

[44] A. Mason, S. Wylie, A. Thomas, H. Keele, A. Shaw, and A. Al-Shammaa, "HEPA FILTER MATERIAL LOAD DETECTION USING A MICROWAVE CAVITY SENSOR," *International Journal on Smart Sensing & Intelligent Systems,* vol. 3, 2010.

[45] O. Korostynska, A. Mason, and A. Al-Shamma'a, "Proof-of-concept microwave sensor on flexible substrate for real-time water composition analysis," in *Sensing Technology (ICST), 2012 Sixth International Conference on*, 2012, pp. 547-550.

[46] A. Mason, O. Korostynska, and A. Al-Shamma'a, "Microwave sensors for real-time nutrients detection in water," in *Smart Sensors for Real-Time Water Quality Monitoring*, ed: Springer, 2013, pp. 197-216.

[47] A. S. Abu-Abed and R. G. Lindquist, "Capacitive interdigital sensor with inhomogeneous nematic liquid crystal film," *Progress In Electromagnetics Research B,* vol. 7, pp. 75-87, 2008.

[48] U. Jönsson, M. Malmqvist, and I. Ronnberg, "Adsorption of immunoglobulin G, protein A, and fibronectin in the submonolayer region evaluated by a combined study of ellipsometry and radiotracer techniques," *Journal of colloid and interface science,* vol. 103, pp. 360-372, 1985.

[49] M. S. A. Rahman, S. C. Mukhopadhyay, and P.-L. Yu, "Novel Planar Interdigital Sensors," in *Novel Sensors for Food Inspection: Modelling, Fabrication and Experimentation*, ed: Springer, 2014, pp. 11-35.

[50] A. Mohd Syaifudin, S. Mukhopadhyay, P. Yu, M. J. Haji-Sheikh, C. H. Chuang, and H. P. Wu, "Detection of natural bio-toxins using an improved design interdigital sensors," 2011, pp. 1028-1031.

[51] A. I. Zia, A. M. Syaifudin, S. Mukhopadhyay, P. Yu, I. Al-Bahadly, C. P. Gooneratne*, et al.*, "Electrochemical impedance spectroscopy based MEMS sensors for phthalates detection in water and juices," *Journal of Physics: Conference Series,* vol. 439, p. 012026, 2013.

[52] A. I. Zia, S. C. Mukhopadhyay, P.-L. Yu, I. Al-Bahadly, C. P. Gooneratne, and J. Kosel, "Rapid and molecular selective electrochemical sensing of phthalates in aqueous solution," *Biosensors and Bioelectronics,* vol. 67, pp. 342-349, 2015.

[53] A. Zia, S. Mukhopadhyay, I. Al-Bahadly, P. Yu, C. P. Gooneratne, and J. Kosel, "Introducing molecular selectivity in rapid impedimetric sensing of phthalates," in

Instrumentation and Measurement Technology Conference (I2MTC) Proceedings, 2014 IEEE International, 2014, pp. 838-843.

[54] A. R. M. Syaifudin, M. Yunus, S. Mukhopadhyay, and K. Jayasundera, "A novel planar interdigital sensor for environmental monitoring," 2009, pp. 105-110.

[55] A. R. M. Syaifudin, K. Jayasundera, and S. Mukhopadhyay, "A novel planar interdigital sensor based sensing and instrumentation for detection of dangerous contaminated chemical in seafood," 2009, pp. 701-706.

[56] Y. Yang, G. Chiesura, G. Luyckx, T. Vervust, F. Bossuyt, J. Vanfleteren*, et al.*, "In situ on-line cure monitoring of composites by embedded interdigital sensor," in *16th European conference on Composite Materials (ECCM-16)*, 2014.

[57] M. Dhull and A. Arora, "Design of MEMS Based Microheater for Enhanced Efficiency of Gas Sensors," *Journal of Thermal Engineering and Applications,* vol. 2, pp. 16-21, 2015.

[58] L. Li, F. Yang, J. Yu, X. Wang, L. Zhang, Y. Chen*, et al.*, "In situ growth of ZnO nanowires on Zn comb-shaped interdigitating electrodes and their photosensitive and gas-sensing characteristics," *Materials Research Bulletin,* vol. 47, pp. 3971-3975, 2012.

[59] J. Fischer, H. Dejmkova, and J. Barek, "Electrochemistry of pesticides and its analytical applications," *Current Organic Chemistry,* vol. 15, pp. 2923-2935, 2011.

[60] M. Khafaji, S. Shahrokhian, and M. Ghalkhani, "Electrochemistry of Levo‐Thyroxin on Edge‐Plane Pyrolytic Graphite Electrode: Application to Sensitive Analytical Determinations," *Electroanalysis,* vol. 23, pp. 1875-1880, 2011.

[61] D. Pritchard, H. Morgan, and J. Cooper, "Simultaneous determination of follicle stimulating hormone and luteinising hormone using a multianalyte immunosensor," *Analytica chimica acta,* vol. 310, pp. 251-256, 1995.

[62] C. G. Fox and J. F. Alder, "Surface acoustic wave sensors for atmospheric gas monitoring. A review," *Analyst,* vol. 114, pp. 997-1004, 1989.

[63] M. M. Yunus and S. Mukhopadhyay, "Development of planar electromagnetic sensors for measurement and monitoring of environmental parameters," *Measurement Science and Technology,* vol. 22, p. 025107, 2011.

[64] M. Faramarzi, M. A. M. Yunus, A. S. M. Nor, and S. Ibrahim, "The application of the Radial Basis Function Neural Network in estimation of nitrate contamination in Manawatu river," in *Computational Science and Technology (ICCST), 2014 International Conference on*, 2014, pp. 1-5.

[65] J. Garcia-Canton, A. Merlos, and A. Baldi, "High-quality factor electrolyte insulator silicon capacitor for wireless chemical sensing," *Electron Device Letters, IEEE,* vol. 28, pp. 27-29, 2007.

[66] S. C. Mukhopadhyay, "Novel planar electromagnetic sensors: Modeling and performance evaluation," *Sensors,* vol. 5, pp. 546-579, 2005.

[67] S. Yamada, M. Katou, M. Iwahara, and F. Dawson, "Eddy current testing probe composed of planar coils," *Magnetics, IEEE Transactions on,* vol. 31, pp. 3185-3187, 1995.

[68] N. J. Goldfine, "Magnetometers for improved materials characterization in aerospace applications," *Materials Evaluation,* vol. 51, pp. 396-405, 1993.

[69] S. C. Mukhopadhyay, S. Yamada, and M. Iwahara, "Investigation of near-surface material properties using planar type meander coil," *JSAEM studies on Applied Electromagnetics and Mechanics,* vol. 11, pp. 61-69, 2001.

[70] M. J. Moorcroft, J. Davis, and R. G. Compton, "Detection and determination of nitrate and nitrite: a review," *Talanta,* vol. 54, pp. 785-803, 2001.

[71] M. A. L. de Oliveira, D. do Carmo Soares, G. S. Tostes, M. do Carmo Guimarães, and F. A. S. Vaz, "Optimization of an Alternative Methodology for Simultaneous Analysis

of Nitrite and Nitrate in Water from Urban Stream by Capillary Electrophoresis under Direct UV Detection," *American Journal of Analytical Chemistry,* vol. 3, p. 484, 2012.

[72] F. Della Betta, L. Vitali, R. Fett, and A. C. O. Costa, "Development and validation of a sub-minute capillary zone electrophoresis method for determination of nitrate and nitrite in baby foods," *Talanta,* vol. 122, pp. 23-29, 2014.

[73] E. Martínková, T. Křžek, and P. Coufal, "Determination of nitrites and nitrates in drinking water using capillary electrophoresis," *Chemical papers,* vol. 68, pp. 1008-1014, 2014.

[74] Z. Kalaycıoğlu and F. B. Erim, "Simultaneous Determination of Nitrate and Nitrite in Fish Products with Improved Sensitivity by Sample Stacking-Capillary Electrophoresis," *Food Analytical Methods,* pp. 1-6, 2015.

[75] R. K. Mahajan, R. Kaur, H. Miyake, and H. Tsukube, "Zn (II) complex-based potentiometric sensors for selective determination of nitrate anion," *Analytica chimica acta,* vol. 584, pp. 89-94, 2007.

[76] M. Cuartero, G. A. Crespo, and E. Bakker, "Tandem Electrochemical Desalination–Potentiometric Nitrate Sensing for Seawater Analysis," *Analytical chemistry,* 2015.

[77] M. Badea, A. Amine, G. Palleschi, D. Moscone, G. Volpe, and A. Curulli, "New electrochemical sensors for detection of nitrites and nitrates," *Journal of Electroanalytical Chemistry,* vol. 509, pp. 66-72, 2001.

[78] B. Britz, E. Ng, H. Jiang, Z. Xu, R. Kumar, and L. Dong, "Smart nitrate-selective electrochemical sensors with electrospun nanofibers modified microelectrode," in *Systems, Man and Cybernetics (SMC), 2014 IEEE International Conference on*, 2014, pp. 3419-3422.

[79] S. Aravamudhan, S. Ketkar, and S. Bhansali, "Development of nitrate-selective electrochemical sensor with integrated micro-fluidics," in *Sensors, 2007 IEEE*, 2007, pp. 205-208.

[80] J. Davis, M. J. Moorcroft, S. J. Wilkins, R. G. Compton, and M. F. Cardosi, "Electrochemical detection of nitrate and nitrite at a copper modified electrode," *Analyst,* vol. 125, pp. 737-742, 2000.

[81] S. Leonardi, N. Donato, A. Bonavita, G. Neri, M. Bonyani, and A. Mirzaei, "Ag-doped nanostructured materials for electrochemical sensors," in *AISEM Annual Conference, 2015 XVIII*, 2015, pp. 1-4.

[82] S. Ward‐Jones, C. E. Banks, A. O. Simm, L. Jiang, and R. G. Compton, "An In Situ Copper Plated Boron‐Doped Diamond Microelectrode Array for the Sensitive Electrochemical Detection of Nitrate," *Electroanalysis,* vol. 17, pp. 1806-1815, 2005.

[83] M. Z. Bruckner. *Ion Chromatography*. Available: http://serc.carleton.edu/microbelife/research_methods/biogeochemical/ic.html

[84] A. Dudwadkar, N. Shenoy, J. Joshi, S. D. Kumar, H. Rao, and A. Reddy, "Application of Ion Chromatography for the Determination of Nitrate in Process Streams of Thermal Denitration Plant," *Separation Science and Technology,* vol. 48, pp. 2425-2430, 2013.

[85] S. Chamandust, M. R. Mehrasebi, K. Kamali, R. Solgi, J. Taran, F. Nazari*, et al.*, "Simultaneous determination of nitrite and nitrate in milk samples by ion chromatography method and estimation of dietary intake," *International Journal of Food Properties,* 2015.

[86] T. Bolanča, Š. Cerjan‐Stefanović, G. Srečnik, Ž. Debeljak, and M. Novič, "Development of an Ion Chromatographic Method for Monitoring Fertilizer Industry Wastewater Quality," *Journal of liquid chromatography & related technologies,* vol. 27, pp. 2781-2798, 2004.

[87] M. Tswett, "Flow Injection Tutorial," ed.

[88] A. Ayala, L. Leal, L. Ferrer, and V. Cerdà, "Multiparametric automated system for sulfate, nitrite and nitrate monitoring in drinking water and wastewater based on sequential injection analysis," *Microchemical Journal,* vol. 100, pp. 55-60, 2012.

[89] S. S. Hassan, H. Sayour, and S. S. Al-Mehrezi, "A novel planar miniaturized potentiometric sensor for flow injection analysis of nitrates in wastewaters, fertilizers and pharmaceuticals," *Analytica chimica acta,* vol. 581, pp. 13-18, 2007.

[90] A. Daniel, D. Birot, M. Lehaitre, and J. Poncin, "Characterization and reduction of interferences in flow-injection analysis for the in situ determination of nitrate and nitrite in sea water," *Analytica chimica acta,* vol. 308, pp. 413-424, 1995.

[91] P. Mikuška and Z. Večeřa, "Simultaneous determination of nitrite and nitrate in water by chemiluminescent flow-injection analysis," *Analytica chimica acta,* vol. 495, pp. 225-232, 2003.

[92] E. A. Zagatto and P. Worsfold, *Flow analysis with spectrophotometric and luminometric detection*: Elsevier, 2012.

[93] S. D. Kolev and I. D. McKelvie, *Advances in flow injection analysis and related techniques* vol. 54: Elsevier, 2008.

[94] B. Narayana and K. Sunil, "A spectrophotometric method for the determination of nitrite and nitrate," *Eurasian Journal of Analytical Chemistry,* vol. 4, pp. 204-214, 2009.

[95] K. Horita and M. Satake, "Column preconcentration analysis–spectrophotometric determination of nitrate and nitrite by a diazotization–coupling reaction," *Analyst,* vol. 122, pp. 1569-1574, 1997.

[96] K. M. Miranda, M. G. Espey, and D. A. Wink, "A rapid, simple spectrophotometric method for simultaneous detection of nitrate and nitrite," *Nitric oxide,* vol. 5, pp. 62-71, 2001.

[97] T. Kong, Y. Chen, Y. Ye, K. Zhang, Z. Wang, and X. Wang, "An amperometric glucose biosensor based on the immobilization of glucose oxidase on the ZnO nanotubes," *Sensors and Actuators B: Chemical,* vol. 138, pp. 344-350, 2009.

[98] W. L. Daniel, M. S. Han, J.-S. Lee, and C. A. Mirkin, "Colorimetric nitrite and nitrate detection with gold nanoparticle probes and kinetic end points," *Journal of the American Chemical Society,* vol. 131, pp. 6362-6363, 2009.

[99] N. Xiao and C. Yu, "Rapid-response and highly sensitive noncross-linking colorimetric nitrite sensor using 4-aminothiophenol modified gold nanorods," *Analytical chemistry,* vol. 82, pp. 3659-3663, 2010.

[100] Arduino. (2015). *Arduino Fio*. Available: https://www.arduino.cc/en/Main/ArduinoBoardFio

[101] H. J. Zhang. (2013, Basic Concepts of Linear Regulator and Switching Mode Power Supplies. Available: http://cds.linear.com/docs/en/application-note/AN140fa.pdf

[102] C. S. Eva Murphy. (2004). *All About Direct Digital Synthesis*. Available: http://www.analog.com/library/analogdialogue/archives/38-08/dds.pdf

[103] (2011). *Reveiw of Arduino DAC solutionos*. Available: http://embeddednewbie.blogspot.co.nz/2011/02/review-of-arduino-dac-solutions.html

[104] Atmel. (2013). *Atmel 8-Bit Microcontroller with 4/8/16/32KBYTES In-System Programmable Flash Datasheet*. Available: http://www.atmel.com/images/atmel-8271-8-bit-avr-microcontroller-atmega48a-48pa-88a-88pa-168a-168pa-328-328p_datasheet_complete.pdf

[105] *PWM Sine Wave Generation*. Available: http://web.csulb.edu/~hill/ee470/Lab%202d%20-%20Sine_Wave_Generator.pdf

[106] E. Tutorials. *Active Low Pass Filter*. Available: http://www.electronics-tutorials.ws/filter/filter_5.html

[107] R. Kavitha, G. Nasira, and N. Nachamai, "INTERNATIONAL JOURNAL OF COMPUTER ENGINEERING & TECHNOLOGY (IJCET)," *Journal Impact Factor,* vol. 3, pp. 94-103, 2012.

[108] W. H. Kim, S. Lee, and J. Hwang, "Real-time energy monitoring and controlling system based on Zigbee sensor networks," *Procedia Computer Science,* vol. 5, pp. 794-797, 2011.

[109] L. Jinfeng and C. Shun, "A ZigBee-based Aquiculture Water Quality Monitoring System," 2015.

[110] Q. Zhang, X.-l. Yang, Y.-m. Zhou, L.-r. Wang, and X.-s. Guo, "A wireless solution for greenhouse monitoring and control system based on ZigBee technology," *Journal of Zhejiang University Science A,* vol. 8, pp. 1584-1587, 2007.

[111] S. Lin, J. Liu, and Y. Fang, "ZigBee based wireless sensor networks and its applications in industrial," in *Automation and Logistics, 2007 IEEE International Conference on*, 2007, pp. 1979-1983.

[112] S. Mukhopadhyay and A. Nag, "Occupancy Detection at Smart Home Using Real Time Dynamic Thresholding of Flexiforce Sensor."

[113] N. K. Suryadevara and S. C. Mukhopadhyay, "Wireless sensor network based home monitoring system for wellness determination of elderly," *Sensors Journal, IEEE,* vol. 12, pp. 1965-1972, 2012.

[114] S. Schmit. (2014). *XBee AT Mode - Transmit and Command Mode Example*. Available: https://eewiki.net/display/Wireless/XBee+AT+Mode+-+Transmit+and+Command+Mode+Example#XBeeATMode-TransmitandCommandModeExample-XBeeModuleandAT/APIBackground

[115] S. C. Mukhopadhyay, *Intelligent Sensing, Instrumentation and Measurements*: Springer, 2013.

[116] Y. Xu and Y.-C. Tai, "Selective deposition of parylene C for underwater shear-stress sensors," in *TRANSDUCERS, Solid-State Sensors, Actuators and Microsystems, 12th International Conference on, 2003*, 2003, pp. 1307-1310.

[117] T. A. Bendikov, S. Miserendino, Y.-C. Tai, and T. C. Harmon, "A parylene-protected nitrate selective microsensor on a carbon fiber cross section," *Sensors and Actuators B: Chemical,* vol. 123, pp. 127-134, 2007.

[118] E. C. Hioki, "HIOKI 3532-50 LCR HITESTER Instruction Manual [Z]," *JAPAN. HIOKI EE CORPORATION,* 2001.

[119] A. Ben-David and C. E. Davidson, "Estimation method for serial dilution experiments," *Journal of microbiological methods,* vol. 107, pp. 214-221, 2014.

[120] B. E. U. *Serial Dilution Protocol*. Available: http://www.biologyexams4u.com/2013/12/serial-dilution-protocol-pdf.html#.VkaiHrcwhhE

[121] M. Yunus, S. Mukhopadhyay, and K. Jayasundera, "A novel planar interdigital sensor for environmental monitoring," in *Sensors, 2009 IEEE*, 2009, pp. 105-110.